ANAEROBIC TREATMENT OF SULFATE LADEN IWASTEWATER WITH SIMULTANEOUS REMOVAL OF HYDROGEN SULFIDE USING BIOCHAR

A DISSERTATION SUBMITTED TO THE GRADUATE DIVISION OF THE UNIVERSITY OF HAWAI'I AT MANOA IN PARTIAL FULFILLMENT OF THE REQUIREMENTS FOR THE DEGREE OF

DOCTOR OF PHYLOSOPHY

IN

MOLECULAR BIOSCIENCES AND BIOENGINEERING

October 2019

By

Fernanda Rocha de Oliveira

Dissertation Committee:

Samir Kumar Khanal, Chairperson

Shihwu Sung

Qing Li

Winston Su

Tao Yan

ACKNOWLEDGEMENTS

I would like to express my sincere gratitude to my advisor Dr. Samir K. Khanal for his continuous guidance, patience, enthusiasm and immense knowledge that encouraged me to successfully complete this Ph.D.

My sincere thanks to my committee members, Dr. Qing Li, Dr. Shihwu Sung, Dr. Winston Su and Dr. Tao Yan for their support, insightful comments and encouragement.

A special thank you to Ryan Kurasaki who spent hours helping me to build the reactors.

Thank you to my lab mates Chayanon, Surendra, Sumeth, Duc, Ed, Kwon, Misheel for the laughs, for the barbecues, for the hikings, for TGIFs, for their friendship and mainly for their knowledge and support 24/7 during the Ph.D. program.

Special thank you to my spouse Daniel, and his unlimited support. For being always there for me, for cleaning my tears many times during this program, for listening, for encouraging me every single day, for not letting me quit, for practiced with me for every presentation and exam and for being here today.

Thank you my baby girl Alana that came in the middle of this mess and was one more reason to push me forward. For “kicking” during presentations and proving to me that I could do it. Thank you for being the best baby I could ever have.

ANAEROBIC TREATMENT OF SULFATE LADEN WASTEWATER WITH SIMULTANEOUS REMOVAL OF HYDROGEN SULFIDE USING BIOCHAR

By Fernanda Rocha de Oliveira

Department of Molecular Biosciences and Bioengineering
University of Hawai'i at Manoa

ABSTRACT

This study examined the use of biochar to alleviate sulfide toxicity during anaerobic treatment of high strength sulfate-rich wastewater with concomitant recovery of sulfur. At the highest sulfate concentration tested (6,000 mg SO_4^{2-}/L), the unionized dissolved sulfide (DS) of 131 mg S/L resulted in built-up of total volatile fatty acids concentration up to 3,500 mg/L as acetic acid (HAc), and the reactors were on the verge of failure. Upon integrating biochar columns with anaerobic reactors, sulfide was rapidly removed with removal efficiencies >98% of gaseous H_2S, 94% of DS and 89% of free sulfide, thereby alleviating sulfide toxicity to methanogens (MPA) and sulfate reducing bacteria (SRB) and promoting the stability of the anaerobic process. 16S rRNA gene sequencing analyses revealed that after the removal of H_2S by biochar, the RA of MPA (*Methanobacterium* and *Methanosaeta*) increased from 0.7% to 3.7% in R1, 0.7% to 2.2% in R2 and 0.4% to 2.2% in R3, while the relative abundance of SRB (*Desulfovibrio* decreased from 9.3% to 6.3% in R1, 9.1% to 1.7% in R2 and 4% to 0.5% in R3 indicating the anaerobic treatment was quickly recovered to stable state.

TABLE OF CONTENTS

LIST OF TABLES

LIST OF FIGURES

CHAPTER 1

INTRODUCTION

1.1 Background and Significance

Anaerobic digestion (AD) is a widely adopted technology for treating high-strength industrial wastewaters with concomitant recovery of bioenergy in the form of biogas (Kanjanarong et al., 2017a). Industries such as distilleries, pharmaceuticals, food processing, and pulp and paper among others generate substantial amount of sulfate-rich wastewater (100 – 15,000 mg S/L). Anaerobic treatment of sulfate-rich wastewaters is challenging as it generates hydrogen sulfide (H_2S) due to dissimilatory sulfate reduction (Khanal & Huang, 2005). H_2S is a highly corrosive gas and deters the quality of biogas as an energy resource. More importantly, sulfide, especially uninonized (H_2S) form in aqueous phase imposes toxicity to methane producing archaea (MPA) , which could lead to AD process failure (Khanal & Huang, 2003).

Dissimilatory sulfate reducing bacteria (SRB), a diverse group of chemolithotrophic bacteria, play an important role in the global carbon and sulfur cycles (van den Brand et al., 2015). In AD processes, SRB utilize sulfate (SO_4^{2-}) as a terminal electron acceptor thereby reducing it to sulfide, and utilizing hydrogen and acetate (CH_3COO^-) as electron donors (Muyzer & Stams, 2008; Plugge et al., 2011). The SRB and MPA co-exist in anaerobic systems. There is also a syntrophic relationship between these two groups of microorganisms in AD processes (Khanal & Huang, 2005). However, during anaerobic

treatment of sulfate-rich wastewater, there is a competition between MPA and SRB for the common substrates (H_2 and acetate) (van den Brand et al., 2015). With favorable thermodynamic and kinetic properties, SRB outcompete methanogens in the presence of sulfate. Studies reported that at the threshold free sulfide concentration of 250 mg S/L, SRB outcompeted MPA due to inhibition of methanogenesis thereby resulting in process failure (Bhattacharya et al., 1996; Khanal & Huang, 2003). Because sulfide has no economic (fuel) value (Khanal & Huang, 2005), reduces the infrastructure lifetime (Kanjanarong et al., 2017a) and impairs the performance of wastewater treatment systems (Oliveira et al., 2017), the removal of H_2S from AD system treating sulfate-rich wastewater is critically important. Current methods of sulfide removal include use of chemicals (various metal ions and alkali chemicals) and biological methods (*Thiobacillus* and biofilter) (Khanal and Li, 2016). Chemical methods are not only costly; but often generate chemical wastes; while biological methods are slow and less effective, especially at high sulfide concentration. Above all, both methods do not provide an opportunity for recovery of sulfur as a valuable resource. Numerous studies reported the use of biochar, a carbonaceous by-product of the thermal treatment of biomass (e.g., pyrolysis) under O_2-limiting conditions, for effective H_2S removal from biogas (>98%) via sorption and chemical bonding with various surface functional groups such as COOH and OH (Kanjanarong et al., 2017a; Sethupathi et al., 2017; Shang et al., 2013; Xu et al., 2014). The adsorption efficiency of biochar is influenced by biochar pH, surface area, porosity and moisture content which are mainly governed by biochar production conditions such as pyrolysis temperature, residence time, and feedstock types (Kanjanarong et al., 2017; Oliveira et al., 2017). There are, however, limited in-depth

studies elucidating the mechanisms of H_2S removal by biochars produced from different feedstocks at different conditions, and the subsequent effect on the microbial communities due to alleviation of sulfide toxicity in AD system.

In this comprehensive study, we operated four completely mixed reactors and assess the effects of increasing sulfate concentration from 500–6000 mg SO_4^2/L on the methanogens activity. Here we employed biochar as an efficient and cost-effective bio-based material to remove H_2S from biogas produced during anaerobic treatment of sulfate-laden wastewater. This study provides a new avenue for use of biochar for alleviating sulfide toxicity in anaerobic treatment of sulfur-laden wastewaters, cleaning biogas and recovering sulfur as macro-nutrient for land application in areas with severe sulfur deficiency due to clean coal technology (David et al., 2016; Kanjanarong et al., 2016). This study also highlights the effects of H_2S removal on anaerobic process performance and process microbiology, especially MPA and SRB diversity and abundance.

We exploited scanning electron microscopy (SEM), Fourier transform infrared (FTIR) and x-ray diffraction (XRD) to demonstrate the mechanisms of H_2S adsorption on biochar. Additionally, the microbial community structure was determined using 16S rRNA gene sequence analysis to quantify MPA and SRB diversity and abundance within the reactors through the different concentrations of sulfate before and after biochar treatment.

1.2 Objectives

Biochar will be highly effective in alleviating sulfide toxicity to MPA and thus increase the relative abundance of methanogens in the system which favorably affects the efficiency of the treatment performance. Based on this rationale, the goal of this study was to develop a single-stage anaerobic system to treat high sulfate wastewater with simultaneous removal of H_2S using biochar. The specific objectives of this research include the following:

- Compare the performance of single-fed and multi-fed reactors for anaerobic treatment of high-rate sulfate-laden wastewater.
- Investigate the use of biochar produced from different feedstocks at different conditions, as an efficient and cost-effective material to remove H_2S from biogas produced in the anaerobic treatment of industrial sulfate-laden wastewater.
- Investigate the mechanisms of H_2S removal by biochars and the subsequent effect on microbial communities diversity and abundance due to alleviation of sulfide toxicity in AD

1.3 Scope of the Study

This scope of this research study is illustrated in Figure 1.1. Four continuous stirred tank reactors (CSTR) were used in this study. Synthetic wastewater with glucose as carbon source and potassium sulfate as sulfate source with all essential trace metal elements and nutrients was fed to all reactors. Softwood and hardwood wastes were used to produce biochars at 550 ^{o}C and 800 ^{o}C. A column packed with biochar was used in all reactors to test sulfide adsorption. All reactors were operated at the same time under steady state. Microbial ecology analysis was done in effluent samples during sulfate increments and after biochar treatment.

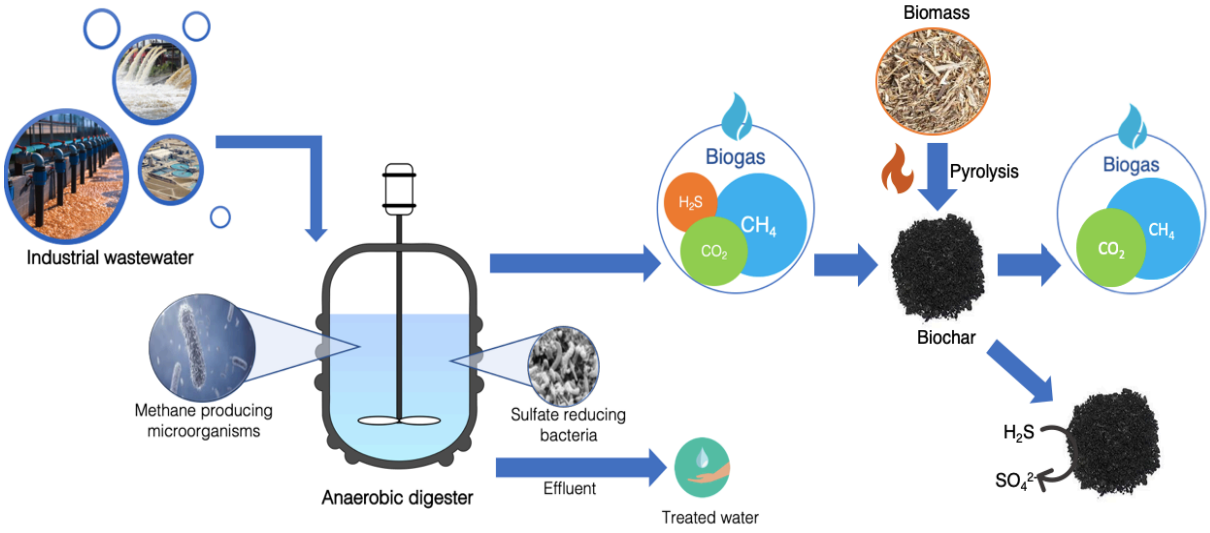

Figure 1.1: Scope of this study.

CHAPTER 2

LITERATURE REVIEW

2.1 High Strength Sulfate-Rich Industrial Wastewater

Industries such as distilleries, pharmaceuticals, food processing, and pulp and paper industries among others generate substantial amounts of sulfate-rich wastewater (100 – 15,000 mg S/L) (Table 2.1). Sulfate-rich wastewaters are produced through the use of sulfuric acid for extractions, bleaching, or pH control in the processes (Pol et al, 1998). Sulfate reduction to sulfide will therefore occur, which is highly undesirable since sulfide is corrosive, imposes toxicity to anaerobes methanogens in aqueous phase, which could lead to process failure and deters the quality of biogas as an energy resource (Khanal & Huang, 2003; Muyzer & Stams, 2008). Besides, depending on the chemical oxygen demand (COD) concentration, the wastewater can be classified as low or high strength sulfate wastewater (Table 2.1).

Table 2.1: Typical characteristics of high strength sulfate-rich industrial wastewater

Wastewater source	COD (mg/L)	Sulfate (mg/L)	References
Molasses Fermentation	55600	7520	(Sun et al., 2013)
Sea food processing	50000	2700	(Li & Khanal, 2016)
Potato-starch factory	37000	102	(Muniraj et al., 2013)

Tannery	56000	18800	(Chowdhary et al., 2017)
Distillery	110000	6500	(Fito et al., 2019)
Edible oil refinery	1,000-8,200	3,100-7,400	(Li & Khanal, 2016)
Pharmaceutical plant	28,540	14,800	(Li & Khanal, 2016)

2.1.2 High Strength Sulfate-Rich Industrial Wastewater Treatment

Industrial wastewater treatment refers to processes that treat or remove soluble organic matter, suspended solids, pathogenic organisms, and chemical contaminants, from wastewater prior to its reuse or discharge into waterbodies. These pollutants are removed from the wastewater using physical (sedimentation), chemical (chlorine disinfection) and biological processes. Anaerobic digestion (AD) is a widely adopted technology for treating high-strength industrial wastewaters with concomitant recovery of bioenergy in the form of biogas (Metcalf & Eddy, 1972).

2.1.3 Anaerobic Digestion of High Strength Sulfate-Rich Industrial Wastewater

AD is the biological degradation of organic matters in the absence of oxygen. It breaks down the organic matter and produces biogas [a mixture of methane (CH_4), carbon dioxide (CO_2), and hydrogen sulfide (H_2S)] (Li & Khanal, 2016). The organic matter degradation pathway is mediated by several groups of microorganisms involved in each

of the four main metabolic stages known as hydrolysis, acidogenesis, acetogenesis, and methanogenesis (Figure **2.1**).

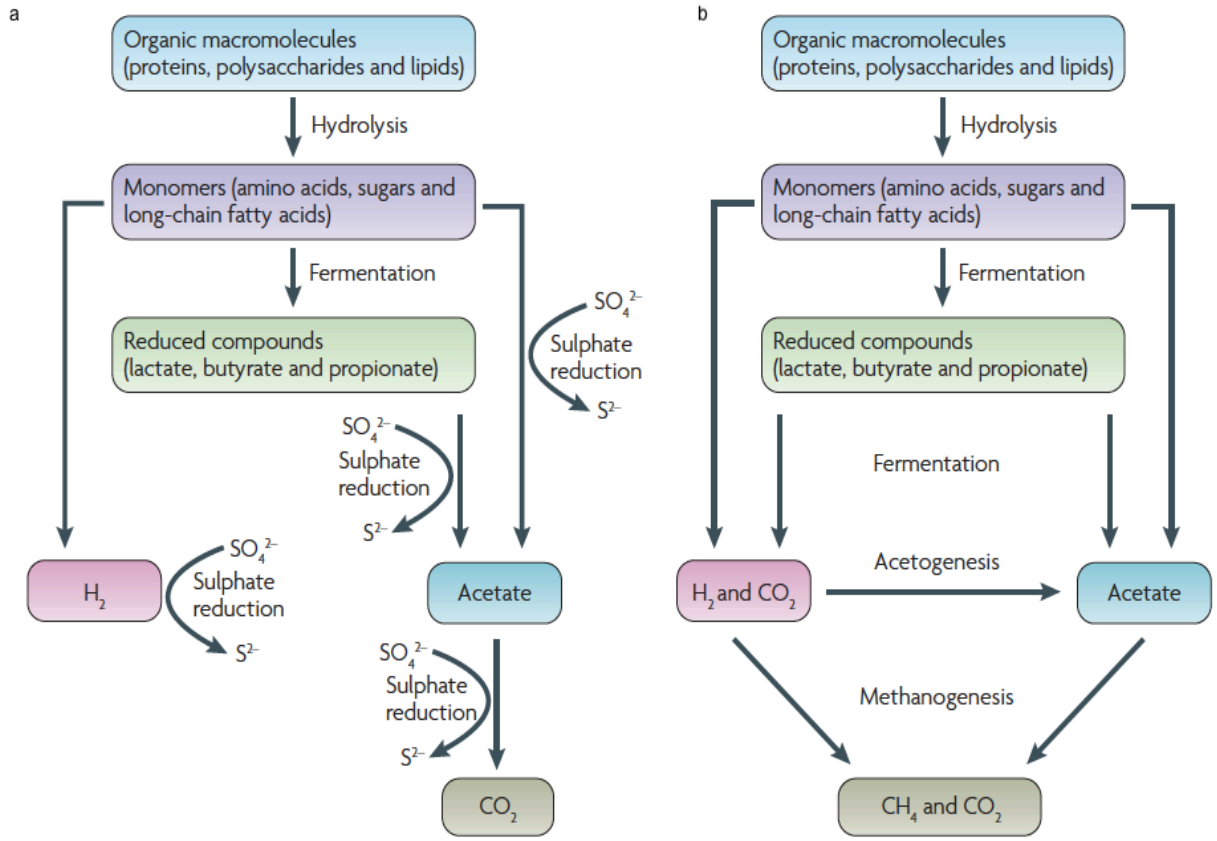

Figure 2.1: Biodegradation pathway of organic matter in (a) presence of sulfate and (b) absence of sulfate (Muyzer & Stams, 2008).

In hydrolysis, hydrolytic bacteria transform complex organic matter such as carbohydrates, proteins, and fats to simple soluble products such as sugars, amino acids, and long chain fatty acids (e.g., cellulose and starch are hydrolyzed into glucose by

Clostridium and *Bacillus*, respectively). Fermentative bacteria (e.g., *Pseudomonas, Bacillus, and Clostridium*) is responsible for the conversion of the soluble products from hydrolysis to volatile fatty acids, H_2, and CO_2 during acidogenesis (Barton & Fauque, 2009; Muyzer & Stams, 2008). Further in acetogenesis, the acetogenic bacteria or syntrophs (e.g., *Syntrophomonas* and *Syntrophobacter*) convert volatile fatty acids, such as propionate, butyrate, and valerate into acetate, CO_2 and H_2. Methane is produced by archaea, methanogens, either through splitting of acetate to CH_4 and CO_2 by acetoclastic methanogens or reduction of CO_2 with H_2 by hydrogenotrophic methanogens. However, the bacteria and archaea are not working separately but synergistically interact with each other to create an interrelated microbial ecology in AD processes (Barton & Fauque, 2009; Muyzer & Stams, 2008)

Sulfate reducing bacteria (SRB) are also involved in the removal of organic matter in anaerobic systems. Dissimilatory sulfate reducing bacteria is a diverse group of chemolithotrophic bacteria that play an essential role in the global carbon and sulfur cycles(van den Brand et al., 2015). In an AD system, SRB utilize sulfate (SO_4^{2-}) as terminal electron acceptor reducing it to H_2S, in which acetate (CH_3COO^-) is used as an electron donor oxidizing it to CO_2 (Muyzer & Stams, 2008; Plugge et al., 2011). The pathways employed in the oxidation of acetate to CO_2 include the acetyl-CoA, as used by *Desulfobacterium, Desulfotomaculum, Desulfococcus*, and *Desulfobacca acetoxidans* or citric acid cycle as used by *Desulfobacter postgatei* (Muyzer & Stams, 2008). The process of dissimilatory sulfate reduction (Figure **2.2**) may occur in two steps, (1) Sulfate reduction requires input of energy in the form of ATP sulfurylase, that results in the formation of adenosine-phosphosulphate (APS) and pyrophosphate. APS is then reduced by the

enzyme APS reductase to form sulfite (SO_3^{2-}) and AMP (2) the dissimilatory sulfite reductase catalyses the reduction of sulfite to H_2S both in the presence of *Desulfovibrio* strain (Barton & Fauque, 2009; Muyzer & Stams, 2008; Plugge et al., 2011)

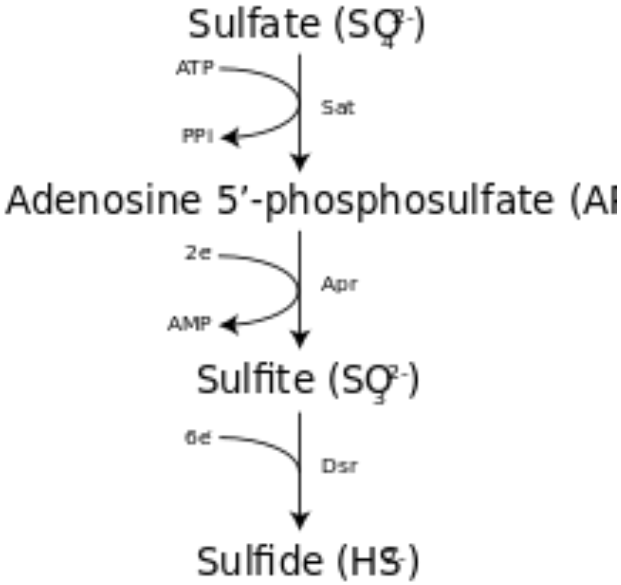

Figure 2.2: Dissimilatory sulfate reduction to sulfide pathway.

2.1.4 Sulfur Transformations

Microorganisms play fundamental role in sulfur transformations (Figure 2.3). The fate of sulfur in the environment has been studied extensively (Edwards, 1998; Muyzer & Stams, 2008; Plugge et al., 2011; Pokorna & Zabranska, 2015). Because sulfur has a broad range of oxidation states, from sulfide -2 (completely reduced) to sulfate +6 (completely oxidized), the interactions and reactions with the environment can follow biological and chemical pathways. SRB have important role in sulfur cycle, they use sulfate as terminal electron acceptor and produce hydrogen sulfide. Subsequently, hydrogen sulfide can be

oxidized to elemental sulfur or sulfate by chemolithotrophic sulfur-oxidizing bacteria (*Thiobacillus*) or phototrophic sulfur bacteria (*Chlorobium*). Sulfate reduction is governed by SRB (*Desulfovibrio* and *Desulfuromonas spp).*

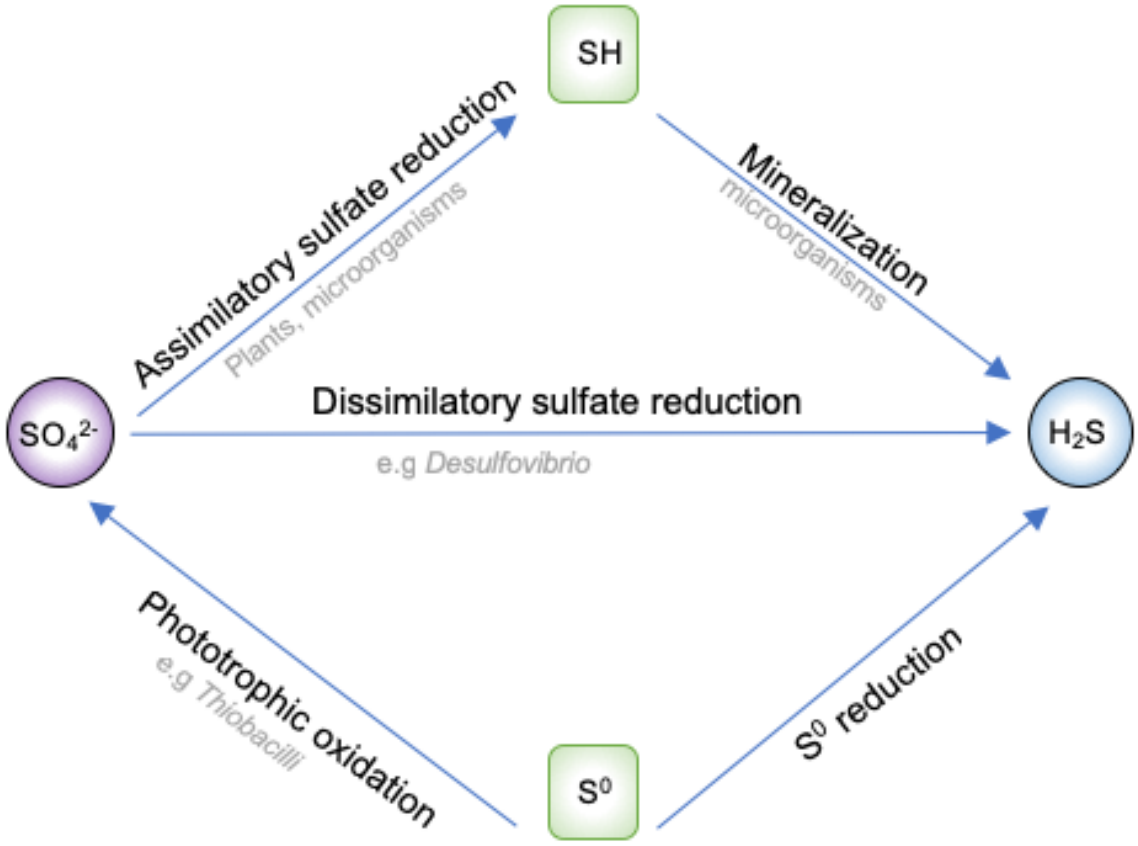

Figure 2.3: Sulfur transformations.

2.1.5 Limitations of Anaerobic Treatment of Sulfate-laden High-strength Industrial Wastewater

Anaerobic treatment of sulfate-rich effluents is challenging as it generates hydrogen sulfide due to dissimilatory sulfate reduction (Khanal & Huang, 2005). H_2S is a highly

corrosive gas and deters the quality of biogas as an energy resource. More importantly, sulfide, especially uninonized, H_2S in aqueous phase imposes toxicity to methane producing archaea (MPA) , which could lead to AD process failure (Khanal & Huang, 2003).

2.2 Interactions Between MPA and SRB

2.2.1 Synergism

SRB and methanogens co-exist in anaerobic systems. There is a syntrophic relationship between these two groups of microorganisms during the degradation of the organic matter. SRB can grow on propionate, lactate, ethanol, butyrate, H_2, and acetate; while methanogens utilize H_2, CO_2, and acetate (van den Brand et al., 2015).

2.2.2 Competition

In an environment rich in sulfate and low in redox potential (e.g., anaerobic treatment of sulfate-rich wastewater), there is a competition between MPA (*Methanosaeta* and *Methanosarcina* species) and SRB (*Desulfovibrio* and *Desulfomicrobium* species*)* for the common sources of electron (H_2 and acetate) and carbon (acetate) (van den Brand et al., 2015). With favorable thermodynamic and kinetic properties, SRB have capability to outcompete methanogens for common substrates in the presence of sulfate.

2.2.3 Factors Affecting the Competition Between MPA and SRB

2.2.3.1 Thermodynamics

The reduction of sulfate to sulfide yields more energy than methanogenesis as demonstrated from the Gibb's free energy change ($\Delta G^{o'}$) in Table 2.2.

Table 2.2. Thermodynamics of reactions mediated by SRB and methanogens (Thauer et al., 1977).

Equation	**$\Delta G^{o'}$ (kJ/reaction)**
Sulfate-reducing reactions	
$4\ H_2 + SO_4^{2-} + H^+ \rightarrow HS^- + 4\ H_2O$	-151.9
$Acetate^- + SO_4^{2-} \rightarrow 2HCO_3^- + HS^-$	-47.6
Methanogenesis reactions	
$4\ H_2 + 2HCO_3^- + H^+ \rightarrow CH_4 + 3\ H_2O$	-135.6
$Acetate^- + H_2O \rightarrow CH_4 + HCO3^-$	-31.0

2.2.3.2 Kinetics

In respect to kinetics (Table 2.3), SRB also demonstrate superiority over methanogens based on lower Ks (or higher affinity to substrate).

Table 2.3. Kinetic properties between SRB and methanogens (Khanal & Huang, 2005).

Substrate uptake	**K_s (mg/L)**
Sulfate-reducing bacteria	
Acetate	11.8
Hydrogen	0.002
Methanogens	
Acetate	177
Hydrogen	0.012

2.2.3.3 COD/SO_4^{2-} ratio

COD/SO_4^{2-} ratio also plays a crucial role in the competition for substrate. Following the stoichiometric equation,

$$8e + 8H^+ + SO_4^{2-} \rightarrow S^{2-} + 4H_2O \qquad (1)$$

the oxidation of COD is coupled to the reduction of sulfate, in a COD/SO_4^{2-} ratio of 0.67. This ratio theoretically implies that for a wastewater with COD/SO_4^{2-} ratio of 0.67, there is enough sulfate to accept electron to completely oxidize the organic matter - if sulfate is not the limiting substrate (Li & Khanal, 2016). While a ratio lower than 0.67 would need an external carbon source, a higher ratio would favor the growth of methanogens that uptake most of the available substrate. Therefore, studies report that optimal COD/SO_4^{2-} ratio for the success of anaerobic treatment range from 1 to 20. These diverse findings may be related to differences in the composition of the carbon source, sulfate concentration and other environmental factors.

2.2.3.4 pH

The maintenance of the system pH in the proper range (between 6.5 and 7.6) is required for an efficient anaerobic digestion. The pH is the controlling factor for dissociation of molecular aqueous form ($H_2S_{(aq)}$) into the gaseous form ($H_2S_{(g)}$), hydrogen sulfide ion (HS^-), and sulfide ion (S^{2-}) in wastewater (Yongsiri et al., 2004). The physicochemical transfers of H_2S in wastewater treatment plants can be expressed by the transfer of the H_2S dissociation is described to be a function of pH and Ka, where Ka is a function of temperature and conductivity (Figure 2.4). Moreover, with pKa=7.0 for this acid-base equilibrium, any variations in pH range significantly affect biogas production. As the pH

increases, the H_2S dissociates into its ions HS^- (bisulfide) and S^{2-} (sulfide), while under acidic conditions favor the amount of H_2S.

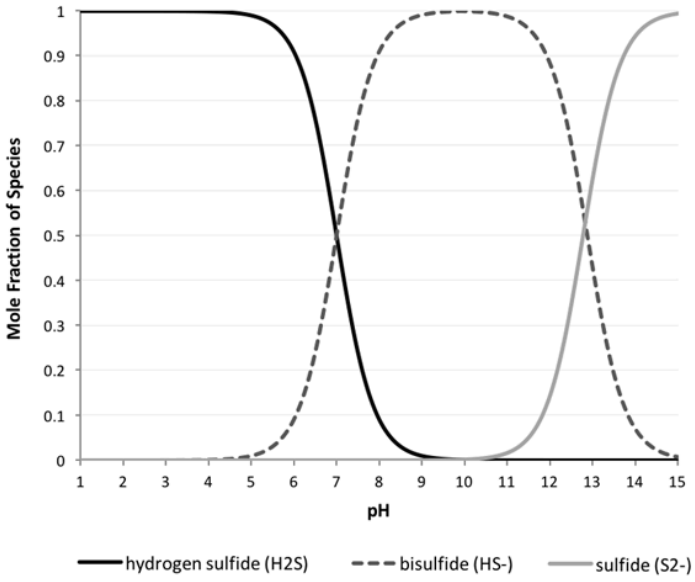

Figure 2.4: Sulfide solubility chart showing the molar fraction of each sulfide species at different pH; H_2S = hydrogen sulfide, HS^- = hydrosulfide, S^{2-} = sulfide.

The pH has relative impact in the bioactivities of SRB and MPA. The methanogens are more sensitive to lower pH ranges (pH < 7.0). Sulfate reducing bacteria are more resilient and have shown to support pH as low as 2 in habitats such as acid drainage sites and as high as 10 in soda lakes (Muyzer & Stams, 2008).

2.3 Sulfide Toxicity

Sulfide is toxic at higher concentrations for many microorganisms. The inhibitory effect of H_2S on several microorganisms can result in serious issues in an AD process such as reduction of methane yield, malodor, and corrosion (Liu et al., 2015). Moreover, a decrease in the efficiency of reactor performance can lead to complete process failure.

2.4 Eliminating Sulfide Toxicity

2.4.1 Methods of Sulfate Removal

The available technologies to remove H_2S in AD processes include absorption into a liquid either water or caustic solution; adsorption on iron oxide based materials, activated carbon or impregnated activated carbon and biological conversion by which sulfide oxidizing microorganisms convert sulfur compounds into elemental sulfur by with addition of air/oxygen (Liu et al., 2015). However, these strategies are expensive, include the addition of chemicals, slow, and can cause the reduction of the microbial activity within the bioreactor. Moreover, those methods do not provide an opportunity for recovery of sulfur as a valuable resource.

2.4.1.1 Biological Methods

Microorganisms have been used to remove H_2S from biogas. Chemotrophic bacterial species (*Thiobacillus* genus) are commonly used. They utilize CO_2 as carbon source and chemical energy from the oxidation of H_2S. Biofilters and Biotrickling filters are used for immobilization of sulfate oxidizing bacteria (SOB) to oxidize H_2S to elemental sulfur.

2.4.1.2 Chemical Methods

Chemical oxidants are the most often used method to control H_2S. A variety of different liquid solvents have been applied to absorb H_2S from biogas such as sodium hydroxide (NaOH) and sodium hypoclorite (NaOCl). The oxidants are continuously used in the process and to avoid salt precipitation, the scrubber solution is frequently replenished. Moreover, the spent caustic used must be carefully disposed and they are not regenerable.

2.4.1.3 Physicochemical Methods

a. Absorption

i. Water Scrubbing

Water scrubbing is used to dissolve H_2S and later remove it by reducing the pressure. Since water is widely available and low-cost, this method can be easy to operate. However, losses of product as high as 10% have been reported due to the pressure changes necessary to remove the H_2S from the water.

ii. Alkanolamines

Alkanolamines such as monoethanolamine (MEA) and diethanolamine (DEA) are water soluble and have great capacity to absorb acid gases. Amine groups are able to absorb the H_2S and dissolve it in an amine stream. Part of this amine is lost or dissolved along the H_2S and it is expensive and energy intensive to regenerate the solution.

b. Adsorption

Adsorption material can attract gaseous molecules to its surface until they saturate. Depending on the gas molecule and the reactivity of the adsorbent surface, the bonding between the gas molecule and the surface can be either physical (physisorption) or

chemical (chemisorption). Physisorption (reversible adsorption) is characterized by weak van der Waals forces with binding energy below 0.25 eV while chemisorption (irreversible adsorption) binding energy can reach 1 eV. H_2S if firstly removed by physical adsorption onto the water film in the surface of the adsorbent and further dissociates to HS^-. Reactions with metal oxides, alkaline species and surface functional groups give redox reactions products. Regeneration methods can be costly and time consuming.

i. Metal Oxides

Metal oxides are often used for H_2S removal. It involves the formation of insoluble iron sulfides “iron sponges” in the forms of Fe_2O_3 and Fe_3O_4. Although the efficiency is approximately 85%, this method is chemical intensive and costly. Zinc oxide, calcium oxide and magnesium oxide have also been tested for H_2S removal but showed problems with low separation efficiency, low selectivity, high cost and low sorption/desorption rates.

ii. Zeolites

Commonly referred to as molecular sieves, they are a highly porous hydrated aluminosilicates material used for H_2S removal. They are very effective to remove polar compounds (H_2S) from non-polar gas streams (CH_4) by ion exchange.

iii. Activated Carbon

Due to high surface area, porosity and surface chemistry, activated carbon is often used for removal of H_2S from biogas. The impregnation of strong bases such as sodium hydroxide (NaOH) or potassium hydroxide (KOH) to act as catalyst, remove H_2S at a higher rate than un-impregnated activated carbons. Much research has focused on this method of H_2S removal, and although it can be effective, the addition of caustic lowers the ignition temperature and therefore the material can self-ignite and there is a high cost for regeneration of the material.

iv. Biochar

Numerous studies reported the use of biochar, a carbonaceous by-product of the thermal treatment of biomass (e.g., pyrolysis) under O_2-limited conditions, for effective H_2S removal from biogas (>98%) via sorption and chemical bonding with surface radical groups such as COOH and OH (Kanjanarong et al., 2017; Sethupathi et al., 2017; Shang et al., 2013; Xu et al., 2014). Preliminary studies in our lab showed that an AD system with an integrated column packed with biochar for biogas recirculation is an effective method to adsorb H_2S from biogas and it is influenced by biochar pH, surface area, porosity and moisture content which are mainly governed by biochar production conditions such as pyrolysis temperature, residence time, and feedstock types (Kanjanarong et al., 2017;Oliveira et al., 2017). Systems that add biochar into the

anaerobic reactor were reported to result in failure of the treatment due to high particulate matter that clogged the pipes and accumulated VFAs.

2.5 Biochar Production

Biochar is the solid product derived from the pyrolysis of waste biomass in the absence of oxygen (Lu et al., 2014a), however, several factors should be considered when determining biochar application, such as the desired biochar characteristics, sustainability requirements, possible toxicity of the biochar and end use. Consequently, the characteristics of any biochar depend on the type of feedstock, thermochemical treatment, production temperature, production residence time, heating rate and oxygen level during production (Windeatt et al., 2014). Achieving the highest biochar yield from the raw material for improving soil productivity and sequestering atmospheric carbon is a very important criteria during biochar production.

2.5.1 Feedstock Selection

Naturally, biomass is composed of cellulose, hemicellulose and lignin. Cellulose and lignin undergo thermal degradation at temperatures ranging between 240-350ºC and 280-500ºC, respectively (Kambo & Dutta, 2015). The proportion of each component determines the amount of the biomass structure that is retained during pyrolysis, at any given temperature. Pyrolysis of wood-based feedstock produces rougher and more

resistant biochars with carbon contents of up to 80%, as the rigid ligninolytic nature of the source material is retained in the biochar residue (Agriculture, 2007). Palm shell biomass has high lignin content as shown in Table **2.4** and therefore, produce high biochar yields, given the stability of lignin to thermal degradation, as revealed by (Demirbas, 2004). Carbon content correlates with the typical lignocellulosic composition and ash content. Corn stover feedstock has high ash content at 135 g kg-1 and low lignin content while the palm shell having low ash content (20 g kg 1) and the highest lignin content for plant feedstock. The same comparison can be made on animal manure feedstock, where chicken waste has higher ash content at 287 g kg-1 and its lignin content is low whereas cattle manure ash content is the lowest (130 g kg-1) and high lignin content. Elemental and ultimate analysis of plant and animal biomass to produce biochar are shown in Table 2.5.

Table 2.4: Typical cellulose, hemicellulose and lignin content of raw feedstocks.

	Cellulose (%)	Hemicellulose (%)	Lignin (%)	References
		Plant feedstock		
Palm Shell	30	18	53	(Windeatt et al., 2014)
Sugar cane bagasse	39	26	24	
Rice husk	38	18	22	
Coconut shell	20	49	30	
Cotton stalk	35	39	21	
Olive pomace	34	15	20	
Wheat straw	35	25	19	(Bruun, et al., 2012)
Corn stover	38	26	19	(Lee et al. , 2007)
		Animal feedstock		
Chicken litter	8	18	5	(Champagne, 2007)
Swine waste	13.5	20.9	5.4	(Chen et al., 2003)
Poultry waste	11	20.2	8.5	
Cattle waste	23	18	19	(Tu et al., 2008)

Table 2.5: Elemental and ultimate analysis of plant and animal feedstocks to produce biochar.

Feedstock	C (%)	H (%)	N (%)	S (%)	O (%)	O/C	Moisture (%)	Volatiles (%)	Fixed carbon (%)	Ash (%)	Reference
Plant feedstock											
Palm shell	53.1	7.1	0.7	0.0	46.8	0.88	3.0	74.1	25.9	2.0	(Windeatt et al., 2014)
Sugarcane bagasse	45.9	6.7	0.9	0.2	59.2	1.3	5.8	85.3	14.7	4.4	
Rice husk	42.5	6.5	1.3	0.0	46.0	1.1	5.7	80.9	19.1	19.6	
Coconut shell	52.6	6.2	2.0	0.0	53.1	1.1	5.7	77.2	22.8	0.6	
Cotton Stalk	46.0	7.6	5.6	0.0	54.5	1.2	6.1	93.1	6.9	4.2	
Olive pomace	49.2	6.8	2.0	0.0	45.8	0.9	5.7	80.5	19.5	4.5	
Wheat straw	43.7	5.6	0.9	0.0	43.9	1.0	5.6	85.9	14.1	7.9	(Bruun et al., 2012)
Corn stover	40.5	6.1	0.7	0.0	38.7	0.7	3.7	72.6	10.2	13.5	(Brewer et al., 2012)
Animal biomass											
Chicken litter	33.6	4.2	5.6	0.5	27.4	0.8	11.4	57.8	6	28.7	(Lin et al., 2013)

Swine waste	30	5.4	3.8	0.6	7.0	0.2	75.4	73.9	70	26.2	(Wang et al., 2015)
Poultry waste	43	6.6	5.7	1.2	6	0.1	20.1	54.3	3.3	11.5	(Acharya et al., 2014)
Cattle	42	5.6	1.7	0.4	50	1.2	86.7	71.4	71	13	(Tu et al., 2008; Wang et al., 2015)

2.5.2 Thermochemical Treatments

Different thermochemical pre-treatments of feedstock are available to produce efficient energy biochar and due to short reaction time and high conversion efficiency they are preferred over biological pre-treatments (Kambo & Dutta, 2015). The techniques available comprise slow or fast pyrolysis, gasification, torrefaction and HTC and different yields are produced and reported in **Table 2.6** (Cox et al., 2012; Kambo & Dutta, 2015). Pyrolysis is the optimized process where the main goal is to produce an agronomically advantageous biochar product with no adverse environmental outcomes (Cox et al., 2012). During the pyrolysis process, lignin, cellulose, fats and starches are thermally broken down into three different fractions: biochar (solid fraction), bio-oil (a volatile matter which can further be partially condensed to liquid phase), and non-condensable gases (CO, CO_2, CH_4, and H_2) (Suliman et al., 2016). Pyrolysis temperature significantly affected biochar properties. Previous studies indicate that when the pyrolysis temperature

is increased from 100°C to 500°C, there is an increase in breakthrough time, carbon content and surface area of biochar (Shang et al., 2013). Additionally, increasing pyrolysis temperature produces biochar with higher aromaticity (less hydrophilic), which is recalcitrant to decomposition. The large variety of feedstock and thermochemical reactions makes the mechanisms of biomass pyrolysis very complex.

Table 2.6: Biochar yields obtained from different thermochemical processes.

Thermochemical process	Temperature (°C)	Residence time	Heating rate	Bio-oil (%)	Syngas (%)	Biochar (%)	References
Slow pyrolysis	~300-650	5 min-12h	10-30 °C/min	30	35	35	(Kambo & Dutta, 2015)
Fast pyrolysis	~500	5-10s	over 300 °C/min	75	13	12	(Ahmad et al., 2014)
Torrefaction	~290	30 min-4 h	10-15 °C/min	0-5	20	80	(Kolk et al., 2013)
Gasification	~750-900	10-20s	50-100 °C/s	5	85	10	(Brewer et al., 2012)
HTC	~180-260	5 min-12 h	5-10 °C/min	25	5	70	(Kim et al., 2015)
Microwave assisted-pyrolysis	300-500	5 min -12 hours	n/a	20	60	20	(Spokas et al., 2012)

2.5.2.1 Slow Pyrolysis

Slow pyrolysis (~300-650 °C in the absence of oxygen) is the most feasible method for high quality biochar and it results in a hydrophobic material with a high surface area, having both positively and negatively charged surfaces that promote adsorption (Sohi, 2009). Slow pyrolysis is characterized by relatively long residence time (from 5 minutes to 12 hours) and low heating rates (10-30 °C/min), which favors high solid product yield (25-35%) (Bruun et al., 2012). This reaction is endothermic and the biochar has a residual energy content of about 30–35MJ kg-1) (Sohi, 2009). Slow pyrolysis often takes place in continuous reactors such as drum pyrolysers, rotary kilns, or screw pyrolysers and is considered as an optimized process to produce biochar without adverse environmental outcomes, inexpensive, uses distinct feedstock's, and consuming less energy (Bruun et al., 2012; Laird et al., 2011). Nevertheless, pyrolysis is the optimized process, where the main goal is to produce an agronomically advantageous biochar product with no adverse environmental outcomes (Oliveira et al., 2017).

2.5.2.2 Fast Pyrolysis

In fast pyrolysis, small-grained organic material is heated (~450 - 600 °C) and exposed to heat transfer for just a few milliseconds to seconds producing 10 to 30% biochars on a weight basis. These biochars contain 15 to 40% of the carbon and nearly all the mineral (ash) content of the original biomass (Brewer et al., 2012; Bruun et al., 2012). The calorific

value of obtained biochar is between 23– 32 MJ kg-1 (Sohi, 2009). Fast pyrolysis biochar has more negatively charged binding sites and tend to be more hydrophilic (Mitchell, Subbiah, Ullman, Frear, & Call, 2015). Low temperatures or large feedstock particles may result in an incomplete pyrolyzed biomass thus, lowering the potential for carbon sequestration in soil affecting its performance (Bruun et al., 2012). Furthermore, fast pyrolysis is optimized to produce bio-oil, which can be upgraded to high-value liquid transportation fuels or processed into a variety of organic chemicals (Lehmann & Joseph, 2015).

2.5.2.3 Torrefaction

Torrefaction is the pretreatment of biomass at temperatures between 200–300 °C with a residence time ranging from 10 min to 2 h, in the absence or low concentration, of oxygen. Approximately, 30% of mass is lost with only 10% of the energy contained within the biomass is lost in the form of gases (Kambo & Dutta, 2015). However, due to the content of raw biomass that is not totally carbonized, the final product may contain some volatile organic compounds and pollutants such as polycyclic aromatic hydrocarbons (PAHs), furans and dioxins, and therefore, the International Biochar Initiative considers it as a charcoal and not biochar (Tumuluru et al., 2011). This charcoal from torrefaction of corn stover for example, has 35 times more PAHs (18 mg/kg) than the corn stover biochar produced through slow pyrolysis between 400 and 600 °C (0.41 mg/kg), which may exert further phytotoxic effects (Tumuluru et al., 2011).

2.5.2.4 Gasification

Gasification is another thermochemical method for biomass conversion to gaseous products at higher temperatures (900 °C) in the presence of limited oxygen and sometimes at high pressures of 15–50 bars (Sohi, 2009). This process is designed to maximize the production of synthesis gas (CO and H_2) and thus the solid product from gasification is not regarded as an ideal biochar. This is because, either the solid yield is very low or the solid does not have the required properties to be classified as biochar according the International Biochar Initiative (IBI). Although little or no biochar is produced through gasification, the biomass is completely converted to CO, H_2, CO_2 and ash (Kambo & Dutta, 2015; Sohi, 2009).

2.5.2.5 Hydrothermal Carbonization (HTC)

Hydrothermal carbonization treats biomass with hot compressed water instead of drying for hours at 180-260°C under pressure to produce a carbon-rich solid material. These materials tend to be best suited for energy purposes since it eliminates the pre-drying process that requires large amounts of energy (Liu & Balasubramanian, 2012). The behavior of hydrochar in respect to combustion was distinct from raw biomass with increased maximum weight loss rate, high ignition temperature and broad combustion ranges at higher temperatures. Nevertheless, limited evidence on the effect of the

aforementioned parameters for the HTC processing of biomass is available and it seems to be challenging to adapt this process to an industrial scale (Kambo & Dutta, 2015).

2.5.2.6 Microwave Assisted-pyrolysis

Microwave-assisted pyrolysis has been explored as a sustainable method to improve the quality of bio-oil, biochar and syngas using different biomass (Budarin et al., 2009; Lin et al., 2013). It is reported that biochar produced from microwave-assisted pyrolysis has higher surface area and pore volume than that from the conventional thermochemical processes. In addition, it is rapid, selective, provides uniform heating, resulting in improved physical and mechanical properties (Budarin et al., 2009; Mohamed et al., 2016). The maximum temperature recorded for pure switch grass was about 159 °C after ~30 min of microwave irradiation, which is well below the desired pyrolysis temperature (Mohamed et al., 2016). Due to the poor absorption of microwaves by dry biomass, it may be necessary to add absorbers or catalysts to increase the microwave absorption rate, and consequently accelerate the heating rate to achieve pyrolysis temperatures (Budarin et al., 2009). The addition of K_3PO_4 (catalyst) showed a great potential for accelerating microwave heating reaching 400°C after 2.8 min, compared with 28.8 min through conventional heating. This improved the biochar qualities with an increase in surface area from 0.33m^2/g to 76.3m^2/g (Mohamed et al., 2016).

2.5.3 Physicochemical Properties

Pyrolysis conditions as residence time, heat transfer rate, particle size (the smaller the particle size, the shorter the time for sorption equilibrium to be attained and more rapid mass transfer of contaminants to micropore sites (Webber et al., 2013) and feedstock types are key parameters for the physico-chemical characterization of the biochar and its applications (Cayuela et al., 2014).

2.5.3.1 Elemental Analysis

During the pyrolysis of the biomass, oxygen and hydrogen are removed as CO, CO_2, H_2O and other O- and H-containing volatiles, concentrating the carbon and consequently reducing O/C and H/C ratios (Brewer et al., 2012). The atomic ratios of H/C and O/C are correlated with the aromaticity, resistance to microbial and chemical degradation (Crombie et al., 2013) and polarity of biochar. High temperature biochars shows low H/C and O/C ratios compared to biochars produced at low temperatures, indicating a gradual growth in aromaticity (Suliman et al., 2016). Typically, lignocellulosic feedstocks consist of carbohydrates and results in O/C ratios close to 0.4. The molar H/C ratio indicates the degree of carbonization and therefore the stability of the biochar. H/C with values exceeding 0.7 are an indication of non-pyrolytic or pyrolysis deficiencies (IBI, 2013).
Van Krevelen diagram is used to confirm the importance of dehydration (loss of O and H as H_2O) and carbonization reactions during pyrolysis. The rates of decarboxylation (loss

of CO_2 and/or CO) and demethylation (loss of CH_3) indicated by a reduction of O/C and H/C ratio respectively are dependent upon the feedstock source and the pyrolysis temperature (Suliman et al., 2016). H/C and O/C ratios decrease in biochars when compared with their feedstocks due to the removal of H and O during pyrolysis suggesting an increase in the aromatic structure, potential stability of the biochar and the recalcitrance of carbon (Oliveira et al., 2017). Therefore, at high pyrolysis temperatures, woody and herbaceous biomass usually provides a more carbon-rich biochar, compared to other feedstocks such as sewage sludge and animal manures (Gul et al., 2015; Novak et al., 2016). Additionally, 50% of the original carbon content is retained in the biochar, which offers a significant opportunity for creating such a carbon sink (Cox et al., 2012).

2.5.3.2 Oxygen Surface Groups

Oxygen functional groups on biochar surface have large effects on the catalytic and adsorptive properties of H_2S. The chemical structures and respective temperature of decomposition of some functional groups are showed in Figure 2.5.

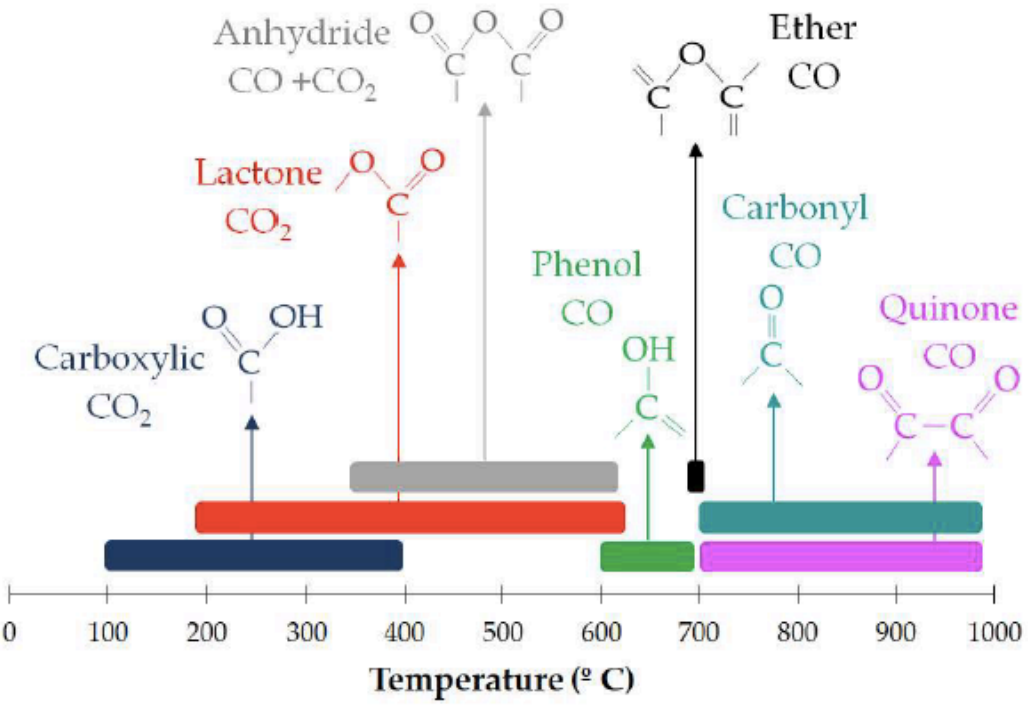

Figure 2.5: Surface oxygen groups on carbons and their approximate decomposition temperature.

2.5.3.2 Surface Area

Highest temperature achieved during pyrolysis leads to an increase in the surface area of biochar which makes it more adsorptive for chemical reactions. However, when combined with a feedstock that has an inorganic component the surface area of the biochar is reduced (Cox et al., 2012). At lower temperatures (300–400°C) there is a partially carbonization of the biomass that results in a biochar with smaller pores and lower surface area (Cox et al., 2012; Lu et al., 2014b). Higher surface area provides a

greater number of adsorption sites for H_2S, thereby increasing the adsorption capacity of biochar (Bagreev, Bandosz, & Locke, 2001).

2.5.3.3 Porosity

Biochar pore size distribution, defined by its surface area, includes nano-pores (<0.9 nm), micro-pores (<2 nm) to macro-pores (>50 nm) (Atkinson et al., 2010). Macro-pores act in function in soil, as for aeration and hydrology and provide a habitat niche for microbes, the larger the pores, the easier water, plant roots and fungal hyphae can penetrate the particle. Micro-pores are considered important for adsorption applications. The porous can also work as a protection for some favorable organisms such as mycorrhizae and bacteria and will have essential effects on its nutrient retention capacity by surface binding of both cations and anions to its surfaces (Liang et al., 2006). Pore size distribution in biochar can be measured by sorptometry that applies micropore analysis by carbon dioxide and meso-pore analysis by nitrogen and by mercury porosimetry, which measures the pores in the macro and meso-pore range and calculates the pore size based on the pressure required to push mercury into the pore (Brewer et al., 2012). Most biochars have a highly porous structure with great adsorptive capabilities and contain several functional groups that are effective in the adsorption of metals when produced at temperatures above 600°C (Lu et al., 2014). The enhanced porosity structure is due to the volatilization of tars and impurities that obstruct the pores and reduce the connectivity.

2.5.3.4 pH

Biochar surface may present hydrophilic, hydrophobic, acidic and basic properties, all of which contribute to their capability to react with soil solution substances. At a higher pH, the carboxylic acids (-COOH) and hydroxyls (-OH) give up protons and become negatively charged (-COO- and -O-, respectively) (Figure 2.6). At low pH, the same groups can accept a proton, hence, the carbon portion of the biochar behaves as a weak acid and buffers the pH of the system. Furthermore, the negatively charged surface functional groups might attract positively charged cations and consequently contribute to the cation exchange capacity (Brewer et al., 2012).

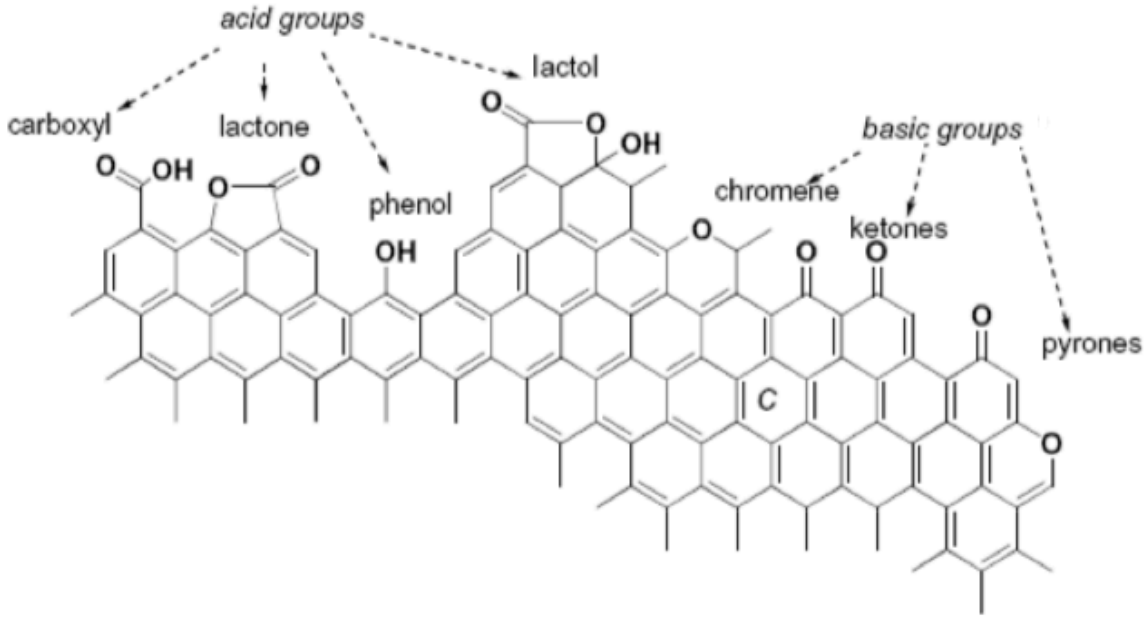

Figure 2.6: Main functional groups on biochar surface (Brennan et al., 2001).

2.5.4 Environmental Applications

An increasing interest in the beneficial application of biochar has opened up a broad spectrum in research development. Using waste biomass for the production of biochar is a reasonable option because such types of feedstock do not have any economic value and moreover do not compete with the food crops for land requirement. Soil amendment with biochar is evaluated globally as a means to improve fertility, plant production and mitigation of climate change (Ahmad et al., 2014; Cayuela et al., 2014). In addition, biochar can be used as a low-cost adsorbent to remove contaminants from wastewater and gaseous streams (Inyang et al., 2012).

2.5.4.1 Removal of Pollutants from Water, Soil and Gaseous Streams

Biochar has wider environmental applications due to its distinctive characteristics, e.g., high adsorption capacity, high specific surface area, microporosity, and ion exchange capacity (Oliveira et al., 2017). Biochar has been applied for the removal of organic and inorganic pollutants from soil, aqueous, and gaseous media. The removal mechanisms are often governed by the interactions of these pollutants with various attributes of biochar. For organic pollutants, the removal is primarily via chemisorption (electrophilic interaction) and physisorption (e.g., pore diffusion, hydrophobic, electrostatic attraction/repulsion via π-π electron donor-acceptor, and H-bonding) through COOH, OH, and R-OH functional groups (Oliveira et al., 2017). Moreover, other mechanisms including partitioning (in non-carbonized phase due to the reduction of substrate polarity), chemical

transformation (via reductive reactions or electrical conductivity) and biodegradation (by diverse microorganisms present on the surface and in the micro-pores of biochar) (Oliveira et al., 2017).

The heavy metals removal mechanisms include ion exchange, surface complexation, precipitation and cationic and anionic interactions between metal ions and active functional groups (COOH, R-OH and OH) on the biochar surface (Ahmad et al., 2014). The variability and predominance of a specific reaction are controlled by specific physiochemical properties of the biochar, which is attributed to feedstock types and pyrolysis conditions used during its production. For example, biochar produced at high pyrolysis temperatures is relatively high in surface area, microporosity, and hydrophobicity (Ahmad et al., 2014); high carbon-to-nitrogen (C/N) ratio, high pH (Novak et al., 2016), and low dissolved organic carbon (Cantrell, Hunt, Uchimiya, Novak, & Ro, 2012); whereas biochar produced at low pyrolysis temperature consists of high dissolved organic carbon content, relatively low porosity, low C/N ratio, and high O-bearing functional groups (Ahmad et al., 2014). These variations in biochar characteristics also have significant implications on its suitability and efficacy in remediation of targeted pollutants.

2.5.4.2 Removal of H_2S from Gaseous Streams

Lower hydrophilicity of biochar helps to create a water film on the surface which in turn increases H_2S removal efficiency (Xu et al., 2014). When H_2S is adsorbed onto the moist

biochar (moisture content of about 80%), the dissociation of H_2S into HS^- and S^{2-} is enhanced in the water film under basic conditions (Kanjanarong et al., 2017a; Xu et al., 2014a). Higher surface area provides a greater number of adsorption sites for H_2S, thereby increasing the adsorption capacity of biochar (Bagreev et al., 2001).

Kinetic models allowed an estimation of sorption rates and rate expressions characteristic of possible reaction mechanisms. The pseudo-first-order and pseudo-second-order kinetic models were used to evaluate the capacity of biochar for H_2S removal through a series of breakthrough studies. It is reported that pseudo-second-order kinetic model (R^2 = 0.9998) is better at predicting the H_2S removal rate than pseudo-first-order model (R^2 = 0.7348) (Kanjanarong et al., 2017a). In pseudo-second-order kinetic model, the rate-limiting step is the surface adsorption that involves chemisorption, where the removal is due to physicochemical interactions between the two phases (Kanjanarong et al., 2017; Robati, 2013; Shang et al., 2013).

CHAPTER 3

MATERIALS AND METHODS

3.1 Anaerobic Digestion Experimental Set-up

3.1.1 Reactors

Four (R1, R2, R3 and R4) 5L working volume CSTR (Figure 3.1) reactors were fabricated on site. Mixing was provided by biogas recirculation through the bottom of each reactor using a diaphragm pump (Parker model L045B11) and a flow meter (Dwyer model 1115). Each reactor was set up differently for further efficiency performance comparison.

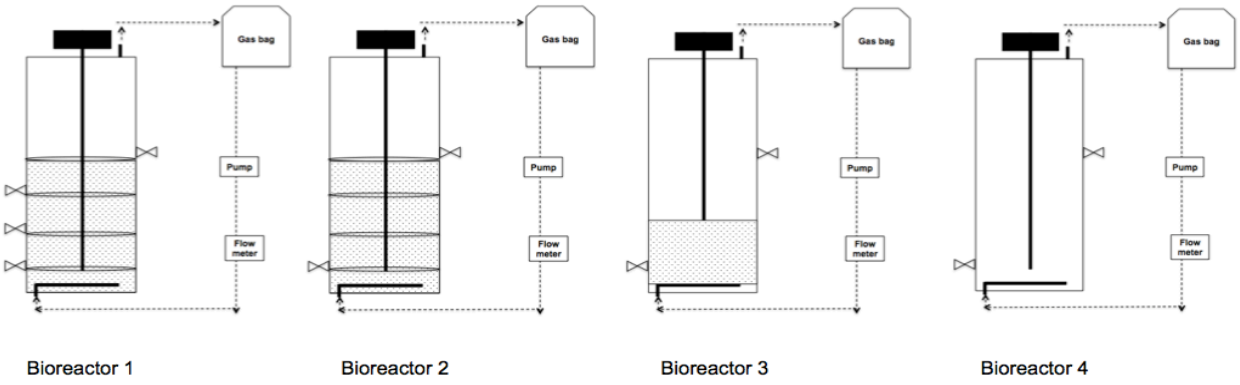

Figure 3.1 Schematic of the reactors set up. Reactor 1: Multi-fed, multiple compartments and with media. Reactor 2: Single-fed, multiple compartments and with media. Reactor

3: Single-fed, single compartment and with media. R4: Single-fed, single compartment and without media.

Reactor 1 (R1)

R1 (Figure 3.2) Consisted of four polypropylene perforated plates placed 12 cm apart from each other to maintain an evenly distribution of 300 g of media within the bioreactor height. Reactor was operated as a multi-fed system, with three influent feeding valves located along the lateral of the reactor to facilitate the homogeneity of the biomass.

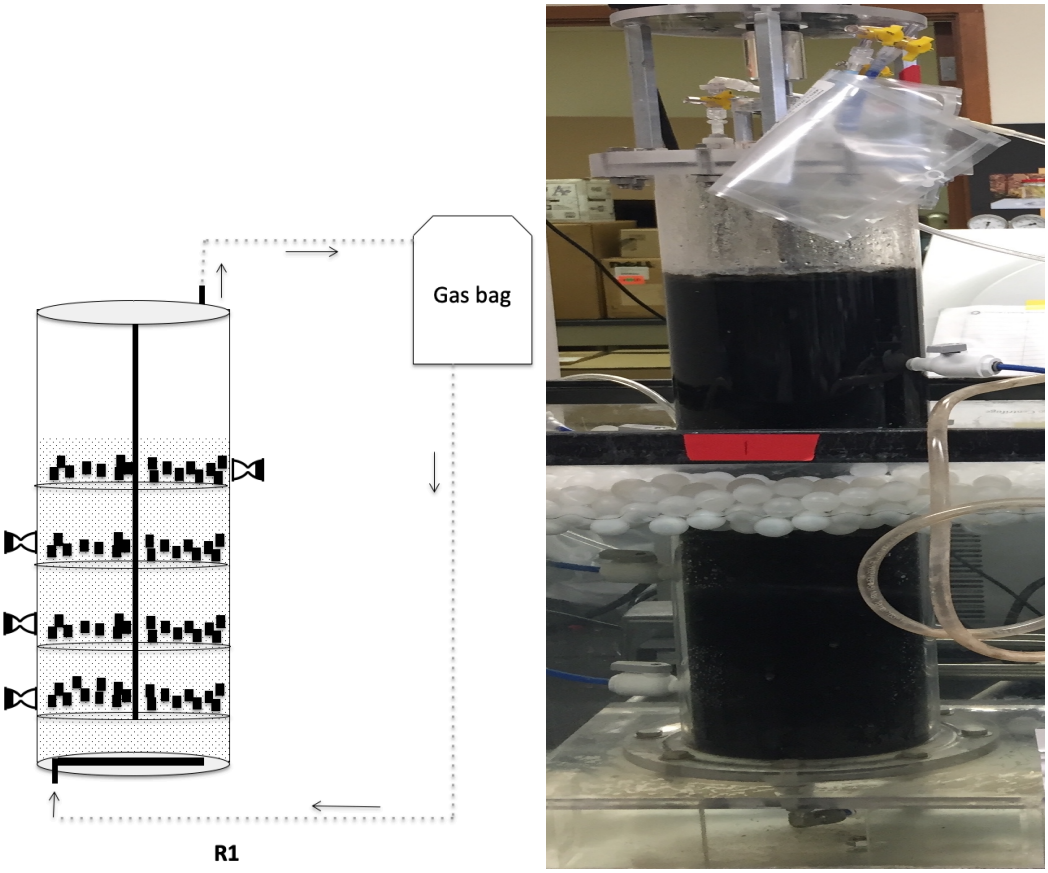

Figure 3.2: Reactor 1 schematics and picture.

Reactor 2 (R2)

R2 (Figure 3.3) consisted of four polypropylene perforated plates placed 12 cm apart from each other to maintain an evenly distribution of 300 g of media within the bioreactor height. Reactor was operated as a single-fed system, with one influent port was located at the bottom/lateral part of the reactor.

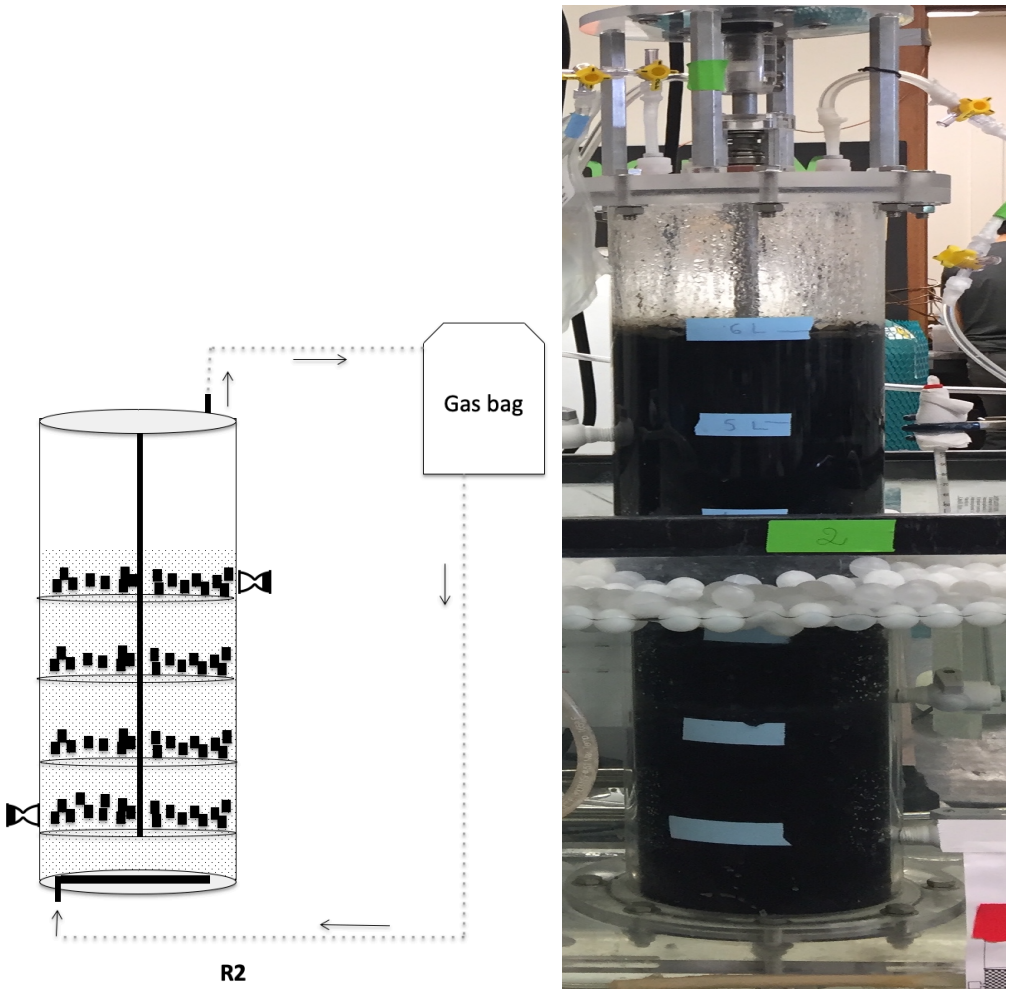

Figure 3.3: R2 schematics and picture.

Reactor 3 (R3)

R3 (Figure 3.4) did not have the perforated plates. Consist of 300 g of media deposited on the bottom of reactor. R3 was operated as a single-fed system with the influent port located at the bottom/lateral part of the reactor.

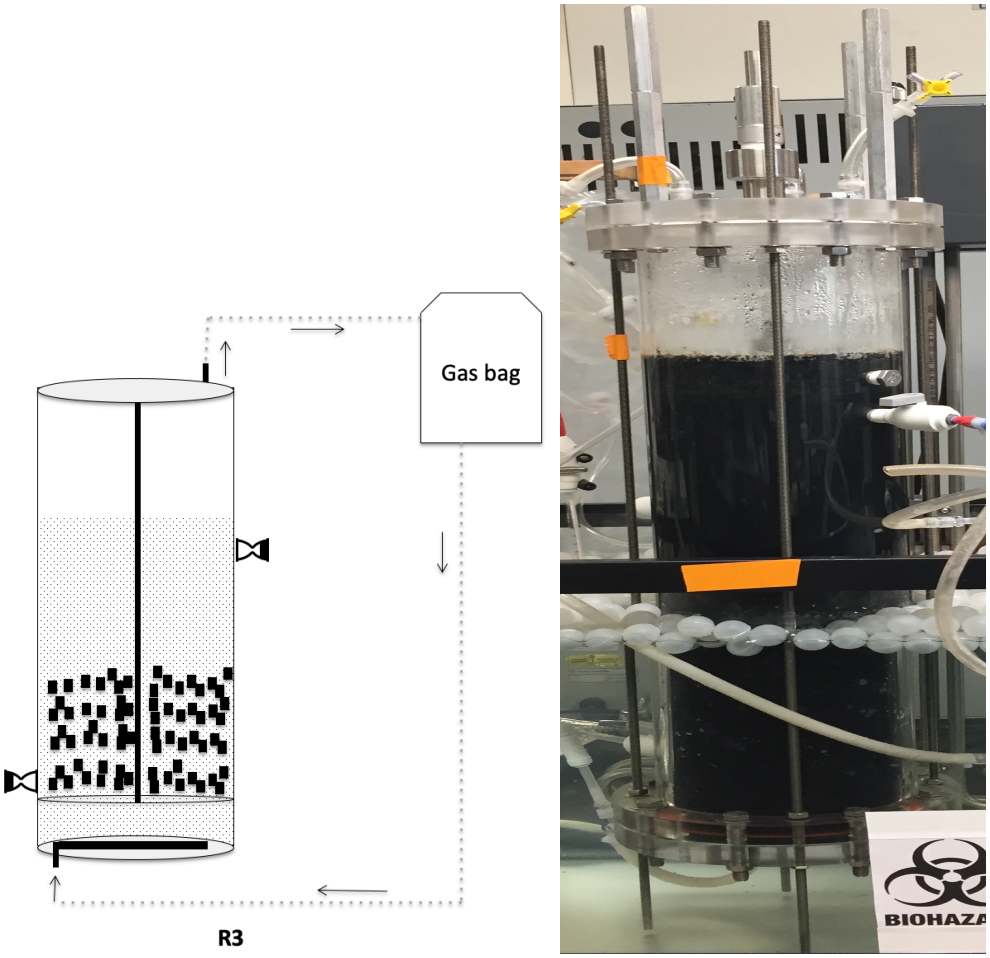

Figure 3.4: R3 schematics and picture.

Reactor 4 (R4)

R4 (Figure 3.5) was operated as single-fed system without media or plates. The influent port was located at the bottom/lateral part of the reactor.

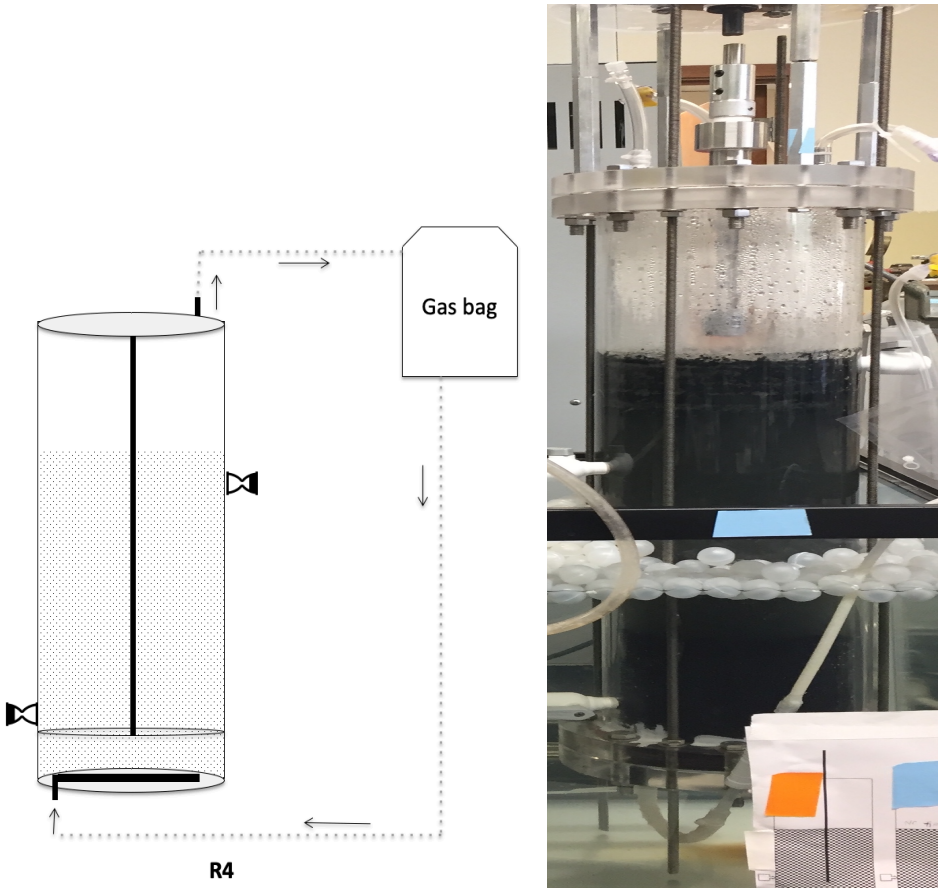

Figure 3.5: R4 schematics and picture.

3.1.2 Packing Media and Specifications

Polypropylene perforated plates (Figure 3.6) were displaced at 12 cm apart from each other. Used in R1 and R2 as means to disperse the media and provide a better homogeneity of biomass. Recycled tire beads (Figure 3.7) were used as packing media (~ 400 pieces) and the main features are presented in Table 3.1.

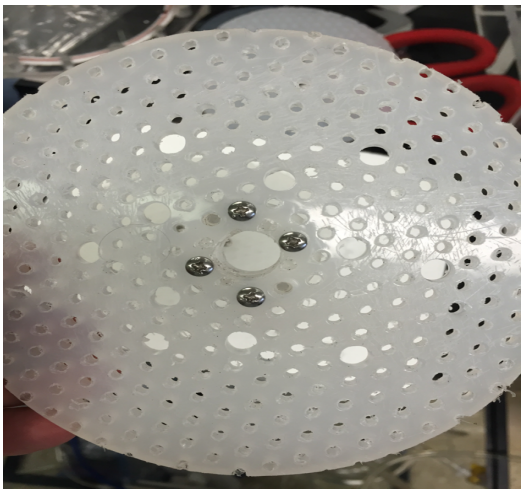

Figure 3.6: Polypropylene perforated plates.

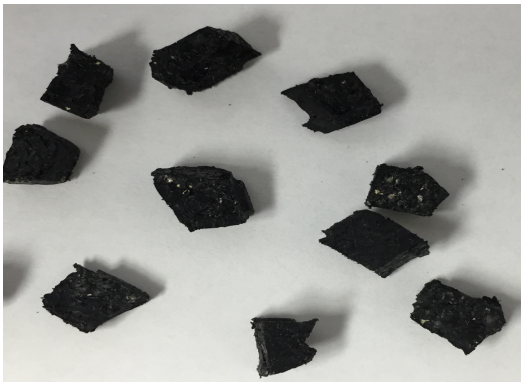

Figure 3.7: Recycled tire beads used as support media.

Table 3.1 Specifications of packing media

Items	Values
Height	1.25 cm
Width	0.62 cm
Length	0.92 cm
Weight	2.2g
Specific surface area	690 m2/m3
Porosity	35%

*300g recycled tire beads were used as packing media in each reactor.

3.1.3 Substrate and Inoculum

The seed sludge used for inoculation was obtained from an anaerobic digester of a local municipal wastewater treatment plant in Oahu, HI and acclimated with synthetic wastewater. Synthetic wastewater containing glucose as carbon source, trace elements and other nutrients (Table 3.2). Substrate was fed to each bioreactor by a peristaltic pump (Cole Palmer, model Masterflex L/S, Vernon Hills, IL). at flow rate of 200 mL/min.

Table 3.2 Substrate composition

Constituents	Concentration	
	For 1000 mg/L COD (mg)	For 5000 mg/L COD (mg)
Glucose	9375	18750
K_2SO_4	Depending on SO_4 concentration	
$NaHCO_3$	3750	7500
NH_4Cl	955	1910
KH_2PO_4	85	170
K_2HPO_4	170	340
$MgCl_2.6H_2O$	300	600
$CaCl_2$	100	200
$CoCl_2$	5.5	11
$FeCl_3$	71	142
$NiCl_2.6H_2O$	80	160
$C_6H_5Na_3O_7.2H_2O$	278	556

3.1.4 Reactor Set-up and Operation

Bioreactors were fed with synthetic wastewater at OLR of 0.5g COD/L-day and incremental of 0.5g COD/L-day until reactor showed signs of stress due to VFA built up (5g COD/L) with hydraulic retention time (HRT) of 10 days. Mesophilic temperature (37±2^{o}C) was maintained by water bath. The detailed operating conditions of reactors can be seen in Table 3.3.

Table 3.3 Operating conditions of reactors

Operating parameters	Bioreactors			
	R1	R2	R3	R4
	Initial set up and operation			
Operation time (days)	~150	~150	~150	~150
HRT* (hrs.)	10	10	10	10
Influent pH value	6.5-7.2	6.5-7.2	6.5-7.2	6.5-7.2
Influent COD concentration (mg/L)	10000, 20000, 40000, 50000	10000, 20000, 40000, 50000	10000, 20000, 40000, 50000	10000, 20000, 40000
	Addition of sulfate loading			
Operation time (days)	~150	~150	~150	n/a
HRT (hrs.)	10	10	10	n/a
Influent pH	6.5-7.2	6.5-7.2	6.5-7.2	n/a
Influent COD concentration (mg/L)	50000	50000	50000	n/a
Influent sulfate concentration (mg SO_4^{2-}/L)	1000, 2000, 3000, 4000, 5000, 6000	1000, 2000, 3000, 4000, 5000, 6000	1000, 2000, 3000, 4000, 5000, 6000	n/a
	Biochar treatment			
Operation time (days)	80	80	80	n/a
HRT (hrs.)	10	10	10	n/a
Influent pH	6.5-7.2	6.5-7.2	6.5-7.2	n/a
Influent COD concentration (mg/L)	50000	50000	50000	n/a
Influent sulfate concentration (mg/L)	6000	6000	6000	n/a
Biochar	BS500, BS800, BH550, BH800	BS500, BS800, BH550, BH800	BS500, BS800, BH550, BH800	n/a

*HRT: Hydraulic retention time.

n/a: not applicable. R4 was discontinued after failure.

3.2 Analytical Methods

Reactors performance was monitored based on biogas production, biogas composition, methane yield, pH, VFA/ALK, individual VFAs composition, total solids (TS), volatile solids (VS) and COD removal.

3.2.1 Sample Preparation

The effluent samples were collected from the gas-liquid separator sampling port. Clear supernatant was obtained by centrifuging (Eppendorf, model 5810R, Waltham, MA) at 12000 RPM for 10 minutes.

3.2.2 pH

The pH value was measured daily using pH meter (Titralab, model AT100, Hach, Germany). The pH meter was calibrated with pH 4.00, 7.00 and 10.00 buffers regularly.

3.2.3 Total Organic Carbon (TOC)

TOC concentration was determined using TOC analyzer (Shimadzu, model V-CSN, Kyoto, Japan) equipped with auto sampler. Potassium phthalate and sodium carbonate were used as calibration standards for organic and inorganic analysis.

3.2.4 Total Volatile Fatty Acids (VFAs)

The total VFAs (measured as mg acetic acid equivalent ((HAceq)/L) and the alkalinity (as mg $CaCO_3$/L) were determined by an automatic titrator (Titralab, model AT100, Hach, Germany) with FOS/TAC software (HACH, Germany) according to the Standard Methods (Apha, 2005).

3.2.5 Individual VFAs (acetic, propionic, iso-butyric, n-butyric, iso-valeric and n-valeric acids)

VFAs (i.e., acetic, propionic, isobutyric, butyric, isovaleric, valeric acids) were quantified using a gas chromatography ((Shimadzu, model GC-2014, Kyoto, Japan) equipped with a flame ionization detector (GC-FID) and a capillary column (ZB-Wax Plus column 30 m length x 0.25 mm inner diameter x 0.25 μm film thickness) (Phenomenex, Torrance, CA).

3.2.6 Suspended Solids (TSS) and Volatile Suspended Solids (VSS)

TSS and VSS were analyzed weekly following US EPA Standard Methods (Apha, 2005)

3.2.7 Sulfate

The turbidimetric method was used to measure the concentrations of sulfate in the effluent following US EPA Standard Methods (Apha, 2005) using HACH kits (Loveland, CO).

3.2.8 Dissolved Sulfide

The methylene blue method was used to quantify sulfide concentration in the effluent following US EPA Standard Methods (Apha, 2005) using HACH kits (Loveland, CO).

3.2.9 Free sulfide

The free aqueous sulfide was calculated based on the ionization constant (K_{a1}) of 1.49 x 10^{-8} at 35^{o}C (Khanal & Huang, 2003), using the following expression:

$$\text{Free sulfide } (H_2S_{aq}) = \frac{\text{Dissolved sulfide}}{[1+(\frac{Ka1}{10}-\text{ph})]} \quad (2)$$

3.2.10 Biogas

Daily biogas production (CH_4, CO_2, H_2S) was collected in Tedlar gasbag (CEL Scientific Corporation, Cerritos, CA) and the volume was quantified daily using a milli-gas counter (MGC, Ritter, Mauldin, SC). Biogas production and composition was analyzed using gas chromatography equipped with a thermal conductivity detector (TCD) (GC2014, Shimadzu, Japan) using a packed column (80/100 Hayesep D column, 2m x 1/8 inch OD x 2.1 mm ID, Supelco, USA). Argon was used as carrier gas. The operating temperatures

of the column, injection port and detector were 50, 120 and 120°C, respectively. The generation rate of biogas components was converted to normal temperature and pressure and indicated as N. The sample was prepared following Boe et al., (2007). The experiments were conducted in triplicate to confirm the repeatability.

3.3 Statistical Analysis

Analysis of Variance (ANOVA) with a threshold value (α) of 0.05 followed by a post-hoc Tukey test was used to analyze the data. Statistical analysis was performed using JMP statistical software (JMP Pro 12.0.1, SAS Institute Inc., Cary, NC)

3.4 Biochar

3.4.1 Biochar Production

Considering that the wood waste account for 39% of total biomass available in the USA (Jang et al., 2018) and exhibit a superior efficiency to adsorb H_2S, four wood derived biochars were used in this study: softwood derived biochar produced at 550 °C (BS550) and 800 °C (BS800) and hardwood derived biochar produced at 550 °C (BH550) and 800 °C (BH800). Biochars were produced in continuous-flow pyrolytic reactors and obtained commercially from Wakefield Biochar, Columbia, MO, USA (BS550 and BH 800); Pacific

Biochar, Santa Rosa, CA, USA (BS800) and Biochar Merchant, Mentor, OH, USA (BH550). Figures in Appendix A.

3.4.2 Experimental Set-up

A biochar packed-bed column with diameter of 1.4 cm, bed height (2 cm), and moisture content of 80 % (adjusted using distilled water before packing into the column) was connected to each reactor as shown in Figure 3.8 and Figure Appendix A.1. Glass beads were packed above and below biochar bed to prevent wash out. The biogas produced was recirculated through the biochar column before entering back into the bottom of the reactor. All biochars were tested in all reactors and each biochar sample was collected after 20 days of experiment to investigate the mechanisms of H_2S adsorption on biochar. A series of tests were conducted on biochar samples before and after removing H_2S. All experiments were conducted in triplicates.

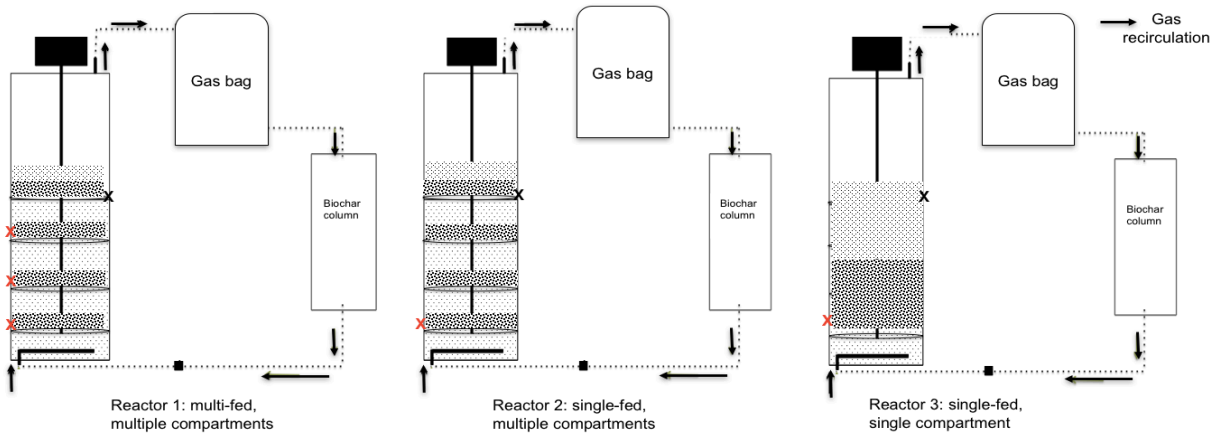

Figure 3.8:Schematic diagram of anaerobic reactors with integrated column of biochar for biogas recirculation. R1: multi-fed, multiple compartments and media. R2: single-fed, multiple compartments and media. R3: single-fed, no divisions, and media.

3.4.3 Biochar Characterization

Biochar were characterized for elemental and proximate composition and surface texture in collaboration with the University of Delaware, USA. X-ray diffraction (XRD), Fourier Transform Infrared (FT-IR) analysis (to quantify the changes in surface functional groups), and scanning electron microscopy (SEM) for solid morphology characterization were performed on all biochar samples.

3.4.3.1 Elemental Composition

Carbon (C), nitrogen (N) and hydrogen (H) content (%) were determined by a CHN Elemental Analyzer (LT Scientific, model Elementar EL cube, Carson City, NV). The oxygen (O) content (%) was calculated by the following equation (Zhao et al., 2017).:

$$O\ (\%) = 100 - (C\ \% + H\ \% + N\ \% + S\ \%) \qquad (3)$$

3.4.3.2 Proximate Composition

3.4.3.2.1 pH

The pH of biochars was measured with a pH meter (Titralab, model AT100, Hach, Germany) at a 1:20 biochar/water ratio after shaking for 30 min(Zhao et al., 2017).

3.4.3.2.2 Volatile Matter (VM)

VM was quantified by using the American Society for Testing and Materials (ASTM) D5142 method (Standard, 2002).

3.4.3.2.3 Ash

Ash was quantified by using the American Society for Testing and Materials (ASTM) D5142 method (Standard, 2002).

3.4.3.2.4 Fixed Carbon

Fixed C content was calculated by the following equation:

$$\text{Fixed C \%} = 100\% - (\text{Ash \%} + \text{VM \%}) \qquad (4)$$

3.4.3.3 Surface Texture Composition

3.4.3.3.1 Surface Area

Surface area of the biochar samples were determined from N_2 adsorption isotherms at 77 K with an accelerated surface area and porosimetry system (Micromeritics, model

ASAP 2020, Norcross, GE). Data was fitted to the Brunauer-Emmett-Teller (BET) equation:

$$\frac{1}{W\left(\left(\frac{P0}{P}\right)-1\right)} = \frac{1}{WmC}+\frac{C-1}{WmC}\left(\frac{P}{P0}\right) \quad (5)$$

Where W= weight of gas adsorbed, P/P0 = relative pressure, Wm= weight of adsorbate as monolayer and C= BET constant.

3.4.3.3.2 Porosity

Porosity was measured using an accelerated surface area and porosimetry system (Micromeritics, model ASAP 2020, Norcross, GE).

3.4.3.3.3 Scanning Electron Microscopy with Energy Dispersive X-ray Spectroscopy (SEM/EDX)

SEM/EDX analysis were performed to evaluate the sulfur deposition on biochar surface after the adsorption of H_2S by using Scanning Electron Microscopy with Energy Dispersive X-ray spectroscopy (Auriga 60 CrossBeam, Oberkochen, Germany) operated at 8 kV and samples coated with Au/Pd film for 60 seconds used to generate high resolution images of biochar surface and quantitative compositional information.

3.4.3.3.4 Fourier Transform Infrared (FTIR)

Surface functional groups on biochars were identified using a Fourier Transform Infrared (FTIR) spectrometer (Thermo Scientific Nicolet 6700, Madison, WI) equipped with an attenuated total reflectance. FTIR spectra from 32 scans were recorded in the wavenumber range 4000–500 cm^{-1} with 2 cm^{-1} resolution.

3.4.3.3.5 X-ray Diffraction (XRD)

XRD was performed on biochar samples to identify the changes in mineral composition by a X-ray diffraction (Bruker, model D8 X-ray, Madison, WI) was performed on biochar samples to identify the changes in mineral composition and used Cu Kα radiation at 1.5418 Å, over a 2θ range of 10–90° using at a scan rate of 2° min^{-1}.

3.5 H_2S Removal Efficiency

The removal efficiency of H_2S was calculated using the following equation:

Removal efficiency (%) = $\frac{(Qin-Qef)}{Qin}\ x\ 100\%$ (6)

Where Q_{In} is the H_2S (ppm) produced in the reactor daily before passing through the biochar column; Q_{Ef} is the H_2S (ppm) exiting the biochar column.

3.6 Adsorption Capacity of Biochars

3.6.1 Isotherms of Adsorption

Freundlich and Langmuir isotherms were applied to describe H_2S adsorption equilibrium at various mass of biochar (0.7, 1.0, 2.0, 3.0, 4.0, and 5.0 mg) under same temperature (25 ^oC). Experiments were carried out with 45 mL of biogas holding 750 ppm H_2S and biochar at different masses. After 3 hrs., equilibrium was established and the biogas was quantified using a gas chromatography (Agilent, model Micro GC 490, Santa Clara, CA) equipped with a thermal conductivity detector (GC-TCD) and a capillary column (CP-Sil 5 CB), a Molsieve 5A and PoraPLOT U columns).

3.6.1.1 Freundlich Isotherm

The Freundlich adsorption isotherm is an empirical equation used to describe the relation between the concentration of a solute on the surface of the adsorbent (Demirbas, 2004). Freundlich isotherm is expressed in Equation (10):

$$qe = K_F Ce^{1/n} \qquad (10)$$

The Freundlich isotherm can be linearized into the logarithmic form (Eq. 11):

$$\ln(q_e) = \ln(K_F) + \frac{1}{n}\ln(C_e) \qquad (11)$$

To validate Freundlich isotherm, we plot $\ln(q_e)$ x $\ln(C_e)$. The slope of the straight line provides the value of 1/n, while the intercept on the y-axis presents the value of log *k* (Jang et al., 2018).

3.6.1.2 Langmuir

The Langmuir isotherm describes the monolayer adsorption of a compound onto a homogeneous surface as presented in Equation 12:

$$q_e = \frac{K_L q_m C_e}{1 + K_L C_e} \quad (12)$$

The Langmuir isotherm can be linearized as:

$$\frac{1}{q_e} = \frac{1}{K_L q_m C_e} + \frac{1}{q_m} \quad (13)$$

Where K_F is the binding energy constant reflecting the affinity of biochar to H_2S; *n* is the Freundlich nonlinearity index (the constant n of the Freundlich isotherm was close to 1.0, indicating a linear adsorption); K_L is the Langmuir constant related to adsorption energy (L/µg); q_m is the theoretical maximum adsorption capacity of H_2S by biochar (mg/g).

3.6.2 Kinetics of Adsorption

The pseudo-first-order and pseudo-second-order adsorption models (Eqs. (7) and (8)) were used to investigate the adsorption rate of H_2S by biochar (Robati, 2013):

$$\log(qe - qt) = logqe - \frac{k1t}{2.303} \quad (7)$$

$$\frac{t}{qt} = \frac{1}{k2q2e} + \frac{t}{qe} \quad (8)$$

Where q_t and q_e (mg/g) are the amount of H_2S removed at time t (min.) and at equilibrium, respectively. k_1 is the pseudo-first-order rate constant (1/min.) and k_2 (g/mg·h) is the pseudo-second-order rate constant.

The amount of H_2S adsorbed at equilibrium was calculated using the Equation (9):

$$qe = \frac{(Co - Ce)V}{m} \quad (9)$$

Where *Co* and *Ce* (mg/L) are the concentration of H_2S at initial and equilibrium, respectively. *V* is the volume of gas (0.06 mL) and *m* is the mass of the adsorbent (biochar) (g).

3.6.3 Breakthrough Studies

Column test was conducted to gain a better understanding of the dynamic adsorption behavior. A glass column (diameter of 1.4 cm) was packed with biochar (bed height of 2 cm) and moisture content of 80%. Glass beads were packed above and below biochar

bed to prevent biochar wash out from the column. Inlet flow rate of the biogas containing 50,000 ppm of H_2S and maintained at 380 mL/min was injected into the bottom of the column. Gas sample was taken every 5 min from the top of the column after recirculating into the biochar. H_2S concentration was quantified using gas chromatography (Agilent, model Micro GC 490, Santa Clara, CA) equipped with a thermal conductivity detector (GC-TCD) and a capillary column (CP-Sil 5 CB), a Molsieve 5A and PoraPLOT U columns). The test was stopped at the breakthrough concentration of 50,000 ppm H_2S in the outlet biogas, indicating the complete utilization of adsorption sites in the biochar.

3.7 Material Balance

3.7.1 Carbon Balance

Carbon mass balance quantified the distribution of the different carbon components. The TOC was balanced against the effluent organic and inorganic carbon (TOC and IC), carbon fraction from methane and carbon dioxide and effluent VSS. Based on the biomass formula $C_5H_7O_2N$, the carbon content of VSS was taken as 53%. Calculations are shown in Table B.1 and presented in Figure 4.7.

3.7.2 Sulfur Balance

Sulfur mass balance quantified the distribution of the different sulfur components at various influent sulfate levels. The influent sulfate was balanced against residual sulfate, ionized ($HS^- + S^{2-}$) and unionized (H_2S_{aq}) sulfide and H_2S biogas. The above parameters were regularly monitored whereas the amount of sulfide precipitated by metals and biomass consume of sulfur were not measured or accounted for in the sulfur balance. Detailed information on sulfur balance calculation are given in Tables B_2, B_3 and B_4 in Appendix B and presented in Figure 4.8.

3.8 Microbial Community Analysis

3.8.1 Extraction of Genome DNA

Biomass samples were collected in triplicates from all reactors during the sulfate loadings of 4000, 5000 and 6000 mgSO_4^{2-}/L and before and after the treatment with biochar at sulfate loading of 6000 mgSO_4^{2-}/L for DNA extractions. DNA was extracted using DNA extraction kit for the corresponding sample. DNA integrity and purity were monitored on 1% agarose gels. DNA concentration and purity were measured using the NanoDrop One (Thermo Fisher Scientific, MA) at the same time.

3.8.2 Amplicon Generation

16S rRNA/18SrRNA/ITS genes of distinct regions (e.g. Bac 16S: V3-V4/V4/V4-V5; Fug 18S: V4/V5; ITS1/ITS2; Arc 16S: V4-V5 et. al) were amplified used specific primer (e.g.

16S: 338F and 806R/515F and 806R/515F and 907R; 18S: 528F and 706R/817F and 1196R; ITS5-1737F and ITS2-2043R/ITS3-F and ITS4R; Arc: Arch519F and Arch915R et. al) with 12bp barcode. Primers were synthesized by Invitrogen (Invitrogen, Carlsbad, CA). PCR reactions, containing 25 μl 2x Premix Taq (Takara Biotechnology, Dalian Co. Ltd., China), 1 μl each primer(10 mM) and 3 μl DNA (20 ng/μl) template in a volume of 50 μl, were amplified by thermocycling: 5 min at 94°C for initialization; 30 cycles of 30 s denaturation at 94°C, 30 s annealing at 52°C, and 30 s extension at 72°C; followed by 10 min final elongation at 72°C. The PCR instrument was BioRadS1000 (Bio-Rad Laboratory, CA).

3.8.3 PCR Products Detection, Pooling and Purification

The length and concentration of the PCR product were detected by 1% agarose gel electrophoresis. Samples with bright main strip between (e.g. 16S V4: 290-310bp/16S V4V5: 400-450bp et. al)can be used for further experiments. PCR products were mixed in equidensity ratios according to the GeneTools Analysis Software (Version4.03.05.0, SynGene). Then, mixture PCR products was purified with EZNA Gel Extraction Kit. Each project selects the appropriate primers for amplification.

3.8.4 Library Preparation and Sequencing

Sequencing libraries were generated using NEBNext® Ultra™ DNA Library Prep Kit for Illumina® (New England Biolabs, MA) following manufacturer's recommendations and index codes were added. The library quality was assessed on the Qubit@ 2.0

Fluorometer (Thermo Fisher Scientific, MA) and Agilent Bioanalyzer 2100 system (Agilent Technologies, Waldbron, Germany). At last, the library was sequenced on an IlluminaHiseq2500 platform and 250 bp paired-end reads were generated.

3.8.5 Sequencing Data Processing

3.8.5.1 Paired-end Raw Reads Quality Control

Quality filtering on the paired-end raw reads were performed under specific filtering conditions to obtain the high-quality clean reads according to the Trimmomatic (V0.33, http://www.usadellab.org/cms/?page=trimmomatic) quality controlled process.

3.8.5.2 Paired-end Clean Reads Assembly

Paired-end clean reads were merged using FLASH(V1.2.11, https://ccb.jhu.edu/software/FLASH/) according to the relationship of the overlap between the paired-end reads, when at least 10 of the reads overlap the read generated from the opposite end of the same DNA fragment, the maximum allowable error ratio of the overlap region of 0.1, and the spliced sequences were called Raw Tags.

3.8.5.3 Raw Tags Quality Control

Sequences were assigned to each sample based on their unique barcode and primer using Mothur software (V1.35.1, http://www.mothur.org), after which the barcodes and primers were removed and got the effective Clean Tags.

3.8.6 OTU Cluster and Species Annotation

3.8.6.1 OTU Cluster

Sequences analysis were performed by usearch software (V8.0.1517 , http://www.drive5.com/usearch/). Sequences with ≥97% similarity were assigned to the same OTU. An OTU is thought to possibly represent a species. The most frequently occurring sequence was extracted as representative sequence for each OTU and was screened for further annotation.

3.8.6.2 Singleton OTU and Chimera Removal

During the clustering, usearch removed the chimera sequence and singleton OTU at the same time. For each representative sequence, the silva (for 16S, 18S, chloroplast and mitochondria, self-organized, https://www.arb-silva.de/) and Unite (for ITS, http://unite.ut.ee/index.php) database were used to annotate taxonomic information (set the confidence threshold to default to ≥0.5).

3.8.6.3 Pollution OTU Removal

Removed the OTU and its tags, which were annotated as chloroplasts or mitochondria (16Samplicons) and could not be annotated to the kingdom level.

3.8.6.4 Phylogenetic Relationship Construction of Single Sample

Phylogenetic relationship of different OTUs used the KRONA software (http://sourceforge.net/projects/krona/) to visualize the results of individual sample annotations. Species composition and abundance information in the samples used the GraPhlAn software (http://huttenhower.sph.harvard.edu/graphlan) to get a single sample OTU annotation circle graph.

3.8.6.5 Phylogenetic Relationship Construction of all Samples

The difference of the dominant species in different samples (groups). The OTU representative sequence with the relative abundance in the first 50 genus level was selected, multiple sequence alignment were conducted using the FastTree software, and the relative abundance of each OTU and the species annotation information of the representative sequence were combined with the ggtree software package for visual display.

3.8.6.6 Data Normalization

OTU abundance information were normalized using a standard of sequence number corresponding to the sample with the least sequences. Subsequent analysis of alpha diversity and beta diversity were all performed basing on this output normalized data.

3.8.7 Alpha Diversity

Alpha diversity was applied to analyze the complexity of species diversity in a sample. Simpson index was used to identify community diversity whilst observed species index was used to identify community richness. Indices were calculated with QIIME (V1.9.1) and displayed with R software(V2.15.3).

3.8.8 Beta Diversity

Beta diversity analysis evaluated the differences of samples in species complexity. Differences in microbial community composition were explored and visualized using non-metric multidimensional scaling (NMDS) analysis was performed by the ggplot2 package of R software based on the weighted and unweighted Unifrac distance matrix.

CHAPTER 4

RESULTS AND DISCUSSION

4.1 Performance of Anaerobic Reactor at Increasing Organic Loading Rates

The effect of increasing the OLRs on the performance of the anaerobic reactors is shown in Figure 4.1. At OLR of 1 g COD/L-day, all reactors showed stable performance with an average effluent VFAs concentration of 340±19.4 mg HAc/L and TOC concentration of 869±56.8 mg/L. At OLR of 2 g COD/L-day, methane production reached up to 25.8±0.8, 32.5±2.6, 34.6±03.8 and 30±2.1 N mL/g$COD_{removed}$ in R1, R2, R3 and R4, respectively, with stable reactor performance (Kanjanarong et al., 2017a)(Kanjanarong et al., 2017a)(Kanjanarong et al., 2017a). At higher OLR of 4 g COD/L-day, the performance of reactor R4 started to deteriorate with pH as low as 5.08 (Table 4.1) which is below the optimum range for methanogens (between 6.8 and 7.5). The decrease in pH was accompanied by the accumulation of total VFAs to as high as 4260±33.5 mg HAc/L with concomitant decrease in methane yield from 34.6±3.8 to 17.3±0.5 N mL/g$COD_{removed}$ thereby suggesting the overloading of the reactor (Khanal, 2008). The high VFAs value (3500 mg/L as HAc) reached in R4 indicated an imbalance between fermentative bacteria, acetogenic bacteria and methanogens, and is usually associated with reactor overloading and a breakdown of the buffering capacity of the reactor with consequently inhibition of methanogens and deterioration in reactor performance (Khanal & Huang,

2005). The methane yields at OLR of 4 g COD/L-day were 83±6.5, 98±9.4 and 103± 3.2 N mL/g$COD_{removed}$ for R1, R2 and R3, respectively. The increase in methane yield was closely related to the increase in TOC removal, and low effluent VFAs concentration (600 mg HAc/L). The reactors, R1, R2 and R3 showed better adaptability with increasing OLR due to the presence of support media (Figure 4.1). The absence of support media in R4 may have prevented the retention of biomass in the reactor which is critically important for stability of anaerobic process. Usually, conventional CSTRs are operated at HRT of 15 to 30 days under mesophilic conditions of 30-35 °C (Li & Khanal, 2016). The short HRT (~10 days) in R4 possibly caused the decline in pH and washout of slow growing methanogens in R4. The CSTRs with support media facilitated immobilization of microbes in R1, R2 and R3 which resulted in better performance, thereby allowing higher COD loading rates at shorter HRT (~10 days), and promoting better process stability (Qureshi et al., 2005). Since R4 performed poorly and failed before reaching the OLR of 5 g COD/L-day, it was discontinued during the rest of the operation.

The biofilm formation around the support media provides dynamic environments with several merits such as maintaining stable and active microorganisms, faster reaction rates, high volumetric organic loading rate, improved process controls, and improved COD and pathogen removal efficiency among others (Khanal, 2008). However, current biofilm carriers are made of polyethylene, may be costly and are not environmentally friendly. Hence the use of recycled tire beads as carrier is proposed in this work as a way to reuse waste tires that otherwise would cause environmental pollution. Therefore, using recycled media can form the basis for an inexpensive but effective immobilization

technique that enhances the production of CO_2, CH_4 and H_2S as biogas while reducing waste production (Ozadali et al., 1997).

Table 4.1: pH and alkalinity at different organic loading rates*

Reactor	OLR, g COD/L-day	Effluent pH	Alkalinity, mg $CaCO_3$/L
R1	1	7.03 ± 0.03	2153 ± 110
	2	6.87 ± 0.02	1989 ± 78
	4	7.00 ± 0.02	2452 ± 130
	5	7.02 ± 0.03	3243 ± 115
R2	1	7.03 ± 0.03	2159 ± 110
	2	7.06 ± 0.02	2098 ± 87
	4	6.98 ± 0.03	2431 ± 160
	5	7.10 ± 0.02	3732 ± 126
R3	1	7.02 ± 0.02	2161 ± 110
	2	6.09 ± 0.02	1845 ± 95
	4	6.94 ± 0.03	2171 ± 130
	5	7.20 ± 0.03	4172 ± 230
R4	1	7.10 ± 0.02	2077 ± 74
	2	7.09 ± 0.02	2138 ± 103
	4	5.08 ± 0.04	1112 ± 63
	5	-	-

* Mean ± standard deviation of five observations under steady-state conditions.

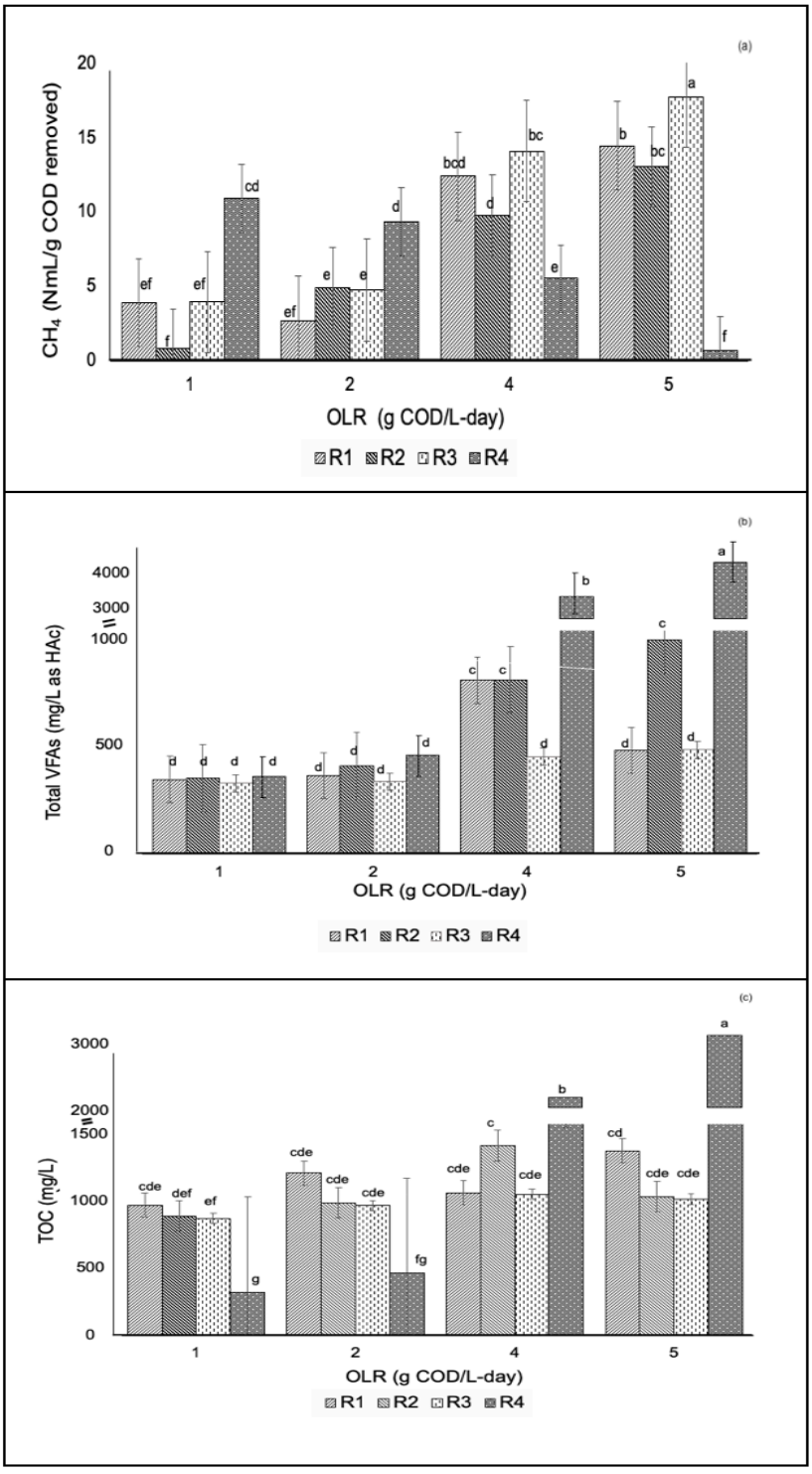

Figure 4.1: Reactor performance at different OLRs. Mean ± standard deviation of five observations under steady-state conditions. (a) Methane yield, (b) Total VFAs and (c) TOC. ($p>0.05$ among R1, R2 and R3 and $p<0.05$ for R4 for methane, VFAs and TOC).

4.1.1 Effect of Compartments on Reactor Performance

The compartments along the reactors R1 and R2 height to distribute the media throughout the reactors, did not show significant difference ($p>0.05$) in terms of reactor performance with that from R3, thereby suggesting that the reactor stability was independent of media distribution. Often, the deposition of media at the bottom of the reactor is associated with obstacle to mixing, leading to poor COD removal in the upper zone in the reactor (Yu et al., 2006). However, reactor mixing with recirculated biogas in this study demonstrated potential to overcome the aforementioned problem. Moreover, there was no significant difference in the treatment efficiency between multi- and single-fed systems ($p>0.05$), which could be due to the limited height of the reactors. Different feeding strategies have been suggested to promote sludge distribution along the height of the reactor with effective utilization of reactor working volume (Yu et al., 2006).

4.2 Performance of Anaerobic Reactor at Increasing Sulfate Concentration

After establishing a steady state condition at OLR of 5 g COD/L-day, the reactors were fed with synthetic wastewater at increasing concentrations of sulfate until the reactor started to show signs of perturbation. The effluent TOC, VFAs, DS and free sulfide concentrations under different sulfate loading rates were determined and are shown in Figure 4.2. No evidence of sulfide toxicity was observed up to sulfate concentration of 5000 mg SO_4^{2-}/L with corresponding TDS of 96.3±5.2, 101.4±2.9 and 103.8±4.9 mg S/L,

free sulfides of 32.3±2.4, 27.3±2.1 and 30.24±1.3 mg S/L and biogas H_2S levels of 50,480±421, 43,222±289 and 46202±718 ppm, in R1, R2 and R3, respectively. During this period, the mean TOC removal efficiency was >90% in all reactors. Though, there was no clear sign of sulfide toxicity, this level of H_2S in biogas could limit the applications of biogas as an energy resource (Khanal and Li., 2017).

However, when sulfate influent was increased to 6000 mg SO_4^{2-}/L, a rapid drop in pH to as low as 5.0 was observed in all reactors with concomitant increase in effluent total VFA concentration to 3000±89, 3340±86 and 3500±47 mg HAc/L (Figure 4.2 b) and effluent TOC to 2102±89, 2261±83 and 2486±106 mg/L (Figure 4.2 c) in the effluent in R1, R2 and R3 respectively, thereby suggesting a process instability. This was consistent with O'Flaherty et al., 1998 who reported that SRB may not be sufficient to completely oxidize intermediate volatile acids such as propionic acid to acetate, thereby the reactor accumulates VFAs and drop the pH value. As the methanogens are vulnerable to abrupt pH changes from the optimal value (6.6 – 7.6), their activity may be inhibited in acidic environments, mainly with high sulfide levels (O'Flaherty et al., 1998).

At 6000 mg SO_4^{2-}/L, the hydrogen sulfide levels in the effluent showed similar trend in all reactors. An increase in dissolved sulfides to 121±2.4, 110±4.1 and 131±0.6 mg S/L with corresponding free sulfides of 53±3.7, 48±4.0 and 53±0.5 mg S/L in reactors R1, R2 and R3, respectively resulted in an inhibition of the methanogens as apparent from decrease in methane yields from 135±3.7, 152±2.2 and 161.7±4.6 without sulfate to 63±3.5, 73±1.5 and 75±4.6 N mL/$gCOD_{removed}$ at sulfate concentration of 6000 mg SO_4/L in R1, R2 and R3 (Figure 4.2 a). Microbial community and state with detailed discussion is provided in section 3.5. This was in consistent with several studies who reported inhibition of

methanogenesis at this concentration (Khanal and Huang, 2003). These findings suggest that DS and free sulfides may promote inhibitory effect on both MPA and *Desulfovibrio*-type SRB detected in our system. Bhattacharya et al. (1996) reported sulfide tolerance at dissolved sulfide of 161 mg S/L and free sulfide of 64 mg S/L. Khanal & Huang (2005) observed sulfide toxicity at a much higher DS and free sulfide of 613 and 228 mg S/L, respectively, and they suggested that the higher tolerance could be due to acclimatization at high sulfate level for a long period of time (>2 years).

4.3 Alleviation of Sulfide Toxicity Using Biochar

When the reactors' performance started to deteriorate due to sulfide toxicity, biogas recirculation through the external biochar column was initiated. H_2S in biogas, DS and free sulfides in the effluent decreased significantly from 65000±123 ppm, 130±0.6 mg S/L and 54±1.4 mg S/L to 1140±99 ppm, 20±3.3 mg S/L and 8.1±0.5 mg S/L; 3540±153 ppm, 10±1.8 mg S/L and 10±0.9 mg S/L; 683±189 ppm, 8±1.1 mg S/L and 5±0.9 mg S/L and 3400±734 ppm, 16±1.1 mg S/L and 14±1.9 mg S/L, with BS550, BS800, BH550 and BH880, respectively (Figure 4.2). As a result, the TOC removal efficiency improved to 90% with rapid drop in total VFAs to 779±35 mg HAc/L, thereby suggesting the alleviation of sulfide toxicity to MPA. The methane yields also increased from 63±3.5, 73±1.5 and 75±4.6 N mL/$gCOD_{removed}$ to 158±2.7, 159.5±0.5 and 154.3±1.7 N mL/$gCOD_{removed}$ in R1, R2 and R3, respectively with stable reactor performance. All biochars showed similar trend in terms of reactor performance with no significant difference ($p>0.05$). Upon integrating biochar columns with anaerobic reactors, sulfide

was rapidly removed with removal efficiencies >98% of gaseous H_2S, 94% of DS and 89% of free sulfide (Figure 4.2), thereby alleviating sulfide toxicity to methanogens and sulfate reducing bacteria and promoting the stability of the anaerobic process.

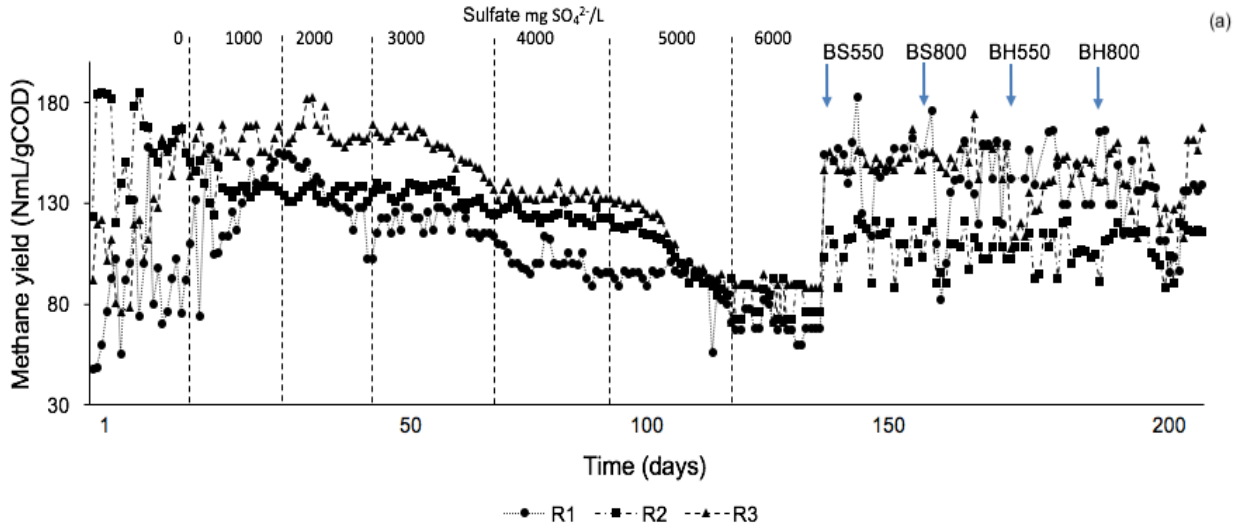

(b)

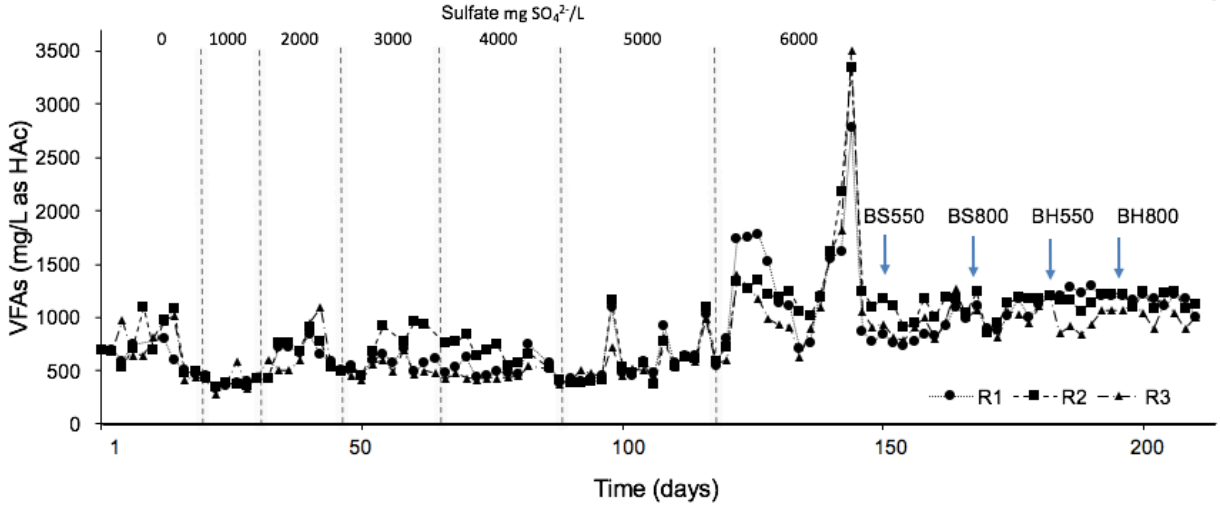
Sulfate mg SO_4^{2-}/L
0
1000
2000
3000
4000
5000
6000
VFAs (mg/L as HAc)
BS550
BS800
BH550
BH800
R1
R2
R3
Time (days)

(c)

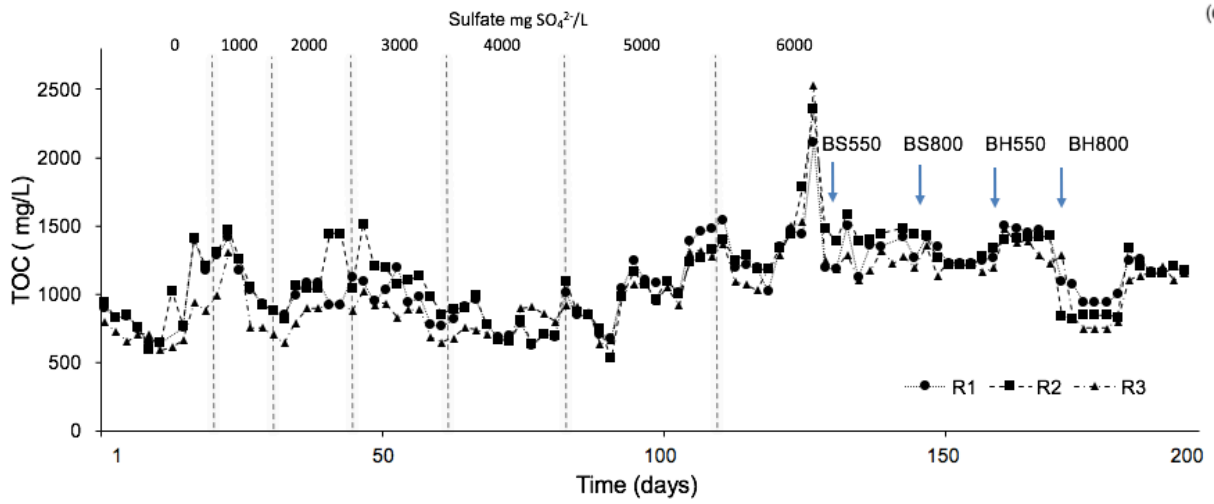
Sulfate mg SO_4^{2-}/L
0
1000
2000
3000
4000
5000
6000
TOC (mg/L)
BS550
BS800
BH550
BH800
R1
R2
R3
Time (days)

(d)

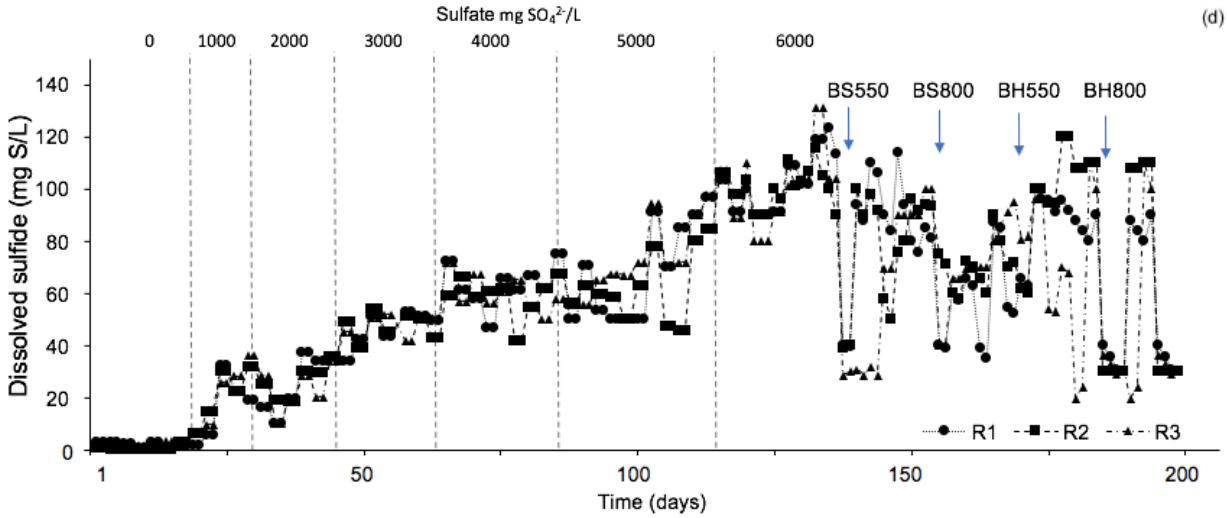
Sulfate mg SO_4^{2-}/L
0
1000
2000
3000
4000
5000
6000
Dissolved sulfide (mg S/L)
BS550
BS800
BH550
BH800
R1
R2
R3
Time (days)

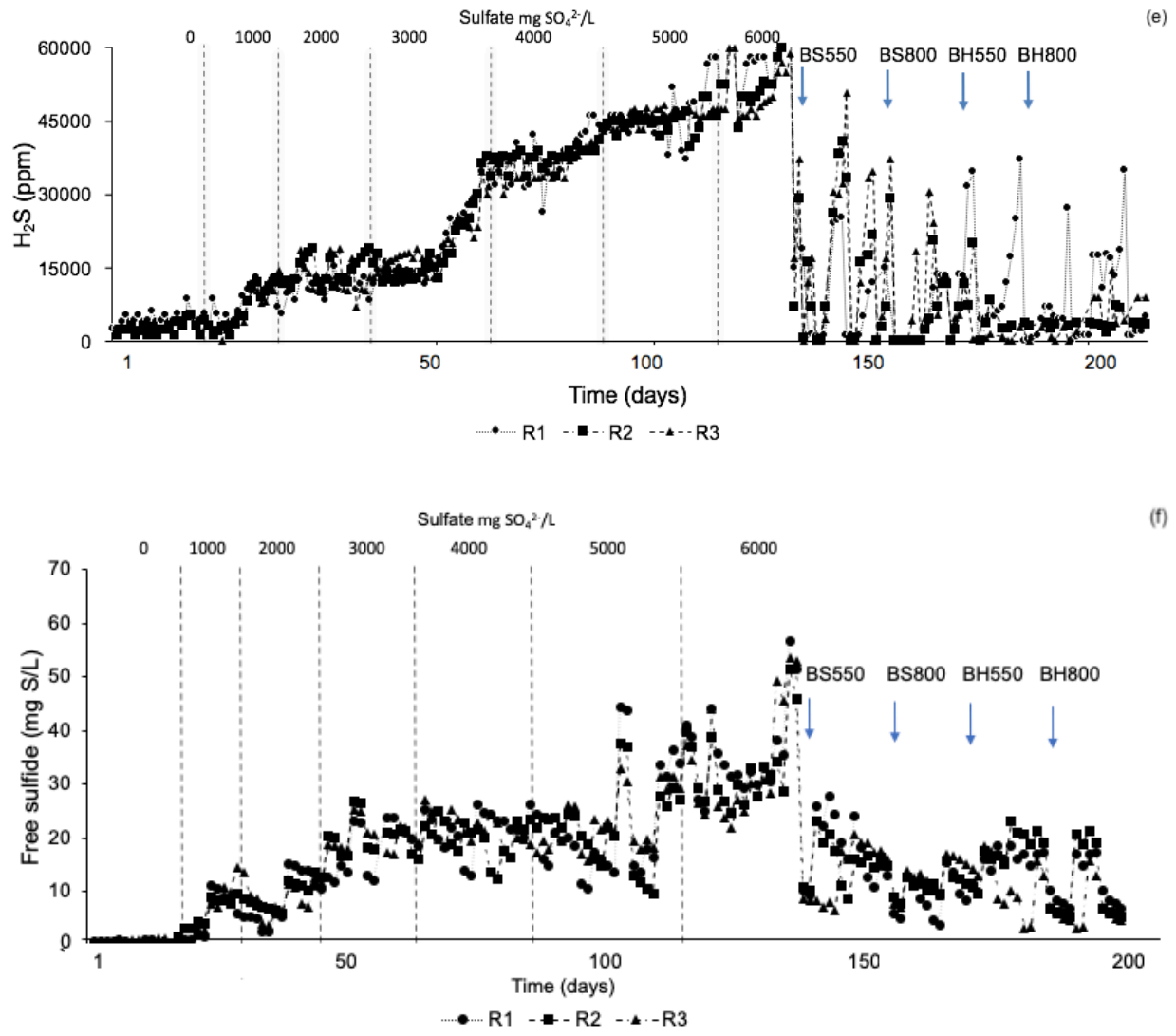

Figure 4.2: Reactor performance with and without biochar. * Mean ± standard deviation of five observations under steady-state conditions. (a) Methane yield, (b) VFAs, (c) TOC, (d) dissolved sulfide (e) H_2S production and (f) free sulfide at increasing sulfate concentration from 1000 to 6000 mg SO_4^{2-}/L.

4.4 Biochar Characterization

4.4.1 Physicochemical Characterization

The elemental, proximate and textural compositions and the atomic ratios of the biochars are summarized in Table 4.2. Understanding the biochar properties is important to assess the quality and commercial value of the biochar as well as the potential suitability of the biochar on the adsorption of H_2S or as amendment in degraded or low fertility soils. The chemical composition of the biochars is listed in Table 4.2.

Table 4.2: Elemental, proximate and textural analysis of biochar, on a dry wt% basis.

Sample		BS550	BS800	BH550	BH800
Elemental analysis	C (%)	70.0±1.7	73.0±3.0	64.5±2.6	77.5±2.2
	H (%)	5.5±0.1	4.3±0.2	6.3±0.8	5.7±0.3
	N (%)	0.25±0.01	0.20±0.02	0.28±0.01	0.40±0.02
	O (%)	24.2±1.4	22.0±1.2	28.6±2.1	16.4±1.4
	H/C	0.08	0.06	0.09	0.07
	O/C	0.11	0.03	0.23	0.10
	C/N	280	360	228	192
	Ash (%)	9.60±0.2	29.18±2.3	3.31±0.2	5.48±0.2
	pH	8.64±0.1	9.64±0.2	8.18±0.1	8.69±0.1

Textural analysis	BET surface area (m^2/g)	105.44	76.63	38.62	36.80
	t-Plot Micropore Area (m^2/g)	31.45	8.40	4.82	n/a
	t-plot Micropore volume (cm^3/g)	0.12	0.07	0.04	0.03
	Average pore width (4V/A by BET) (nm)	6.55	6.59	6.67	6.79

Value represents means; ± represents standard error.

The carbon content in the biochar increased from 70% to 73% and from 64% to 77% in softwood and hardwood feedstock respectively, with increasing pyrolysis temperature, whereas oxygen and hydrogen were removed as CO, CO_2, H_2O, and other O- and H-containing volatiles, thereby concentrating the carbon and consequently reducing the O/C

and H/C ratios (Brewer et al., 2012). Above 550°C, the graphene sheets continue to increase the aromatic content and therefore, producing a biochar recalcitrant to decomposition (Zambon et al., 2016).

4.4.1.1 van Krevelen Diagram

van Krevelen diagram (Figure 4.3) is used to confirm the importance of dehydration (loss of O and H as H_2O) and carbonization reactions during pyrolysis. Because of the dehydration of feedstock during pyrolysis at higher temperature (800 °C), biochar loses more surface functional groups as OH- and C- bound oxygen and hydrogen atoms than pyrolysis at lower temperature (550 °C) due to structural core degradation (Novak et al., 2016). Therefore, biochars BS550 and BH550 were likely to have more surface functional groups (e.g., -COOH, R-OH, C=O) available and higher capacity for H_2S adsorption. Ash content of the biochars increased with increasing temperature from 500 °C to 800 °C as a result of a concentration of minerals and volatilization of lignocellulosic matter. Several studies show an exponential increase in ash content with pyrolysis temperature (Oliveira et al., 2017; Rafiq et al., 2016; Xu et al., 2014). While H_2S removal efficiency was nearly 99% for all biochars**,** the biochars produced at higher temperatures (BH800 and BS800) saturated more often than those produced at lower temperatures (BH550 and BS550).
The molar ratios O/C and H/C of biochar indicate the polarity, aromaticity, stability and degree of carbonization (Oliveira et al., 2017; Zambon et al., 2016). O/C ratio is the number of polar sites (hydroxyl, carboxylate, and carbonyl groups) per carbon atom

(Batista et al., 2018) and at higher temperatures results in a less hydrophilic surface of biochars as we demonstrated in and BS800 and BH800 (Figure 4.3). Lower hydrophilicity of biochar helps to create a water film on the surface which in turn increases H_2S removal efficiency (Xu et al., 2014a). H/C ratio of ≤0.2 indicates dehydration and decarboxylation processes that are related to an increase in aromaticity and degree of condensation of the biochar (Rafiq et al., 2016).

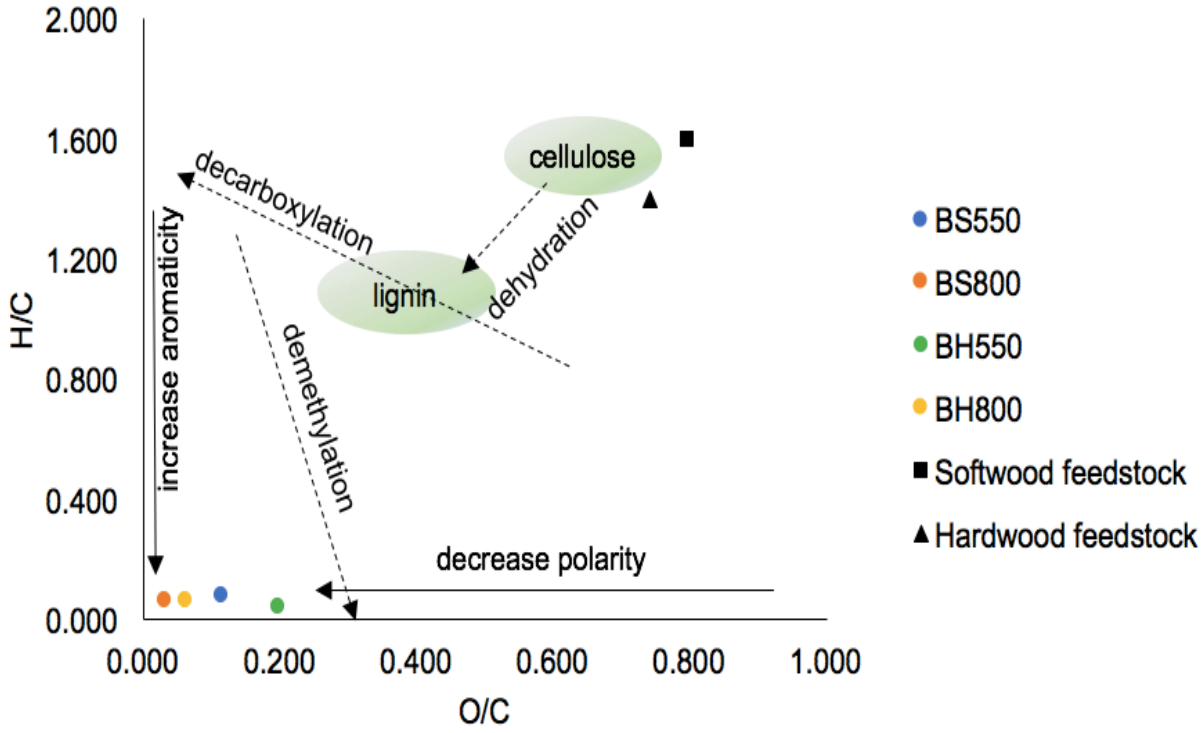

Figure 4.3: van Krevelen diagram of biochars. (feedstock data from (Anca-Couce & Obernberger, 2016 and Willems & Militz, 2013).

Ash content of the biochars increased with increasing temperature from 500 °C to 800 °C as a result of a concentration of minerals and volatilization of lignocellulosic matter. Literature findings shows an exponential increase of ash content with pyrolysis temperature (Oliveira et al., 2017; Rafiq et al., 2016; Xu et al., 2014). Surface area and pore properties of biochars were reported in Table 4.3. Even though literature reported that as pyrolysis temperature increases, the accessible surface area increases, a relatively lower surface area is observed in both feedstocks when temperature rises. Possibly, extending the holding time during pyrolysis cause the reactions to continue at the pore surface area reducing the number of micro-pores and/or filling them total or partially with inorganic material (Rafiq et al., 2016). BET surface area and pore volume are important factors during adsorption of H_2S on carbon structures. A reduction in the pore volume and surface area (Table 4.3) is expected due to the reaction of biochar surface with H_2S until saturation. Although those parameters play important role on adsorption process, proper combination with surface chemistry is essential. Feng et al., 2005 summarizes that both the contribution of pore structure and surface chemistry occur during H_2S removal and mainly depend on the experimental conditions.

Table 4.3: Pore volume of biochar before and after sulfide adsorption

	Pore volume (cm^3/g)		BET Surface area m2/g	
Biochar	Before H_2S	After H_2S	Before H_2S	After H_2S
BS550	0.155	0.062	105.44	51.49
BS800	0.042	0.015	76.63	7.83
BH550	0.057	0.008	38.62	7.78
BH800	0.031	0.004	36.80	7.21

4.5 Mass Balance

4.5.1 Carbon Balance

The total carbon recovery was higher than 80% (Figure 4.4). At 333 mg S/L, between 3.7 – 4% of the influent carbon was in the effluent in all reactors. An increase in sulfate to 666 to 1333 mg S/L, maintained the same TOC % contribution in all reactors, suggesting that up to 1333 mg S/L there was no sulfide toxicity affecting the microorganisms and the organic removal was constant. However, at 1666 to 2000 mg S/L, the effluent TOC increased to 12.22, 15.00 and 12,78% in R1, R2 and R3 respectively, indicating reactor deterioration due to stress imposed on the AD system as a result of increasing sulfide levels. Methane production was also affected by sulfide toxicity. Initially at 333 mg S/L, the percentage of carbon represented 21.83, 24.6, and 25.4% of the total influent carbon in R1, R2 and R3 respectively. The decrease of carbon % due to sulfide toxicity to MPB

reached levels as low as 13% in all AD treatments. (Khanal & Huang, 2005) also observed decrease in methane production and TOC removal with increasing influent sulfate levels more than 1333 mg S/L. Once the biogas was recirculated through the biochar column, the TOC rapidly decreased to initial levels of 3.89, 5 and 5.5% in R1, R2 and R3 respectively. It was also observed a sharp increase in methane production to 22, 26 and 30% of total influent carbon in R1, R2 and R3 respectively. This was because the biochar retained the sulfur within its pores, reducing the SO_4^{2-} available in the reactor as a source of electron acceptor to SRB, hence reducing the sulfide toxicity to MPA. All reactors recovered and indicated that a biochar column integrated to the AD system is a fair alternative to remove the sulfide from the biogas and consequently keep the reactor efficiency for AD treatment.

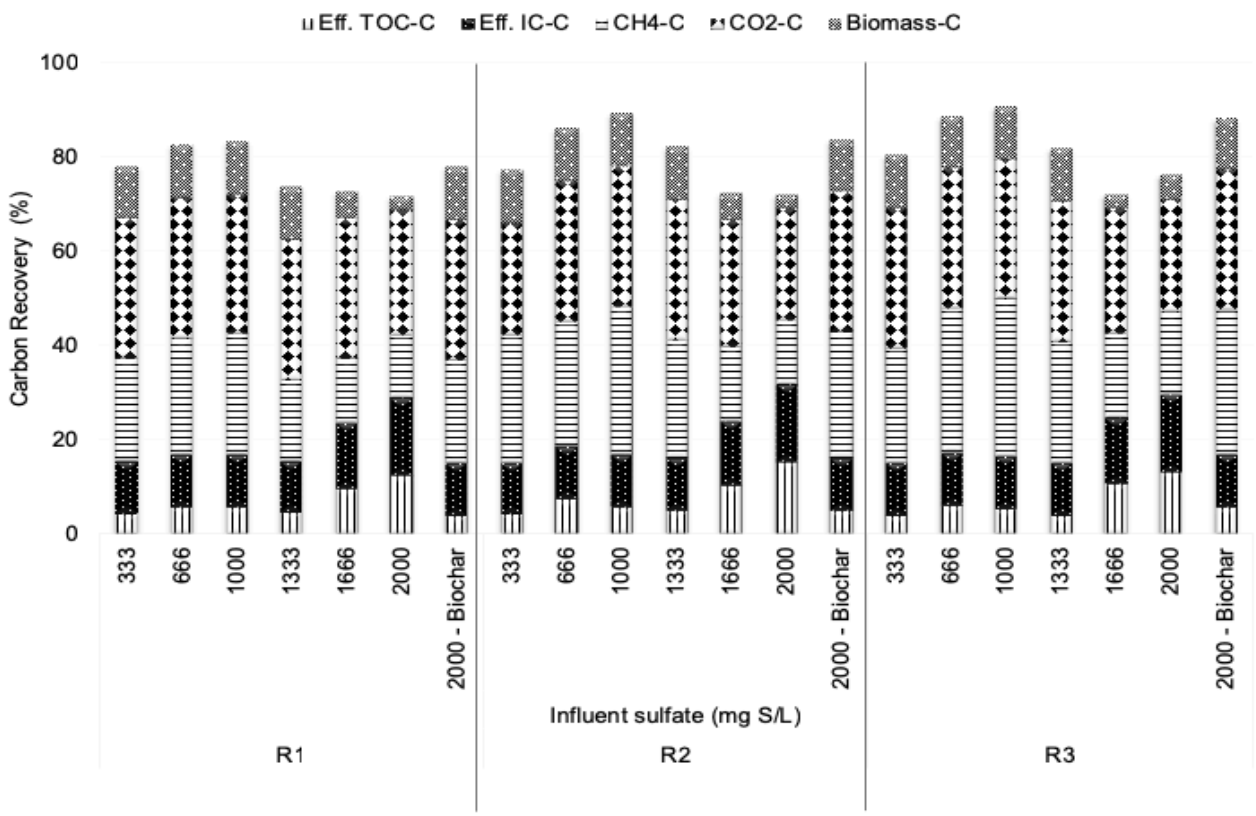

Figure 4.4: Carbon balance under different influent sulfate concentrations before and after biochar.

4.5.2 Sulfur Balance

The influent sulfate was balanced against the sum of effluent sulfate, effluent dissolved sulfide, effluent free sulfide and biogas sulfide (Figure 4.5). The above parameters were regularly monitored whereas the amount of sulfide precipitated by metals and biomass consume of sulfur were not measured or accounted for in the sulfur balance. The total sulfur recovery ranged from 65 to 85% at 333, 666, 1000, 1333 and 1666 mg S/L. It was evident the most of the influent sulfate was converted to gas phase. Figure 4.5 shows the a constant distribution of sulfur species during the sulfate levels up to 1666 mg/SL. At

2000 mg S/L a slightly decrease in sulfide gas and an increase in the unionized S (dissolved sulfide) and sulfate, indicated sulfide toxicity to SRB. At this point, the pH of all reactors were as low as 5 and all reactor were on the verge of failure. The use of a column packed with biochar for biogas recirculation and simultaneous sulfide adsorption was initiated once reactors performances started to deteriorate. Biogas sulfide and dissolved sulfide levels decreased to less than 10% and 5% in all reactors and no sulfide toxicity was observed since the reactors recovered. Microbial relative abundance for methanogens and sulfate reducing bacteria during increase in sulfate loadings before and after biochar treatment supports this data and is reported in later section of this dissertation.

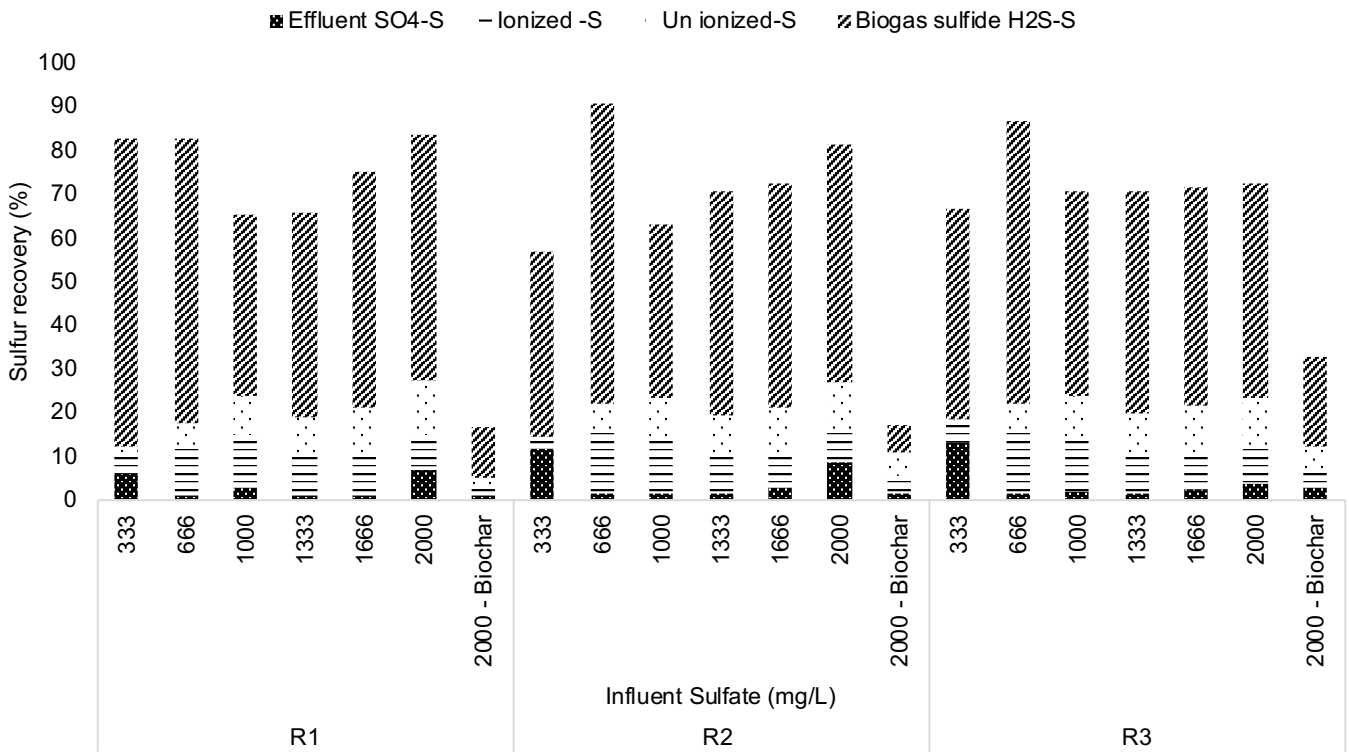

Figure 4.5: Sulfur balance at different influent sulfate concentration before and after biochar.

4.6 Adsorption Capacity of Biochars

Our previous study (Kanjanarong et al., 2017) showed that when the moisture content of biochar was adjusted at about 80%, adsorption of H_2S proceeded mainly via chemisorption, and greater internal porosity would allow greater accessibility to the active sites by the dissociated hydrogen sulfide ions. Thus, a higher adsorption capacity was obtained.

4.6.1 Adsorption Isotherms

Langmuir and Freundlich adsorption isotherms were used to describe the adsorption process in which both Langmuir (R^2 = 0.89 to 0.96) and Freundlich (R^2 = 0.87 to 0.95) isotherms showed to fit to the experimental data (Figure 4.6 and Figure 4.7). However, Langmuir isotherm yielded greater R^2 value than the Freundlich isotherm generated for the same biochar (Table 4.4). Similar behavior was also reported by Fidel et al. (2018) in which both Langmuir and Freundlich isotherms fitted well the experimental data of inorganic compounds adsorption onto corn stover biochar. The adsorption parameters are summarized in Table 4.4. Among all four biochars ($p<0.05$) tested, BS550 had the highest adsorption capacity of H_2S (160.4 mg H_2S/g biochar) followed by BH550 (143.5 mg H_2S/g biochar). Biochars BS550 and BH550 were superior to adsorb H_2S from gaseous streams compared to BS800 (106.3 mg H_2S/g biochar) and BH800 (105.1 mg

H_2S/g biochar). Adsorption capacity between biochars produced at higher temperatures (800 ^oC) were not significantly different ($p>0.2$). These findings are in agreement with other studies in which biochar produced at lower pyrolysis temperatures (500 ^oC) was more effective to remove inorganic pollutants than the biochar produced at higher pyrolysis temperatures (800 ^oC) due to a higher carbon content, presence of numerous functional groups and more hydrophilic surface (Bagreev et al., 2001; Kanjanarong et al., 2017; Xu et al., 2014; Oliveira et al., 2017). Studies showed that the wood-derived biochars exhibited a greater potential to adsorb pollutants due to high aromatic organic composition, low ash content, large surface area and porosity (Bagreev et al., 2001). Our results using wood-derived biochars also demonstrated higher maximum adsorption capacity in comparison with camphor (109.3 mg H_2S/g) (Shang et al., 2013), sewage sludge (104.5 mg H_2S/g) and pig manure (59.6 mg H_2S/g) derived biochars (Xu et al., 2014).

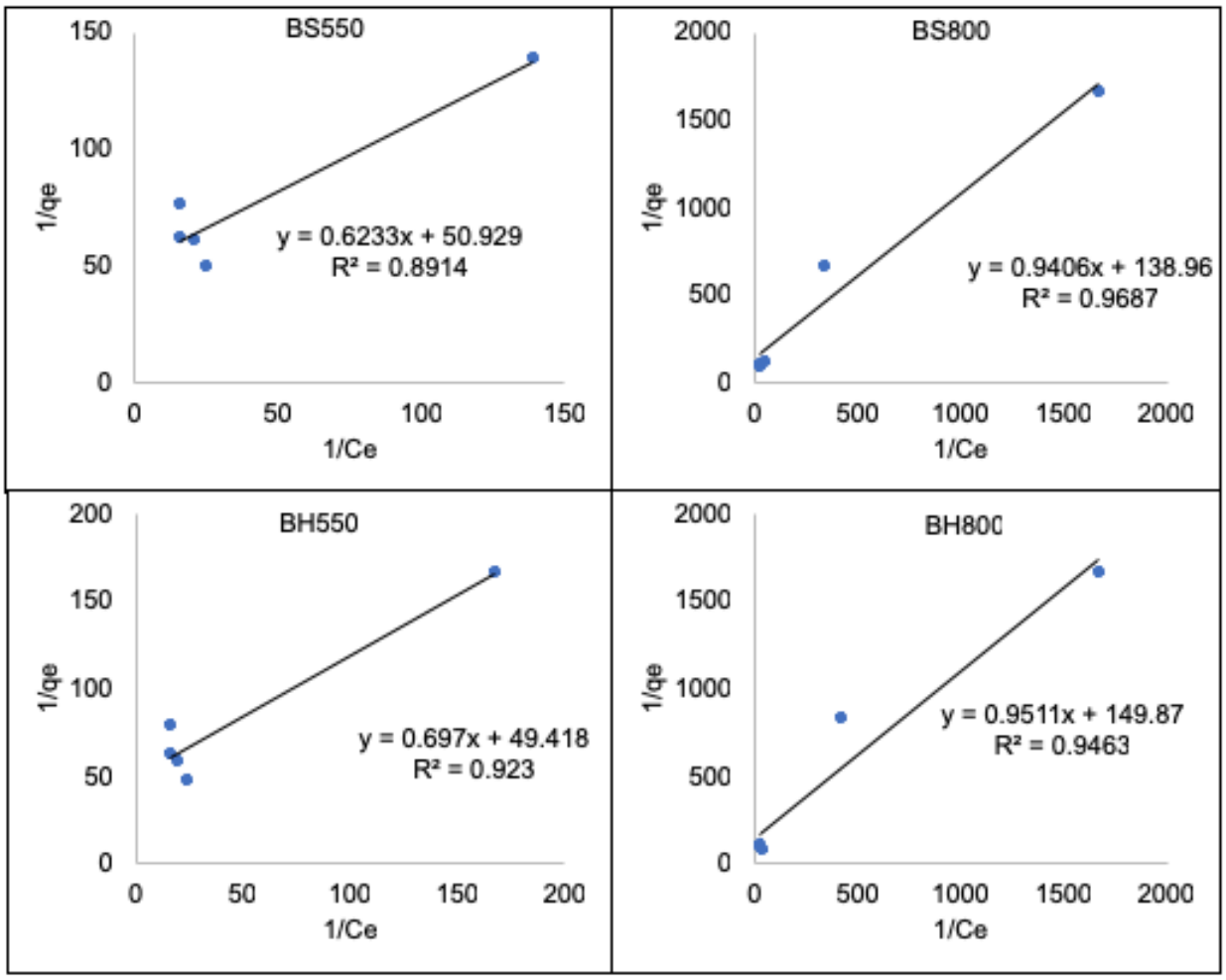

Figure 4.6: Langmuir isotherm plots for H2S adsorption on BS550, BS800, BH550 and BH800.

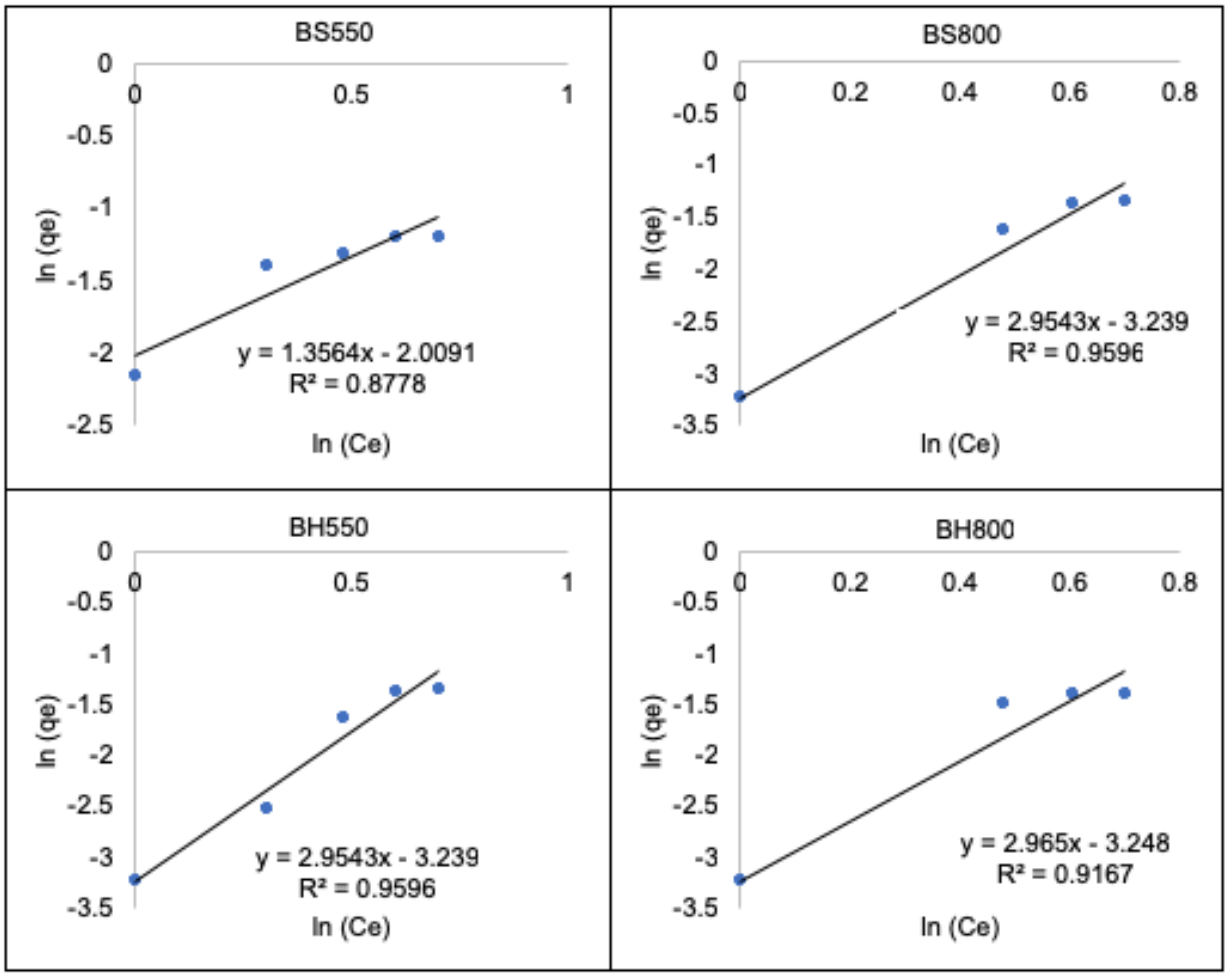

Figure 4.7: Freundlich isotherm plots for H2S adsorption on BS550, BS800, BH550 and BH800.

Table 4.4: Adsorption parameters for Langmuir and Freundlich isotherms

Biochar	Langmuir			Freundlich		
	$q_e = (K_L q_m C_e) / (1 + (K_L C_e))$			$\text{Log } q_e = \log K_F + 1/n \log C_e$		
	q_m (mg/g)	K_L (L/mg)	R^2	K_F (mg/g)	1/n	R^2
BS550	$160.44^a \pm 0.4$	0.02	0.89	0.13	1.54	0.87
BS800	$106.32^c \pm 0.4$	0.01	0.96	0.02	3.07	0.95
BH550	$143.47^b \pm 0.4$	0.02	0.92	0.11	1.71	0.91
BH800	$105.14^c \pm 0.4$	0.01	0.94	0.02	3.23	0.91

Each superscript letter indicates statistically significant differences between biochars. ($p<0.05$)

4.6.2 Kinetic Models

The pseudo-first-order adsorption kinetics showed lower R^2 value (<0.81) compared to pseudo-second order R^2 value (>0.94) for all biochars studied. Thus, pseudo-second-order kinetics represents well the H_2S adsorption onto biochar. In pseudo-second-order kinetic model, the rate-limiting step is the surface adsorption that involves chemisorption, where the removal is due to physico-chemical interactions between the two phases (Kanjanarong et al., 2017; Shang et al., 2013 and Robati, 2013).Thus, a higher capacity of adsorption was obtained. The adsorption parameters are summarized in Table 4.5.

Table 4.5: Parameter for pseudo-first-order and pseudo-second-order kinetics

	Pseudo first-order		Pseudo second-order		
	k1	R^2	q_e	k2	R^2
BS550	0.008	0.61	0.33	0.15	0.94

BS800	0.002	0.81	0.35	0.14	0.94
BH550	0.003	0.63	0.33	0.21	0.95
BH800	0.001	0.69	0.63	0.15	0.97

4.6.3 Breakthrough Curves

Column test was conducted to gain a better understanding of the dynamic adsorption behavior. Breakthrough curves for H_2S adsorption on biochars are presented in Figure 4.8, where C_0 and C were the inlet H_2S concentration and outlet H_2S concentration in ppm at time *t*, respectively. Initially, adsorption was rapid because of large availability of sites in the adsorbent, and as the biogas entered the packed bed and was adsorbed, it filled up the available sites and reached equilibrium with the adsorbent (Patel, 2019). At this point, concentration of adsorbate was zero, hence the ratio $C/C_0=0$. Subsequently, the upper layer of biochar bed was gradually saturated with feeding H_2S_{gas} and become less efficient. Therefore, more adsorbate came out in the outlet biogas (C/C_0 >0 and <1) until biochar was completely exhausted ($C/C_0=1$) and adsorption did not occur. When the concentration of H_2S in the outlet biogas matched the inlet concentration (exhaust point), the adsorbent required replacement. The breakthrough times for BS800 (5 min) and BH800 (5 min) were shorter and steeper than those of the BS550 (10 min) and BH550 (min), suggesting a poor sorption capacity of BS800 and BH800 compared to BS550 and BH550. While >94% H_2S removal efficiency was obtained with all biochars in R1, R2 and R3**,** biochars produced at higher temperatures (BH800 and BS800) saturated more often and had to be replaced more times. Shang et al., (2016) stated that longer breakthrough times indicate better retention of adsorbate and that the breakthrough capacity is

governed by biochar pH and pyrolysis temperature. Patel (2019) reported that breakthrough time and exhaustion are slower with increasing bed height of column. Increased surface area and the number of binding sites available for adsorption increase the volume of treated adsorbate and time for interaction of adsorbate-adsorbent.

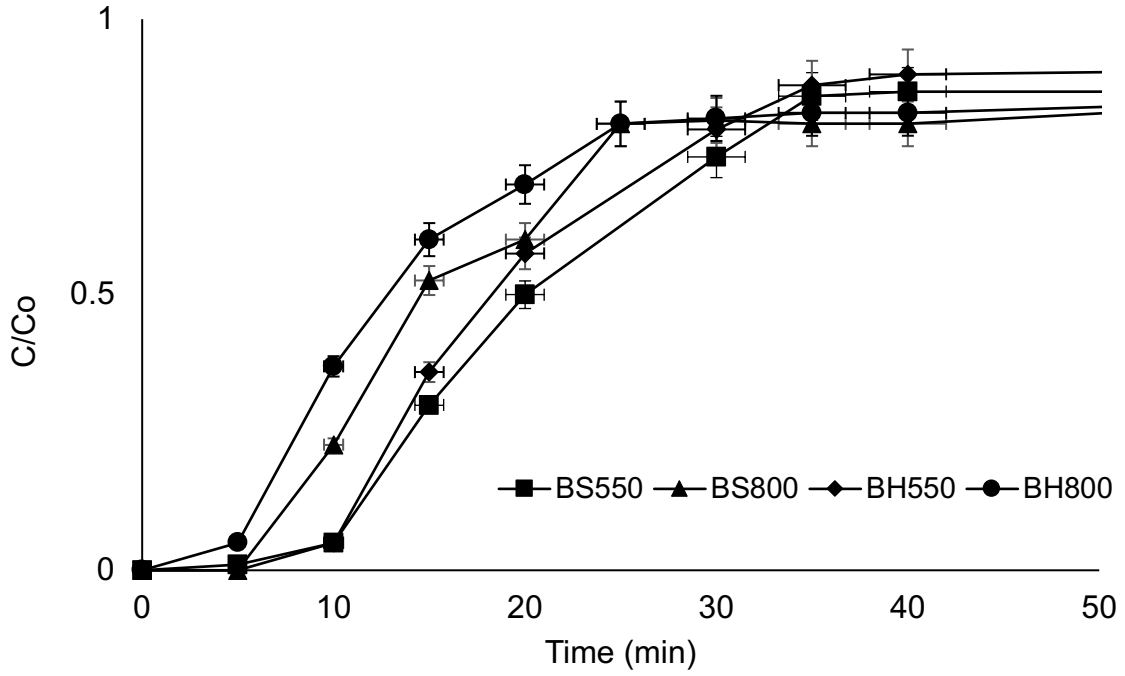

Figure 4.8: Breakthrough curves for BS550, BS800, BH550 and BH800.

4.7 Mechanisms of H_2S Adsorption on Biochar

There are several mechanisms by which H_2S can be adsorbed onto biochar (Figure 4.9). Chemisorption of heterogeneous molecules requires the diffusion of reactant molecules into the surface, adsorption on the surface and reaction of the adsorbed species. Adsorption via functional groups (e.g., carboxylic, lactone, phenol, carbonyl, ether, pyrone) complexation, plays an important role in promoting these reactions. Firstly, H_2S molecules are trapped into the pores or surface of the biochar by weak van der Waal's forces. Secondly, H_2S diffuses into the water film under basic conditions and dissociates into HS^- and H^+. Lastly, thiol (-SH) structures are formed on the carbon structure and are further attacked by oxygen functional groups, resulting in oxidized species of sulfur (S^0 and SO_4^{2}) (Xu et al., 2014).

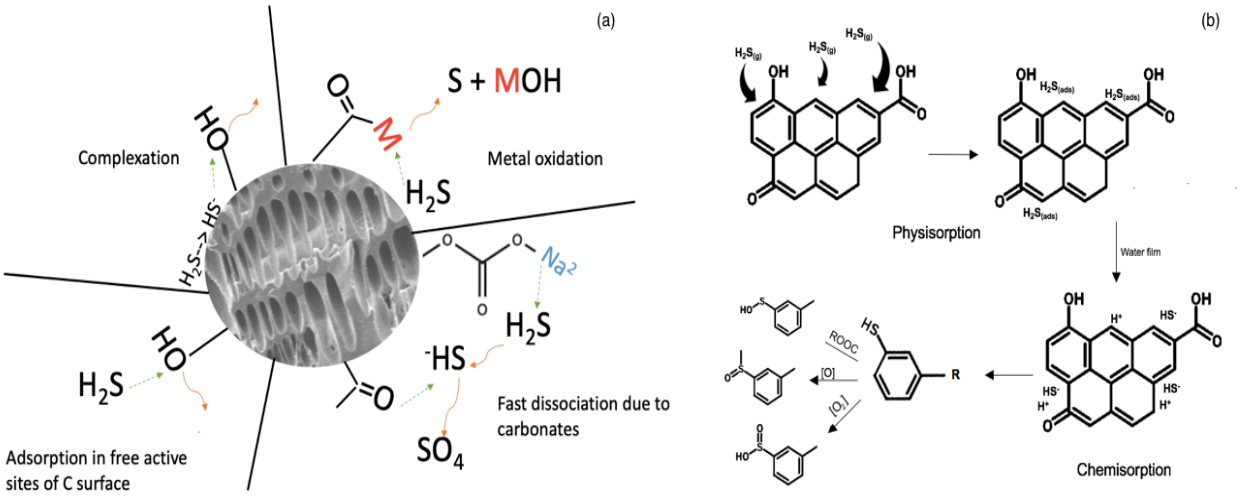

Figure 4.9: (a) Possible mechanisms of H_2S adsorption on biochar; (b) Mechanism of H_2S adsorption via functional groups complexation on biochar.

The acidic dissociation is only possible when the pH value of biochar is higher than the pKa constant (7.2) of H_2S (Kanjanarong et al., 2017; Xu et al., 2014). The biochars BS500, BS800, BH550 and BH800 had pH of 8.64±0.1, 9.64±0.2, 8.18±0.1 and 8.69±0.1, respectively. pH is influenced by pyrolysis temperature and decomposition of organic and inorganic materials. At higher temperatures, more organic compounds are decomposed, thereby giving an alkaline characteristic to the biochar surface (Shang et al., 2015). Therefore, all biochars tested had favorable condition for first dissociation of H_2S without alkaline pretreatment, which is often used to enhance the adsorption capacity of activated carbons. Usually, SO_4^{2-} is formed on the surface of the biochar where O_2 is sufficient while elemental sulfur (S^0) is formed in the pores of biochar due to limited O_2 (Kanjanarong et al., 2017).

Based on SEM-EDX analysis of biochars surface (Figure 4.10) before sulfide removal, C, O, Si and Ca were the major constituent elements in the adsorbent, whereas after H_2S adsorption, there was presence of S along with C, O, Si and Ca. The presence of the peak corresponding to sulfur in biochar confirms the effective removal of sulfide. Following H_2S adsorption onto the biochar, the sulfur content increased from 0 (wt %) to 7.2±0.2, 3.2±0.3, 14.2±0.7 and 7.2±0.4 (wt %) in BS550, BS800, BH550 and BH800, respectively. XRD analysis further revealed the presence of gypsum ($CaSO_4.2H_2O$) onto biochar surface at 2θ = 11.6 and 29.2 and the formation of elemental sulfur (S^0) at 2 θ = 22.8 and 25.**7** (Figure 4.11). These results demonstrated that S^0 and SO_4^{2-} were formed after H_2S adsorption (Xu et al., 2014). Moreover, the complete oxidation of H_2S to sulfate was expected on the surface of the biochar where more oxygen would be available,

whereas limited O_2 diffusion into the pores would result in the formation of S^0 (Xu et al., 2014).

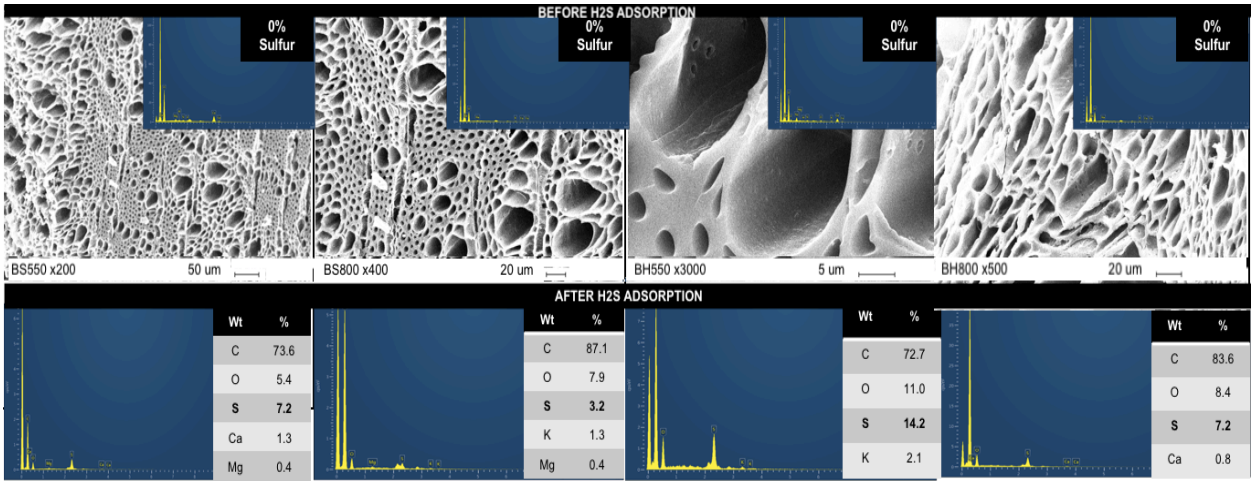

Figure 4.10: SEM/EDX images of biochar surface before and after sulfide removal (a) BS550, (b) BS800, (c) BH550 and (d) BH800.

Hardwood biochars also showed peaks around 1577-1590 cm^{-1} for COO- asymmetric stretching and significant weak bands at 1470 cm^{-1} which could be attributed to C-O stretching vibration of phenol (Figure 4.12) (Kanjanarong et al., 2017). Structural changes that occurred in biochar after H_2S removal include the additional presence of IR bands on 617- 692 cm^{-1} representing S-O bending in biochar samples and 752-775 cm^{-1} representing S-S stretching in sulfides. Moreover, the reduction in intensity of the stretching vibrations due to COOH groups (1724 cm^{-1}), further confirmed the role of oxygen functional groups in sulfide adsorption onto biochar. As the pyrolysis temperature increased, biochars began to show higher aromatic C=C stretching on 1440 cm^{-1} and a decrease in aromatic C=C and C=O stretching of conjugated ketones and quinones on 1578 cm^{-1} (Zhao et al., 2017) suggesting a decrease in the polar functional groups.

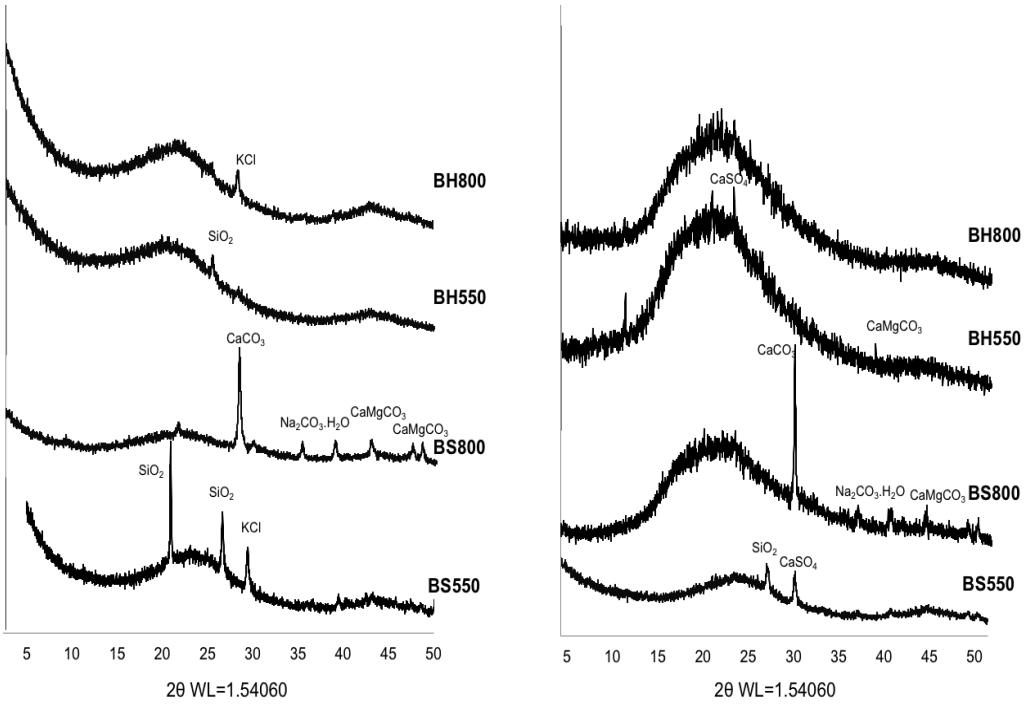

Figure 4.11: XRD patterns of biochars (a) before and (b) after H_2S adsorption.

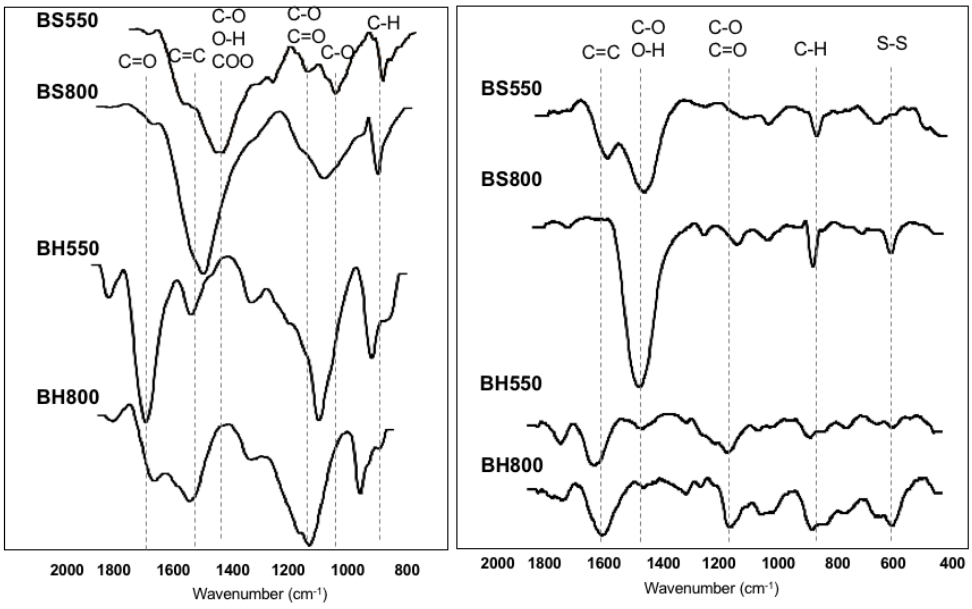

Figure 4.12: FTIR spectra (c) before and (d) after H_2S adsorption

Biochars produced at higher temperature usually are more alkaline with more carbonate compounds that facilitate the dissociation of H_2S to HS^- ions. Alkaline biochar and inorganic minerals present on biochar surface also play an important role in sorption of H_2S and final forms of sulfur (Kanjanarong et al., 2017; Xu et al., 2014). All biochars tested exhibited a weak and sharp peak at 875 cm^{-1} that corresponds to Ca-O stretching of the calcium carbonate species present on the surface of biochar, a peak on 1040-1088 cm^{-1} to C-O stretching and deformation in C-OH (Herbert et al., 2012). The proposed mechanism involves dissociation of $CaCO_3$ (Eq. 14), dissociation of H_2S (Eq. 15) and finally the oxidation of HS to sulfate or elemental sulfur (Eq. 16).

$$CaCO_3 + H_2O \rightarrow Ca_2 + HCO_3^- + OH \quad (14)$$

$$H_2S + CO_3^{-2} \rightarrow HS + H_2CO_3 \quad (15)$$

$$HS + O_2 \rightarrow S \text{ or } SO_4 \quad (16)$$

Ionic interactions with COOH and OH groups (Eq. 6) could result in the formation of soluble $(K, Na)_2SO_4$ or less soluble ($CaSO_4$) forms (Xu, et al., 2014). The peak at 1158 cm^{-1} indicated the possible formation of SO_4^{2-}. This is consistent with the XRD data that showed the formation of $CaSO_4$ after the treatment with H_2S in all biochars. Moreover, SEM-EDX analysis showed that all biochars contained as much as 1.3% Ca and 2.1% K, which may combine with SO_4^{2-} to form K_2SO_4 and $CaSO_4$. Lee et al. (2002) suggested that impregnating biochar with basic hydroxide ions could significantly affect the degree of adsorptivity. According to Bagreev et al. (2001), NaOH impregnation on biochar shifts

the dissociation of H_2S forward and increase the HS^- ions, thus facilitating the oxidation (Eqs. (17), (18) and (16)).

$$MeOH + H_2S \rightarrow Me_2S + H_2O \quad (17)$$

$$MeHS + 1/2\ O2 \rightarrow HS + MeOH \quad (18)$$

$$HS + O_2 \rightarrow S \text{ or } SO_4 \quad (16)$$

4.8 Microbial Community Structure

4.8.1 Alpha Diversity

4.8.1.1 Species Diversity and Richness

Multivariate data analysis in microbial ecology analyze the relationship between microbial molecular diversity of bacterial communities under different environments. Data pretreatment including samples ID, sulfate concentration, reads, clean tags, number of sequences and GC can be seen in Table B.1. 16S ribosomal gene sequencing was used to assess the bacterial community composition and diversity changes within reactors before and after sulfide removal with biochar (Figure 4.13). The most abundant phyla in all reactors were *Firmicutes* (3 - 18%), *Bacteroidetes* (12 – 39%) and *Spirochaetes* (13 - 44%). These microorganisms are active during the hydrolysis of polysaccharides, acidogenesis and acetogenesis steps of anaerobic processes and are the major phyla found in anaerobic digestion systems (Raskin et al., 1996). The diversity of *Firmicutes* with a total of 45 different OTUs (34 assigned to *Clostridia*) was higher than the *Bacteroidetes* with only 29 OTUs. While *Bacteroidetes* were more resistant to sulfide,

Firmicutes were more sensitive and some OTUs disappeared (e.g., OTU_10, 16, 23, 29, 33, 36, 40, and 41). The fact that the reactors were dominated by *Bacteroidetes* and *Spirochaetes*, suggests that the resistant OTUs quickly adapted to increased sulfide concentration (Goux et al., 2015).

Given the interaction between MPA and SRB, as well as the competition for substrate, the relative abundance of MPA and SRB was further evaluated to better understand their effects in anaerobic treatment of sulfate-laden high strength wastewaters **(Figure 4.13).** Microbial community analyses of three reactors at 4000, 5000 and 6000 mg SO_4^{2-}/L before biochar use and at 6000 mg SO_4^{2-}/L after biochar treatment identified that the majority of SRB belong to genus *Desulfovibrio*, which has the highest affinity to sulfate among all SRB (Muyzer and Stams, 2008). The dominant methanogens were hydrogenotrophic methanogens associated to genus *Methanobacterium* (accounted for 71-93% of total archaea sequenced) that produce methane from either H_2/CO_2 or formate, and the mixotrophic *Methanosaeta* (3-29% of total archaea sequenced). *Methanobacterium* plays important role in methanogenesis because they tolerate high concentration of sulfate and VFAs, and are known to dominate and thrive in anaerobic environments. No acetoclastic methanogens *Methanosarcina* was identified in the reactors, which could be due to the fact that *Methanosarcina* are more sensitive to sulfide toxicity than hydrogenotrophic methanogens (Zabranska and Pokorna, 2017). Raskin et al. (1996) reported that, in general, *Methanosarcina* spp. has more favorable kinetic parameters (μmax, K, μmax/K, q_{max}, and minimum thresholds) than *Methanosaeta* spp., indicating that, under high sulfate level and low acetate concentrations, *Methanosaeta* spp. has a competitive advantage over *Methanosarcina* spp. These findings support the

findings of Franke-Whittle et al. (2014) who reported a syntrophic relationship between acetate oxidizers and hydrogenotrophic methanogens as the main pathway for acetate degradation and methane production in mesophilic reactors. Nevertheless, Goux et al. (2015) suggests that a shift from acetoclastic methanogenesis to syntrophic acetate oxidation coupled with hydrogenotrophic methanogenesis maintains process stability.

Figure 4.13 illustrates the relative abundances of the SRB and MPA during increments of sulfate loading and after biochar treatment at sulfate concentration of 6000 mg SO_4^{2-}/L. As the sulfate loading increased from 4000 to 5000 and then to 6000 mg SO_4^{2-}/L, relative abundance of SRB in R1 increased proportionally from 5% to 8% and then to 10% of total microbial sequences. Similar trends of increasing SRB population as sulfate loading increased were also experienced in other replicated reactors (Figure 4.13). This finding illustrated that SRB could rapidly adapt and grow in environment with excess sulfate, resulting in high H_2S released at higher sulfate concentration. Since SRB and MPA utilize same substrates (acetate and hydrogen as electron donors) and SRB have intrinsic kinetic and energetic advantages (Muyzer & Stams, 2008), high abundance of SRB could out-compete MPA, thereby suppressing MPA's growth and methane yield. This phenomenon was apparent in all reactors when influent sulfate was increased from 4000 to 6000 mg SO_4^{2-}/L. The relative abundance of SRB increased from 5 to 10%, 4 to 10% and 2 to 4%, in R1, R2 and R3, respectively while the relative abundance of MPA reduced from 2.4% to 0.7% in R1, 1.7% to 0.7% in R2 and 1.5% to 0.4% in R3. Several authors reported that a reduction in *Methanobacterium* species occurs due to the fact that SRB outcompete hydrogenotrophic methanogenic archaea for the available hydrogen (Jiménez et al., 2018; Muyzer & Stams, 2008). Concurrently methane yield decreased by

47% in R1, 33% in R2 and 41% in R3 (Figure 4.2). The drops in MPA population and methane production were also caused by the sulfide toxicity as H_2S in biogas reached 65,000 ppm, DS was 131.2 mg S/L with free sulfide of 54 mg S/L (Figure 4.2).

Simpson's index (Figure 4.13) was used to measure the biodiversity of a habitat taking into account the number of species present and their relative abundance. A lower Simpson's index (0.85) was observed at 6000 mg SO_4^{2-}/L before sulfide removal compared with >0.90 after sulfide removal with biochar in all reactors ($p=0.016$). The index value may have changed in response to disturbances in the reactors caused by sulfide toxicity. VFAs accumulation and reduction of pH are reported to contribute to a decrease in richness and diversity of the archaeal community (Goux et al., 2015), hence the lower index value at 6000 mg SO_4^{2-}/L before sulfide removal.

After the removal of H_2S by biochar, the relative abundance of MPA increased from 0.7% to 3.7% in R1, 0.7% to 2.2% in R2 and 0.4% to 2.2% in R3, while the relative abundance of SRB decreased from 9.3% to 6.3% in R1, 9.1% to 1.7% in R2 and 4% to 0.5% in R3 (Figure 4.13). Simultaneously methane yield increased from 63.5±3.5, 73.5±1.5 and 75.3±4.6 N mL/$gCOD_{removed}$ to 158.2±2.6, 121.5±1.2 and 154.3±1.69 N mL/$gCOD_{removed}$ in R1, R2 and R3 respectively, indicating the anaerobic treatment was quickly recovered. The aforementioned results indicate that biochar could effectively capture H_2S from biogas, thereby alleviating sulfide toxicity to methanogens and sulfate reducing bacteria and promote the stability of the anaerobic process.

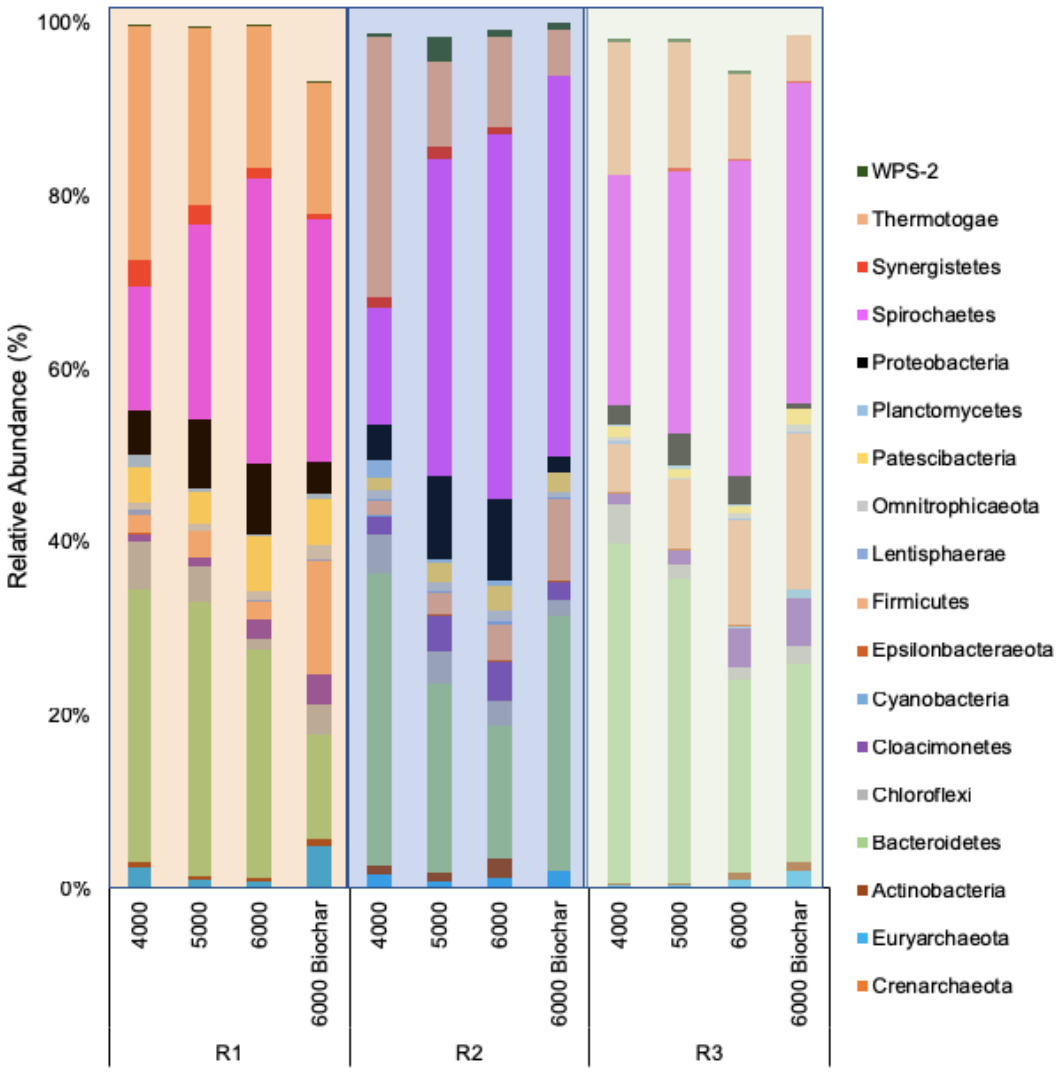
100%
80%
60%
40%
20%
0%
Relative Abundance (%)
4000
5000
6000
6000 Biochar
R1
R2
R3
WPS-2
Thermotogae
Synergistetes
Spirochaetes
Proteobacteria
Planctomycetes
Patescibacteria
Omnitrophicaeota
Lentisphaerae
Firmicutes
Epsilonbacteraeota
Cyanobacteria
Cloacimonetes
Chloroflexi
Bacteroidetes
Actinobacteria
Euryarchaeota
Crenarchaeota

(b)

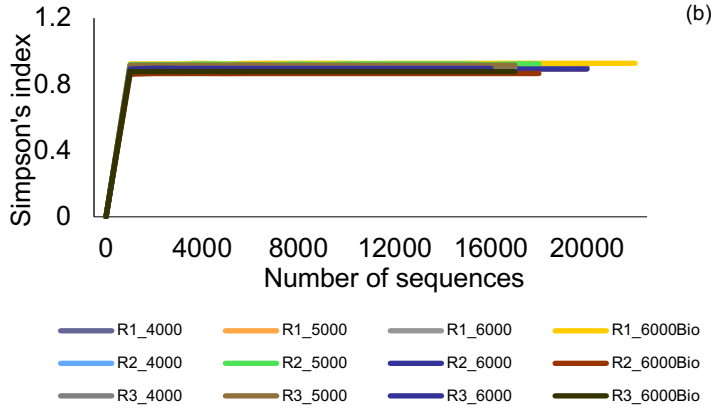
1.2
0.8
0.4
0
Simpson's index
0
4000
8000
12000
16000
20000
Number of sequences
R1_4000
R1_5000
R1_6000
R1_6000Bio
R2_4000
R2_5000
R2_6000
R2_6000Bio
R3_4000
R3_5000
R3_6000
R3_6000Bio

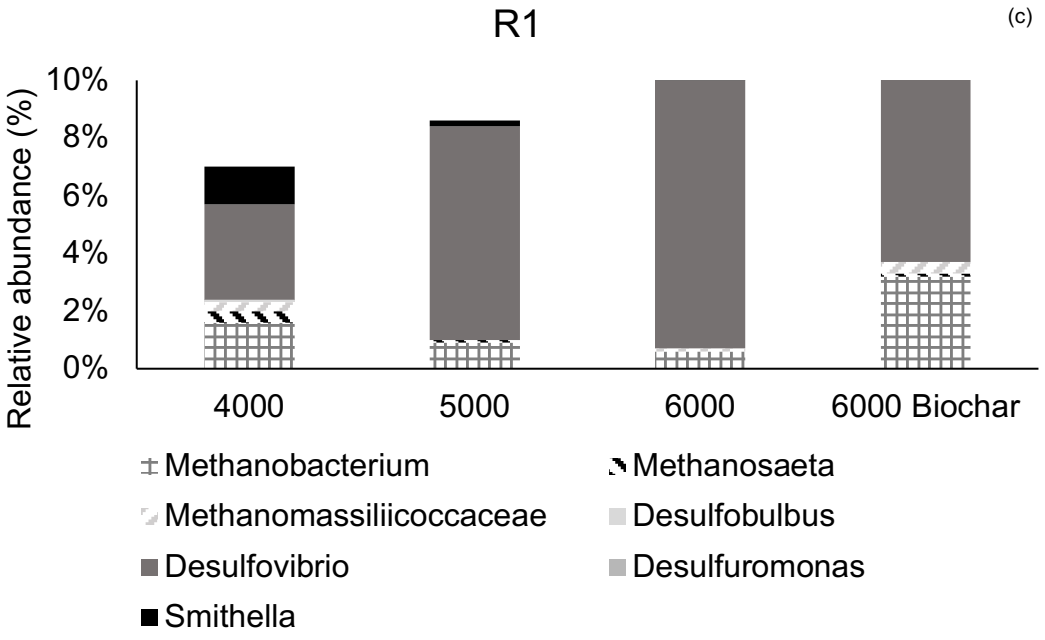
R1
(c)
Relative abundance (%)
10%
8%
6%
4%
2%
0%
4000
5000
6000
6000 Biochar
Methanobacterium
Methanosaeta
Methanomassiliicoccaceae
Desulfobulbus
Desulfovibrio
Desulfuromonas
Smithella

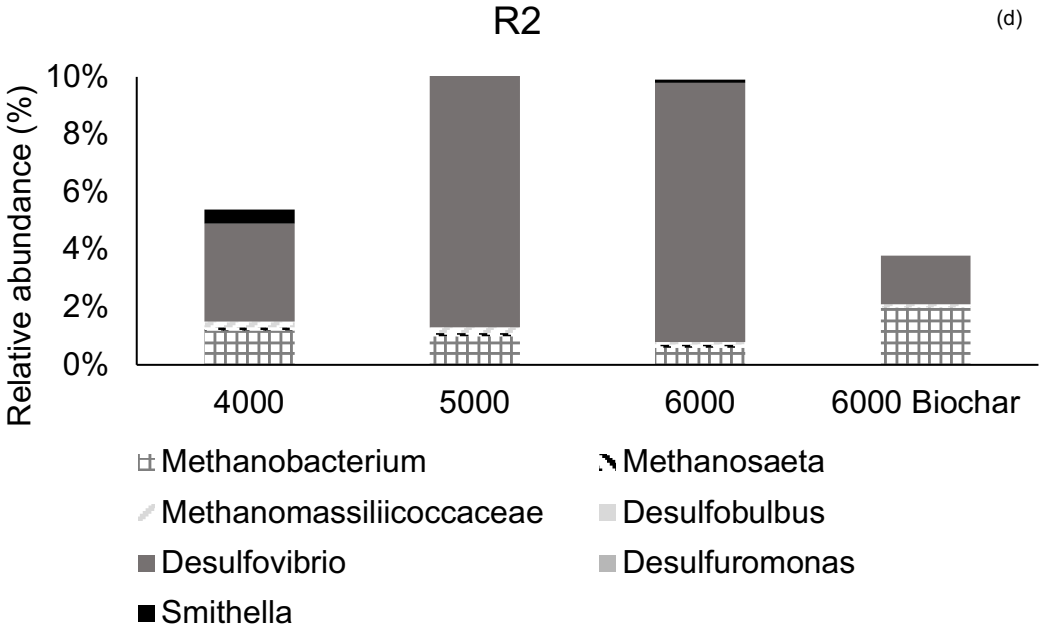
R2
(d)
Relative abundance (%)
10%
8%
6%
4%
2%
0%
4000
5000
6000
6000 Biochar
Methanobacterium
Methanosaeta
Methanomassiliicoccaceae
Desulfobulbus
Desulfovibrio
Desulfuromonas
Smithella

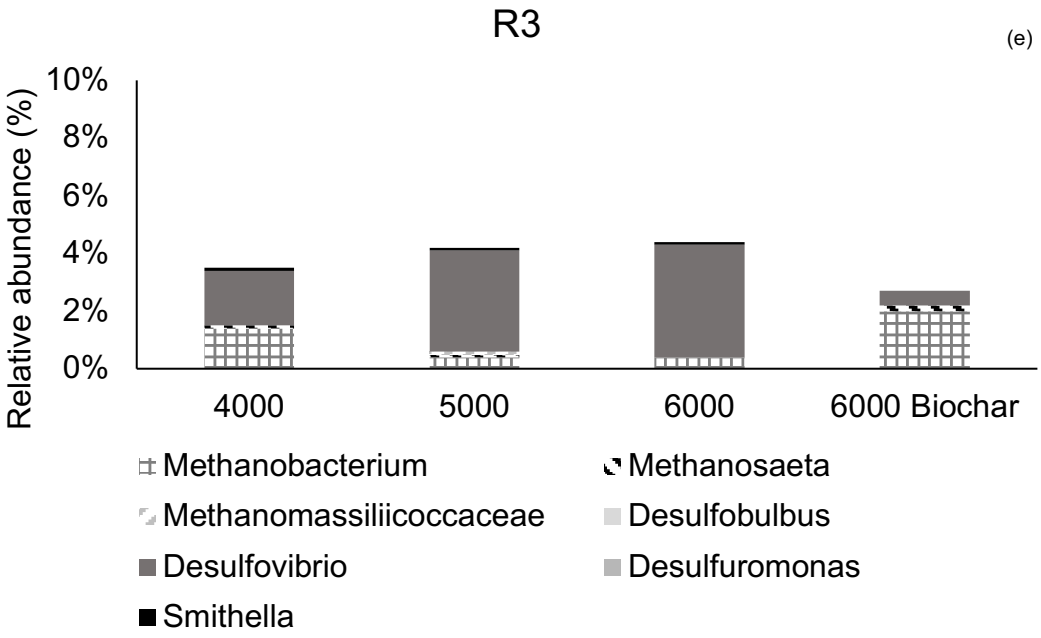

Figure 4.13: Alpha diversity. (a) Relative abundance (%) at the genus level in R1, R3 and R3, (b) Simpson's index. Relative abundance of MPA and SRB while increasing the sulfate concentration from 4000 to 6000 mg SO_4^{2-}/L before using biochar and at 6000 mgSO_4^{2-}/L after biochar treatment in (c) R1, (d) R2 and (e) R3.

4.8.2 Beta Diversity

4.8.2.1 Non-metric Multidimensional Scaling (NMDS)

The beta diversity of the archaeal and bacterial communities was presented in a non-metric multidimensional scaling (NMDS) analysis based on the unweighted UniFrac

distances (Figure 4.14). Two distinct clusters were identified, (i) containing similarity of microbial abundance of all species while increasing sulfate concentration to 4000, 5000 and 6000 mg SO_4^{2-}/L within reactors R1, R2 and R3 (cluster 1) and (ii) similarity of microbial abundance of all species after H_2S removal in R1, R2 and R3 (cluster 2). As can be seen in Figure 4.14, our results revealed that microbial communities structure and diversity in anaerobic reactors changed under environmental disturbances. Therefore, the balance in RA between MPA and SRB have direct effect in the degradation of substrates and methane production, thus the performance of anaerobic reactor and the efficiency of the wastewater treatment.

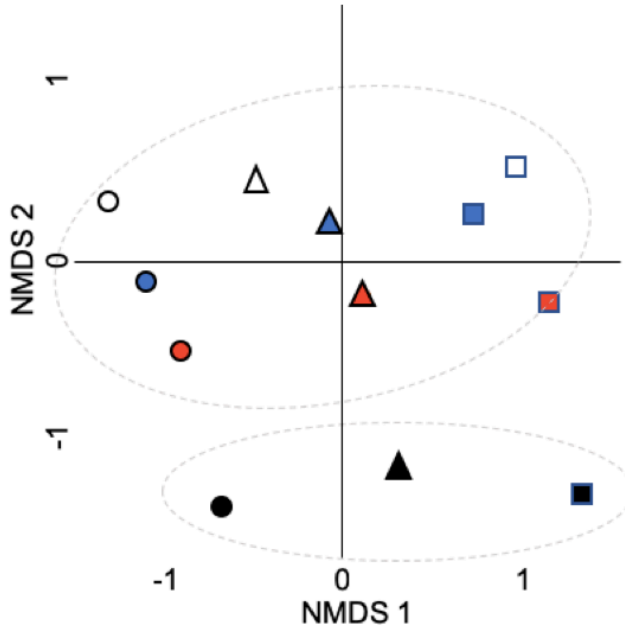

Reactor	Sulfate concentration (mg SO_4^{2-}/L) before biochar			Sulfate concentration (mg SO_4^{2-}/L) after biochar
	4000	5000	6000	6000
R1	○	●	●	●
R2	△	▲	▲	▲
R3	□	■	■	■

Figure 4.14: Beta diversity. NMDS biplot of unweighted Unifrac distance metrics based

on the taxonomic similarities between samples at genus level. Different symbols and colors are used for different reactors (R1, R2 and R3) at increasing sulfate concentration to 4000, 5000 and 6000 mg SO_4^{2-}/L and at 6000 mg SO_4^{2-}/L after biochar treatment to remove H_2S. Stress: 0.109.

CHAPTER 5

ENGINEERING APPLICATION

An innovative decentralized anaerobic treatment system for sulfate laden industrial wastewater was developed in this study. Robustness and ability to quickly recover under stress situations were the main parameters this study focused on. The use of perforated propylene plates to space out the recycled tire beads (media) throughout reactor height demonstrated no effect when compared with the reactor without their use. Moreover, the use of recycled tire beads itself showed to be an affordable and efficient way to create a biofilm for microorganisms attachment and prevention of biomass wash out. Major challenge encountered in high strength wastewater in AD systems is the removal of H_2S from the biogas produced that results in increasing costs with continuous upkeep and maintenance (Robert and Bowker, 1991) and inhibition of microbial activity, thereby reducing biogas production. The advantages of using biochar over activated carbon is that it dispenses activation and/ or regeneration, hence, reducing costs of production, reuse and disposal. Moreover, biochar production demands 15 times less energy than activated carbon and has less global warming potential as shown in Table 5.1. Biochar can be applied to land as a fertilizer after biogas purification processes, hence avoiding costs with regeneration or disposal.

Table 5.1: Energy demand and global warming potential of biochar and activated carbon (Alhashimi & Aktas, 2017).

	Activated Carbon	Biochar
Cost of Production (USD/Kg)	1.44	0.58
Energy demand (MJ/kg)	97	6.1
Emissions (kg CO_{2eq}/kg)	6.6	-0.9

Recently, there has been a significant concern of deficiency of micro-nutrient, especially sulfur, resulting in steadily declined crop yield in watersheds across the eastern United States (David et al., 2016). Most fertilizers contain little sulfur for plant uptake, hence application of sulfur will be necessary to maintain crop yield in the future. Thus, sulfur-rich biochar would provide a new opportunity as a source of micro-nutrient in sulfur deficient soils. This is a more sustainable alternative that reuses organic waste, minimize waste production and reduce safety threats concerns related to H_2S production.

Scaling up the packed bed column

The AD process was integrated with a biochar-packed column for sulfide removal. The distinct characteristics of each biochar produced resulted in different sulfide adsorption capacities. By increasing the temperature of production, biochar loses oxygen functional groups that are directly related to adsorption capacities.

Typical biochar size range of 1 to 2 mm. The empty bed contact time (EBCT) and linear velocity are the main parameter to be followed to scale up a packed bed column. Usually the EBCT is between 3 and 15 minutes and linear velocity range between 5 and 20 m/h.

Contact time (minute)= $\frac{carbon\ volume\ (m3)*60(\frac{min}{h})}{flow\ rate\ (\frac{L}{h})}$

Linear velocity (m/h)= $\frac{flow\ rate\ (L/h)}{surface\ area\ (m2)}$

Assuming an EBCT of 3 minutes, column diameter of 5 cm and a linear velocity of 10 m/h to avoid pressure drop in the bed, we have the surface area of 19.6 cm2 and the flow rate of 19.6 L/h. If the ratio of biochar bed/column diameter is assumed to be 10, then the height of carbon bed is 55 cm. The pressure drop in the column helps to determine the column height. Using info from a supplier Chemivron Carbon, under a bed height of 55 cm and linear velocity of 10 m/h the total pressure drop in biochar is 16.5 mbar and column height is 60 cm.

Biogas Energy

Assuming the production of 1000 m^3/day with 60% of CH_4, and considering that each cubic meter of biogas contains the equivalent of 6 kWh of heat energy or 2kWh of electrical power, there is a production of 2000 kWh/day of electrical power. In the US, the average daily consumption for a residential utility customer is 30 kWh.

CHAPTER 6

CONCLUSIONS

The reactors with biofilm formation (R1, R2 and R3) facilitated immobilization of microbes in which resulted in higher COD loading rates at shorter HRT (~10 days) and better process stability than the reactor without support media (R4). No evidence of sulfide toxicity was observed up to sulfate concentration of 5000 mg SO_4^{2-}/L when the mean TOC removal efficiency was >90% in all reactors. Under sulfate influent of 6000 mg SO_4^{2-}/L, a rapid drop in pH to as low as 5.0 was observed in all reactors with concomitant increase in effluent total VFA and TOC concentrations to 3500±47 mg HAc/L and 2486±106 mg/L respectively and an increase in dissolved sulfides up to 131±0.6 mg S/L, resulting in the inhibition of the methanogens as apparent from decrease in methane yields in R1, R2 and R3. Upon integrating biochar columns with anaerobic reactors, sulfide was rapidly removed with removal efficiencies >98% of gaseous H_2S, 94% of DS and 89% of free sulfide, thereby alleviating sulfide toxicity to methanogens and sulfate reducing bacteria and promoting the stability of the anaerobic process. While biochar produced under lower temperature (550 ^oC) implied a higher adsorption capacity than at higher temperature (800 ^oC), biochars showed similar trend in terms of reactor performance with no significant difference. 16S rRNA was used to identify and classify the bacteria and archaea relative abundance in the reactors under sulfate concentrations and after sulfide removal. It is demonstrated that methanogens and sulfate reducing bacteria play major role in the performance and stability of anaerobic reactors and

environmental disturbances promote the unbalance of those species. The results reported here are the first to describe the effects of hydrogen sulfide removal by biochar on microbial communities structure in anaerobic treatment of sufate-rich wastewater.

CHAPTER 7

FUTURE WORK

Biochar has demonstrated excellent amendment properties such as such as improving soil texture; water holding capacity, cationic exchange capacity, formation of soil aggregates, and reducing nutrient leaching from soils (Lehmann and Joseph, 2015). Recently, there has been a significant concern of deficiency of micro-nutrient, especially sulfur, resulting in steadily declined crop yield in watersheds across the eastern United States (David et al., 2016). Most fertilizers contain little sulfur for plant uptake, hence application of sulfur will be necessary to maintain crop yield in the future. Thus, sulfur-rich biochar would provide a new opportunity as a source of micro-nutrient in sulfur deficient soils. However, research on bioavailability of S for plants from S-biochar (as S fertilizer) are lacking. Besides, studies on S-deficient soils and high S-demanding plants are required to estimate S-biochar characteristics to apply into soil as efficient S-fertilizer. Field application of biochars have wide characteristics, much of which are yet to be comprehensively understood, especially into soils with the potential to seize these nutrients efficiently.

CHAPTER 8

REFERENCES

Acharya, B., Dutta, A., Mahmud, S., Tushar, M., & Leon, M. (2014). Ash analysis of poultry Litter , willow and oats for combustion in boilers. Jornal of Biomass to Bioefuel, 1, 16-26.

Agriculture, M., Box, P. O., & Winsley, P. (2007). Biochar and bioenergy production for climate change mitigation. Science And Technology, 64(1), 5–10.

Ahmad, M., Upamali, A., Eun, J., Zhang, M., Bolan, N., Mohan, D., … Sik, Y. (2014). Biochar as a sorbent for contaminant management in soil and water : A review. Chemosphere, 99, 19–33.

Alhashimi, H. A., & Aktas, C. B. (2017). Life cycle environmental and economic performance of biochar compared with activated carbon: a meta-analysis. Resources, Conservation and Recycling, 118, 13–26.

Anca-Couce, A., & Obernberger, I. (2016). Application of a detailed biomass pyrolysis kinetic scheme to hardwood and softwood torrefaction. Fuel, 167, 158-167.

Apha, A. (2005). Wpcf. Standard Methods for the Examination of Water and Wastewater, 20.

Atkinson, C. J., Fitzgerald, J. D., & Hipps, N. A. (2010). Potential mechanisms for achieving agricultural benefits from biochar application to temperate soils : a review. Plant and Soil 337(1-2), 1-18.

Bagreev, A., Bandosz, T. J., & Locke, D. C. (2001). Pore structure and surface chemistry of adsorbents obtained by pyrolysis of sewage sludge-derived fertilizer. Carbon,

39(13), 1971–1979.

Barton, L. L., & Fauque, G. D. (2009). Biochemistry, physiology and biotechnology of sulfate-reducing bacteria. Advances in Applied Microbiology, 68, 41–98.

Batista, E. M. C. C., Shultz, J., Matos, T. T. S., Fornari, M. R., Ferreira, T. M., Szpoganicz, B., … Mangrich, A. S. (2018). Effect of surface and porosity of biochar on water holding capacity aiming indirectly at preservation of the Amazon biome. Scientific Reports, 8(1), 1–9.

Bhattacharya, S. K., Uberoi, V., & Dronamraju, M. M. (1996). Interaction between acetate fed sulfate reducers and methanogens. Water Research, 30(10), 2239–2246.

Brennan, J. K., Bandosz, T. J., Thomson, K. T., & Gubbins, K. E. (2001). Water in porous carbons. Colloids and Surfaces A: Physicochemical and Engineering Aspects, 187, 539–568.

Brewer, C. E., Hu, Y., Schmidt-rohr, K., Loynachan, T. E., Laird, D. A., & Brown, R. C. (2012). Extent of pyrolysis impacts on fast pyrolysis biochar properties. Journal of Environmental Quality, 41(4), 1115-1112.

Bruun, E. W., Ambus, P., Egsgaard, H., & Hauggaard-nielsen, H. (2012). Effects of slow and fast pyrolysis biochar on soil C and N turnover dynamics. Soil Biology and Biochemistry, 46, 73–79.

Budarin, V. L., Clark, J. H., Lanigan, B. A., Shuttleworth, P., Breeden, S. W., Wilson, A. J., … Ross, A. (2009). The preparation of high-grade bio-oils through the controlled, low temperature microwave activation of wheat straw. Bioresource Technology, 100(23), 6064–6068.

Cantrell, K. B., Hunt, P. G., Uchimiya, M., Novak, J. M., & Ro, K. S. (2012). Impact of

pyrolysis temperature and manure source on physicochemical characteristics of biochar. Bioresource Technology, 107, 419–428.

Cayuela, M. L., van Zwieten, L., Singh, B. P., Jeffery, S., Roig, A., & Sánchez-monedero, M. A. (2014). Agriculture , ecosystems and environment biochar ' s role in mitigating soil nitrous oxide emissions : A review and meta-analysis. Agriculture, Ecosystems and Environment,191, 5–16.

Champagne, P. (2007). Feasibility of producing bio-ethanol from waste residues: A Canadian perspective: Feasibility of producing bio-ethanol from waste residues in Canada. Resources, Conservation and Recycling, 50(3), 211–230.

Chen, S., Kincaid, R. L., Harrison, J. H., Elliott, D. C., & Brown, M. D. (2003). Value-added chemicals from animal manure. Pacific Northwest National Lab., Richland, WA (US), Environmental Molecular Sciences Laboratory (US).

Chowdhary, P., More, N., Raj, A., & Bharagava, R. N. (2017). Characterization and identification of bacterial pathogens from treated tannery wastewater. Microbiol Res Int, 5(3), 30–36.

Cox, J., Downie, A., Jenkins, A., Hickey, A., Lines-Kelly, R., McClintock, A., … van Zwieten, L. (2012). Biochar in horticulture: prospects for the use of biochar in Australian horticulture. NSW Department of Primary Industries, 104. Retrieved from http://www.dpi.nsw.gov.au/__data/assets/pdf_file/0008/447857/DPI-BioChar-in-Horticulture.pdf

Crombie, K., Masek, O., Sohi, S. P., Brownsort, P., & Cross, A. (2013). The effect of pyrolysis conditions on biochar stability as determined by three methods. GCB Bioenergy, 5(2), 122–131.

Demirbas, A. (2004). Effects of temperature and particle size on bio-char yield from pyrolysis of agricultural residues. Journal of Analytical and Applied Pyrolysis, 72(2), 243–248.

Edwards, P. (1998). Sulfur cycling, retention, and mobility in soils: a review. General Technical Report, NE-250, Radnor, PA: US Department of Agriculture, Forest Service, Northeastern Research Station. 18p., 250. Retrieved from http://www.fs.fed.us/ne/newtown_square/publications/technical_reports/pdfs/1998/gtrne250.pdf

Feng, W., Kwon, S., Borguet, E., & Vidic, R. (2005). Adsorption of hydrogen sulfide onto activated carbon fibers: effect of pore structure and surface chemistry. Environmental Science & Technology, 39(24), 9744–9749.

Fidel, R. B., Laird, D. A., & Spokas, K. A. (2018). Sorption of ammonium and nitrate to biochars is electrostatic and pH-dependent. Scientific Reports, *8*(1), 17627.

Fito, J., Tefera, N., & Van Hulle, S. W. H. (2019). Sugarcane biorefineries wastewater: bioremediation technologies for environmental sustainability. Chemical and Biological Technologies in Agriculture, 6(1), 6.

Franke-Whittle, I. H., Walter, A., Ebner, C., & Insam, H. (2014). Investigation into the effect of high concentrations of volatile fatty acids in anaerobic digestion on methanogenic communities. Waste Management, 34(11), 2080–2089.

Goux, X., Calusinska, M., Lemaigre, S., Marynowska, M., Klocke, M., Udelhoven, T., … Delfosse, P. (2015). Microbial community dynamics in replicate anaerobic digesters exposed sequentially to increasing organic loading rate, acidosis, and process recovery. Biotechnology for Biofuels, 8(1), 122.

Gul, S., Whalen, J. K., Thomas, B. W., Sachdeva, V., & Deng, H. (2015). Physico-chemical properties and microbial responses in biochar-amended soils: Mechanisms and future directions. Agriculture, Ecosystems and Environment, *206*, 46–59.

Herbert, L., Hosek, I., Kripalani, R., & Vanasupa, L. (2012). The characterization and comparison of biochar produced from a decentralized reactor using forced air and natural draft pyrolysis, (June), 1–35.

Inyang, M., Gao, B., Yao, Y., Xue, Y., & Zimmerman, A. R. (2012). Removal of heavy metals from aqueous solution by biochars derived from anaerobically digested biomass. Bioresource Technology, *110*, 50–56.

Jang, H. M., Yoo, S., Choi, Y. K., Park, S., & Kan, E. (2018). Adsorption isotherm, kinetic modeling and mechanism of tetracycline on Pinus taeda-derived activated biochar. Bioresource Technology, 259, 24–31.

Jiménez, J., Barrera, E. L., De Vrieze, J., Boon, N., DeMeester, S., Spanjers, H., … Dewulf, J. (2018). Microbial community dynamics reflect reactor stability during the anaerobic digestion of a very high strength and sulfate-rich vinasse. Journal of Chemical Technology & Biotechnology, 93(4), 975–984.

Kambo, H. S., & Dutta, A. (2015). A comparative review of biochar and hydrochar in terms of production , physico-chemical properties and applications. Renewable and Sustainable Energy Reviews, 45, 359–378.

Kanjanarong, J., Giri, B. S., Jaisi, D. P., Oliveira, F. R., Boonsawang, P., Chaiprapat, S., … Khanal, S. K. (2017). Removal of hydrogen sulfide generated during anaerobic treatment of sulfate-laden wastewater using biochar: Evaluation of efficiency and mechanisms. Bioresource Technology, 234(2016), 115–121.

Khanal, S. K., & Huang, J.-C. (2005). Effect of High Influent Sulfate on Anaerobic Wastewater Treatment. Water Environment Research, *77*(7), 3037–3046.

Khanal, S. K., & Huang, J. (2003). ORP-based oxygenation for sulfide control in anaerobic treatment of high-sulfate wastewater. Water Research, *37(9)*, 2053–2062.

Kim, D., Yoshikawa, K., & Park, K. Y. (2015). Characteristics of biochar obtained by hydrothermal carbonization of cellulose for renewable energy. Energies, *8*(12), 14040–14048.

Kolk, van der, Zwart, K. B., & W, H. J. (2013). Pyrolysis in the countries of the North Sea region: potentially available quantities of biomass waste for biochar production. Interreg IVB Project Biochar.

Laird, D., Rogovska, N., Garcia-Perez, M., Collins, H., Streubel, J., & Smith, M. (2011). Chapter 16 Pyrolysis and biochar- opportunities for distributed production and soil quality enhancement. *Production,* 257–281.

Lee, D., Owens, V. N., Boe, A., & Jeranyama. (2007). Composition of herbaceous biomass feedstocks. North Central Sun Grant Center, South Dakota State University.

Lee, Y.-W., Choi, D.-K., & Park, J.-W. (2002). Characteristics of NO x adsorption and surface chemistry on impregnated activated carbon. Separation Science and Technology, 37(4), 937–956.

Lehmann, J., & Joseph, S. (2015). Biochar for environmental management: science, technology and implementation. Routledge.

Li, Y., & Khanal, S. K. (2016). Bioenergy: principles and applications. John Wiley & Sons.

Liang, B., Lehmann, J., Solomon, D., Kinyangi, J., Grossman, J., O'Neill, B., … Neves, E. G. (2006). Black carbon increases cation exchange capacity in soils. Soil Science

Society of America Journal, 70(5), 1719.

Lin, Y., Munroe, P., Joseph, S., Ziolkowski, A., Zwieten, L. Van, Kimber, S., & Rust, J. (2013). Chemical and structural analysis of enhanced biochars : thermally treated mixtures of biochar, chicken litter, clay and minerals. Chemosphere, *91(1)*, 35–40.

Liu, Z. G., & Balasubramanian, R. (2012). Hydrothermal carbonization of waste biomass for energy generation. Seventh International Conference on Waste Management and Technology (Icwmt 7), 16, 159–166.

Liu, Z., Maszenan, A. M., Liu, Y., & Ng, W. J. (2015). A brief review on possible approaches towards controlling sulfate-reducing bacteria (SRB) in wastewater treatment systems. Desalination and Water Treatment, *53*(10), 2799–2807.

Lu, K., Yang, X., Shen, J., Robinson, B., Huang, H., Liu, D., … Wang, H. (2014). Effect of bamboo and rice straw biochars on the bioavailability of Cd , Cu , Pb and Zn to Sedum plumbizincicola. Agriculture, Ecosystems and Environment *191*, 124–132.

Metcalf & Eddy, I. (1972). Wastewater Engineering. McGraw-Hill.

Mitchell, S. M., Subbiah, M., Ullman, J. L., Frear, C., & Call, D. R. (2015). Evaluation of 27 different biochars for potential sequestration of antibiotic residues in food animal production environments. Journal of Environmental Chemical Engineering *3*, 162–169.

Mohamed, B. A., Kim, C. S., Ellis, N., & Bi, X. (2016). Microwave-assisted catalytic pyrolysis of switchgrass for improving bio-oil and biochar properties. Bioresource Technology, 201, 121–132.

Muniraj, I. K., Xiao, L., Hu, Z., Zhan, X., & Shi, J. (2013). Microbial lipid production from potato processing wastewater using oleaginous filamentous fungi Aspergillus

oryzae. Water Research, *47*(10), 3477–3483.

Muyzer, G., & Stams, A. J. M. (2008). The ecology and biotechnology of sulphate-reducing bacteria. Nature Reviews Microbiology, *6*(6), 441–454.

Novak, J., Lima, I., Xing, B., Gaskin, J., Steiner, C., Das, K., … H, S. (2009). Characterization of designer biochar produced at different temperatures and their effects on a loamy sand. Annals ofEnvironmental Science, *3*, 195–206.

O'Flaherty, V., Mahony, T., O'Kennedy, R., & Colleran, E. (1998). Effect of pH on growth kinetics and sulphide toxicity thresholds of a range of methanogenic, syntrophic and sulphate-reducing bacteria. Process Biochemistry, 33(5), 555–569.

Oliveira, F. R., Patel, A. K., Jaisi, D. P., Adhikari, S., Lu, H., & Khanal, S. K. (2017). Environmental application of biochar: Current status and perspectives. Bioresource Technology, *246*, 110–122.

Patel, H. (2019). Fixed-bed column adsorption study: a comprehensive review. Applied Water Science, *9*(3), 45.

Plugge, C. M., Zhang, W., Scholten, J. C. M., & Stams, A. J. M. (2011). Metabolic flexibility of sulfate-reducing bacteria. Frontiers in Microbiology, *2*, 1–8.

Pokorna, D., & Zabranska, J. (2015). Sulfur-oxidizing bacteria in environmental technology. Biotechnology Advances, *33*(6), 1246–1259.

Pol, L. W. H., Lens, P. N. L., Stams, A. J. M., & Lettinga, G. (1998). Anaerobic treatment of sulphate-rich wastewaters. Biodegradation, *9*(182655), 213–224.

Qureshi, N., Annous, B. A., Ezeji, T. C., Karcher, P., & Maddox, I. S. (2005). Biofilm reactors for industrial bioconversion process: Employing potential of enhanced reaction rates. Microbial Cell Factories, *4*, 1–21.

Rafiq, M. K., Bachmann, R. T., Rafiq, M. T., Shang, Z., Joseph, S., & Long, R. L. (2016). Influence of pyrolysis temperature on physico-chemical properties of corn stover (zea mays l.) biochar and feasibility for carbon capture and energy balance. PLoS ONE, *11*(6), 1–17.

Raskin, L., Rittmann, B. E., & Stahl, D. A. (1996). Competition and coexistence of sulfate-reducing and methanogenic populations in anaerobic biofilms. Appl. Environ. Microbiol., 62(10), 3847–3857.

Robati, D. (2013). Pseudo-second-order kinetic equations for modeling adsorption systems for removal of lead ions using multi-walled carbon nanotube. Journal of Nanostructure in Chemistry, 3(1), 55.

Thauer, R. K., Jungermann, K., & Decker, K. (1977). Energy conservation in chemotrophic anaerobic bacteria. Bacteriological Reviews, *40*(1), 100–181.

Sethupathi, S., Zhang, M., Rajapaksha, A. U., Lee, S. R., Nor, N. M., Mohamed, A. R., … Ok, Y. S. (2017). Biochars as potential adsorbers of CH4, CO2and H2S. Sustainability (Switzerland), 9(1), 1–10. h

Shang, G., Li, Q., Liu, L., Chen, P., & Huang, X. (2016). Adsorption of hydrogen sulfide by biochars derived from pyrolysis of different agricultural/forestry wastes. Journal of the Air and Waste Management Association.

Shang, G., Shen, G., Liu, L., Chen, Q., & Xu, Z. (2013). Kinetics and mechanisms of hydrogen sulfide adsorption by biochars. Bioresource Technology, 133, 495–499.

Sohi, S., Lopez-Capel, E., Krull, E., & Bol, R. (2009). Biochar, Climate Change and Soil: A Review to Guide Future Research. CSIRO Land and Water Science Report 5, no 09:17-31.

Spokas, K. A., Cantrell, K. B., Novak, J. M., Archer, D. W., Ippolito, J. A., Collins, H. P., … Nichols, K. A. (2012). Biochar: a synthesis of its agronomic impact beyond carbon sequestration. *J*ournal of Environmental Quality, 41(4), 973–989.

Standard, A. (2002). ASTM standards-D5142-04 standard test methods for proximate analysis of the analysis sample of coal and coke by instrumental procedures. Annual Book of ASTM Standards, Section, 5.

Suliman, W., Harsh, J. B., Abu-lail, N. I., Fortuna, A., Dallmeyer, I., & Garcia-perez, M. (2016). Biomass and bioenergy influence of feedstock source and pyrolysis temperature on biochar bulk and surface properties. Biomass and Bioenergy, 84, 37–48.

Sun, W., Xu, M., Xia, C., Li, A., & Sun, G. (2013). Enhanced production of laccase by Coriolus hirsutus using molasses distillery wastewater. Frontiers of Environmental Science & Engineering, 7(2), 200–210.

Tu, D., Dong, H., & Shang, B. (2008). Pyrolysis behavior of selected manures using TG-FTIR techniques, (701).

Tumuluru, J., Sokhansanj, S., Hess, J. R., Wright, C. T., & Boardman, R. D. (2011). A review on biomass torrefaction process and product properties for energy applications. Industrial Biotechnology, 7(5), 384–401.

van den Brand, T. P. H., Roest, K., Chen, G. H., Brdjanovic, D., & van Loosdrecht, M. C. M. (2015). Occurrence and activity of sulphate reducing bacteria in aerobic activated sludge systems. World Journal of Microbiology and Biotechnology, 31(3), 507–516.

Wang, K., He, C., You, S., Liu, W., Wang, W., Zhang, R., … Ren, N. (2015). Transformation of organic matters in animal wastes during composting. Journal of

Hazardous Materials, 300, 745–753.

Webber, J. B. W., Corbett, P., Semple, K. T., Ogbonnaya, U., Teel, W. S., Masiello, C. A., … Hu, Q. (2013). Microporous and Mesoporous Materials An NMR study of porous rock and biochar containing organic material. Microporous and Mesoporous Materials, 178, 94–98.

Willems, W., & Militz, H. (2013). Thermal wood modification chemistry analyzed using van Krevelen's representation. International Wood Products Journal, 4(3), 166-171.

Windeatt, J. H., Ross, A. B., Williams, P. T., Forster, P. M., Nahil, M. A., & Singh, S. (2014). Characteristics of biochars from crop residues: Potential for carbon sequestration and soil amendment. Journal of Environmental Management, *146*, 189–197.

Xu, X., Cao, X., Zhao, L., & Sun, T. (2014). Comparison of sewage sludge- and pig manure-derived biochars for hydrogen sulfide removal. Chemosphere, 111, 296–303.

Yongsiri, C., Vollertsen, J., & Hvitved-Jacobsen, T. (2004). Effect of temperature on air-water transfer of hydrogen sulfide. *Journal of Environmental Engineering*, *130*(1), 104–109.

Yu, H.-Q., Zhao, Q.-B., & Tang, Y. (2006). Anaerobic treatment of winery wastewater using laboratory-scale multi-and single-fed filters at ambient temperatures. Process Biochemistry, 41(12), 2477–2481.

Yu, H. Q., Zhao, Q. B., & Tang, Y. (2006). Anaerobic treatment of winery wastewater using laboratory-scale multi- and single-fed filters at ambient temperatures. Process Biochemistry, 41(12), 2477–2481.

Zambon, I., Colosimo, F., Monarca, D., Cecchini, M., Gallucci, F., Proto, A. R., … Colantoni, A. (2016). An innovative agro-forestry supply chain for residual biomass: Physicochemical characterisation of biochar from olive and hazelnut pellets. Energies, 9(7), 1–11.

Zhao, S. X., Ta, N., & Wang, X. D. (2017). Effect of temperature on the structural and physicochemical properties of biochar with apple tree branches as feedstock material. Energies, 10(9).

APPENDIX A

PHOTOGRAPHS OF THE EXPERIMENTAL SET UP, BIOCHAR, AND SET UP

A.1 Pictures of experimental set up

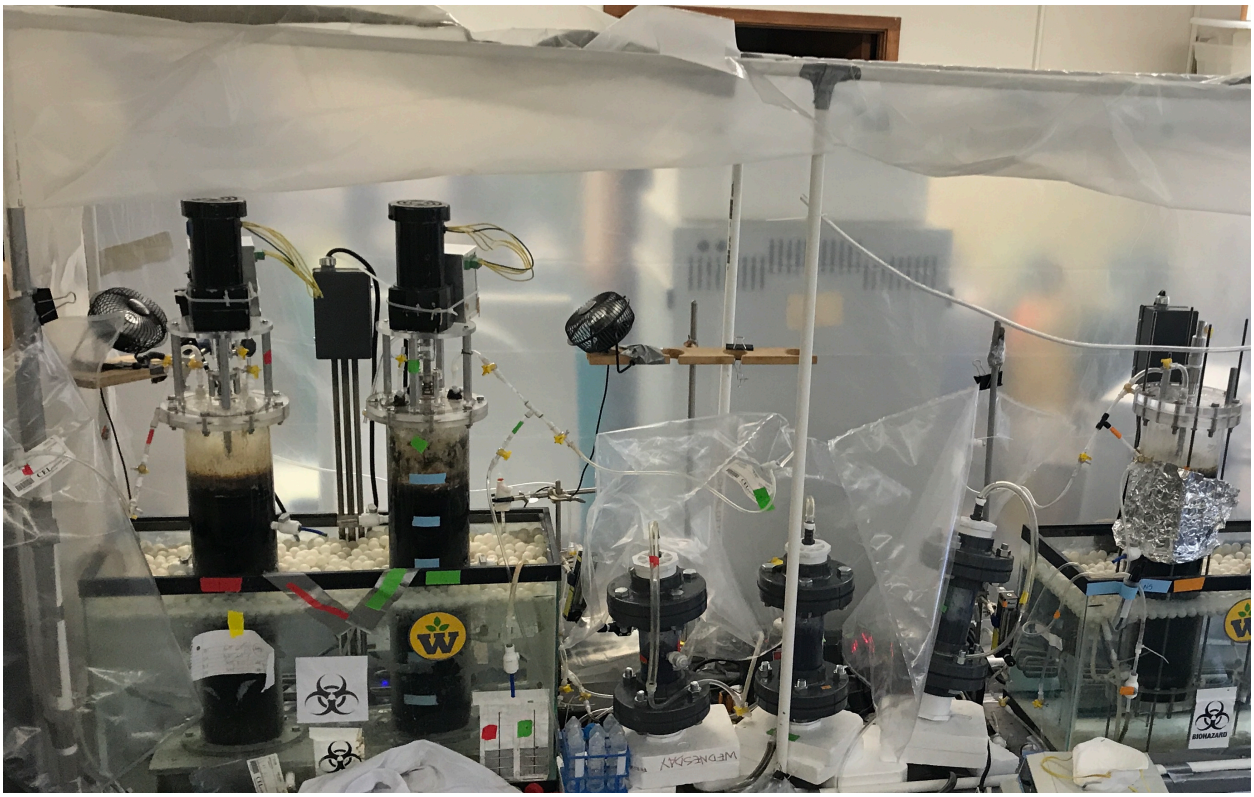
BIOHAZARD

A.2 Reactors R1 and R2

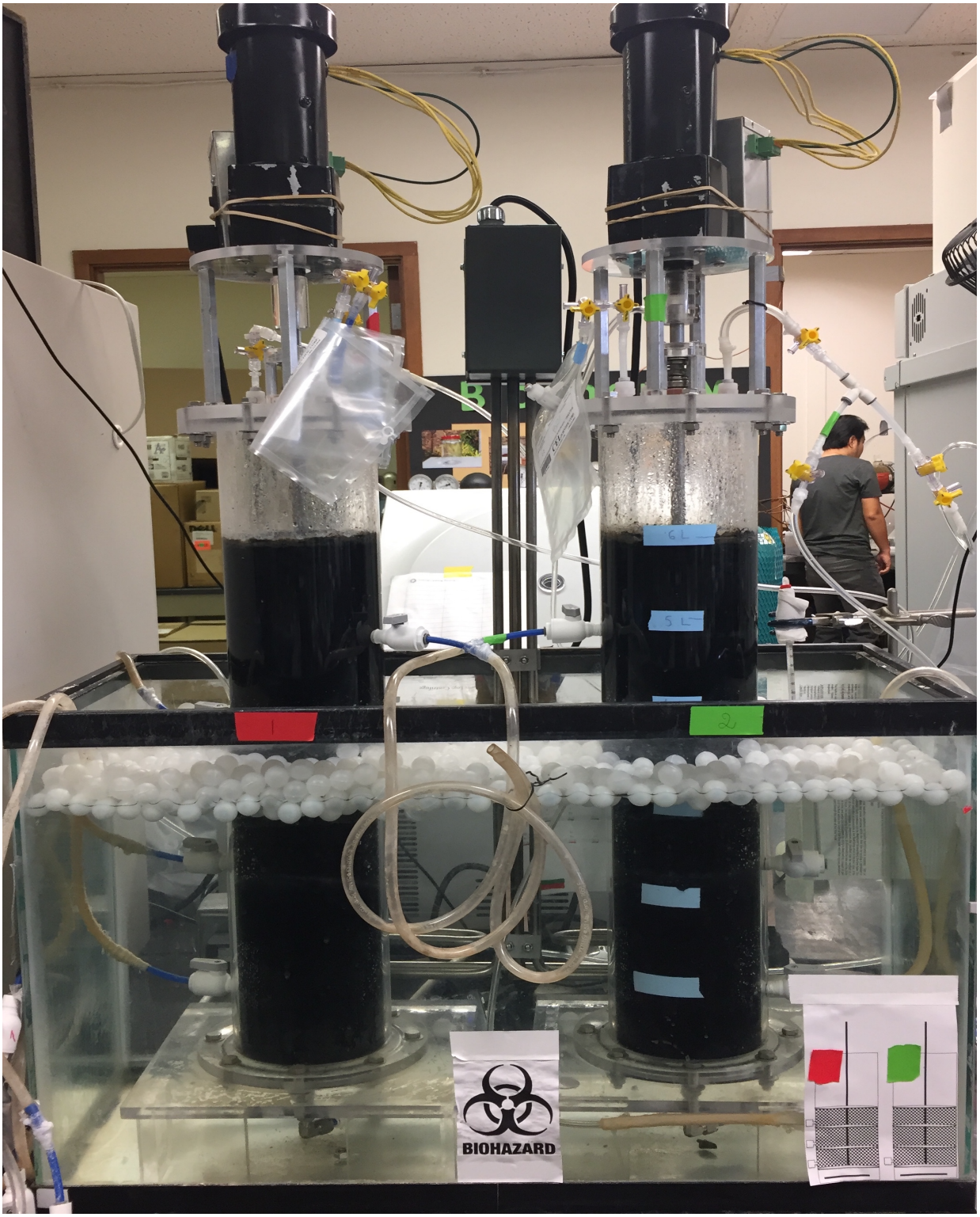

A.3 Reactor R3 and R4

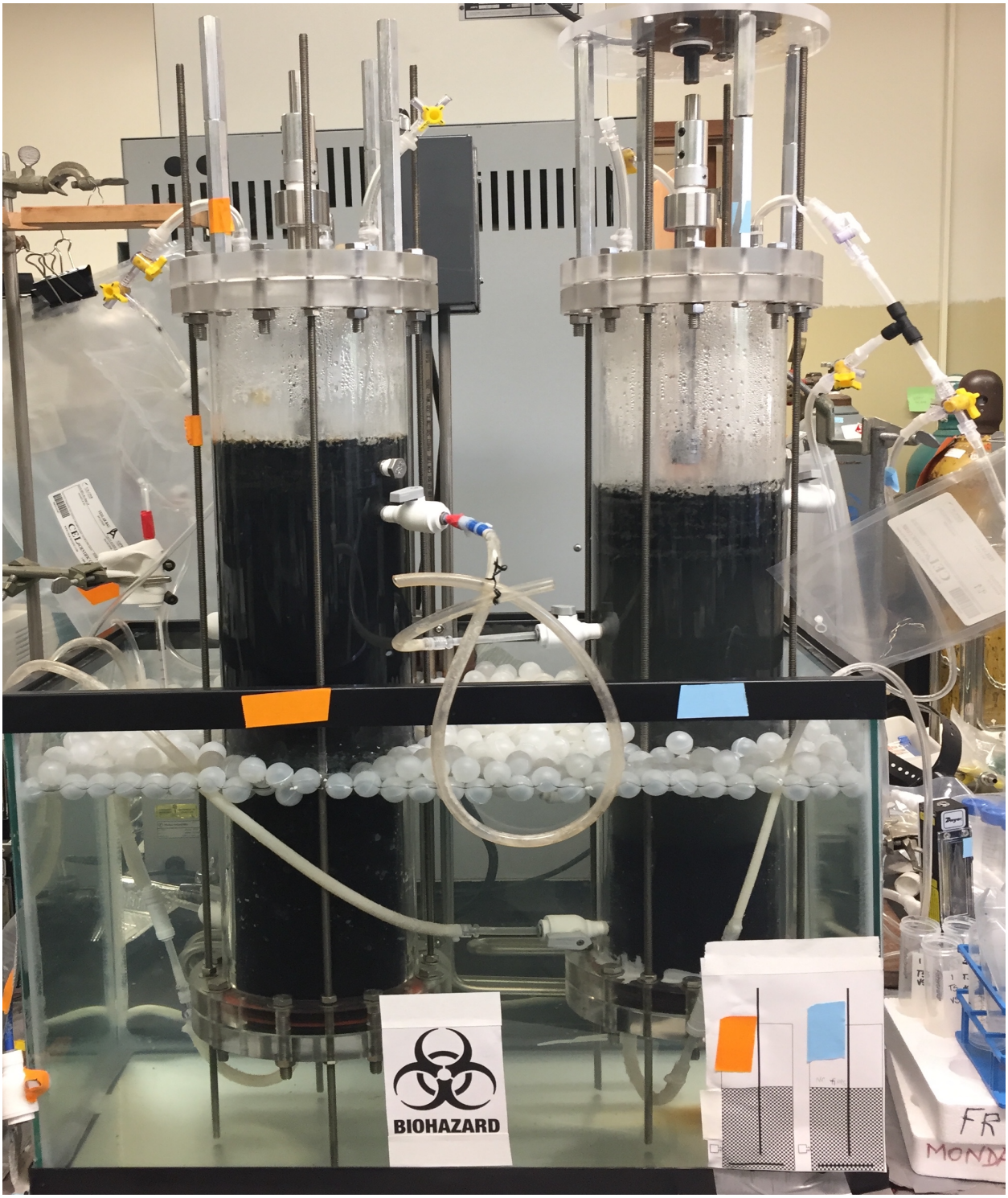

A.4 Biochar column

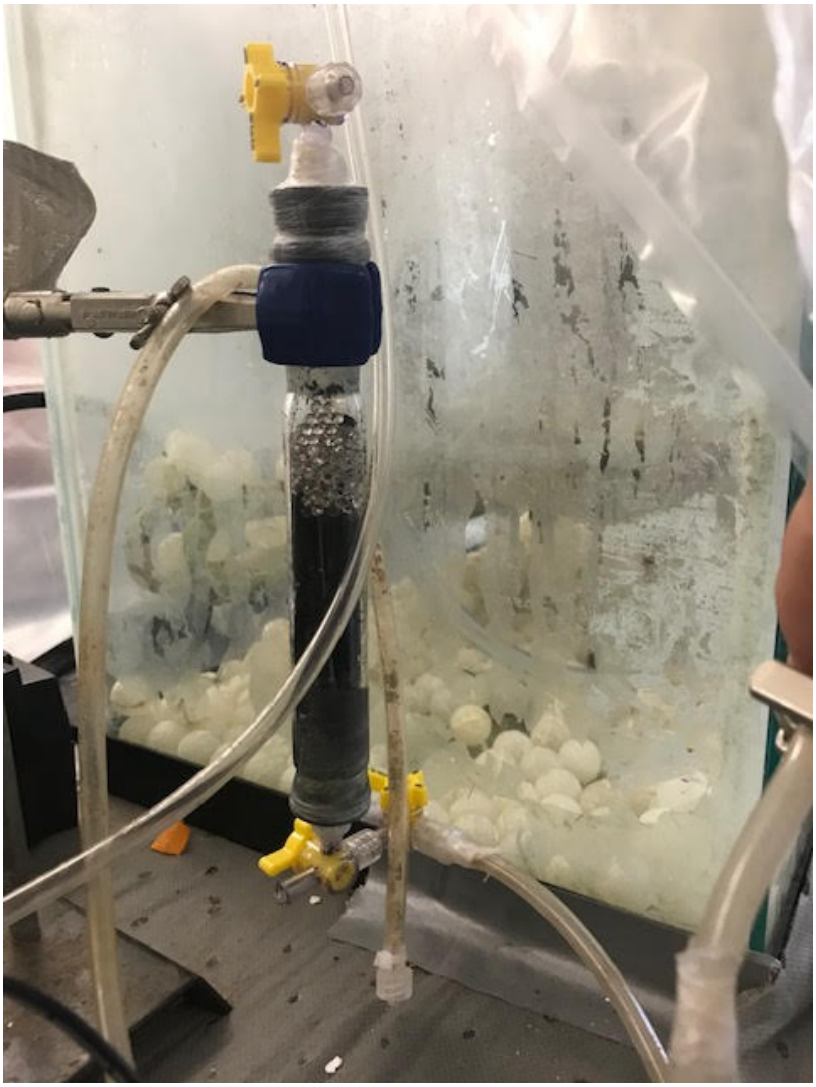

APPENDIX B

COD BALANCE AD SULFUR BALANCE

Table B.1 Parameters for carbon balance

Reactor	Influent sulfate mg/L	TOC influent %	TOC g C	TOC effluent g/d	TOC effluent %	IC g	IC %	CH4 NL/d	g C	CH4 %	CO2 NL/d	g C	CO2 %	VSS g	VSS %	Recovery
R1	1000	100	18	0.74	4.11	2.00	11.11	5.50	3.93	21.83	10.00	5.36	29.76	2.00	11.11	95.29
	2000	100	18	1.03	5.72	2.00	11.11	6.20	4.43	24.60	10.00	5.36	29.76	2.00	11.11	95.79
	3000	100	18	1.03	5.72	2.00	11.11	6.40	4.57	25.40	10.00	5.36	29.76	2.00	11.11	95.93
	4000	100	18	0.80	4.44	2.00	11.11	4.30	3.07	17.06	10.00	5.36	29.76	2.00	11.11	94.43
	5000	100	18	1.70	9.44	2.50	13.89	3.50	2.50	13.89	10.00	5.36	29.76	1.00	5.56	93.36
	6000	100	18	2.20	12.22	3.00	16.67	3.30	2.36	13.10	9.00	4.82	26.79	0.50	2.78	92.68
	6000 - Biochar	100	18	0.70	3.89	2.00	11.11	5.50	3.93	21.83	10.00	5.36	29.76	2.00	11.11	95.29
R2	1000	100	18	0.73	4.07	2.00	11.11	6.80	4.86	26.98	8.00	4.29	23.81	2.00	11.11	95.14
	2000	100	18	1.32	7.33	2.00	11.11	6.70	4.79	26.59	10.00	5.36	29.76	2.00	11.11	96.14
	3000	100	18	1.03	5.73	2.00	11.11	7.90	5.64	31.35	10.00	5.36	29.76	2.00	11.11	97.00
	4000	100	18	0.90	5.00	2.00	11.11	6.30	4.50	25.00	10.00	5.36	29.76	2.00	11.11	95.86
	5000	100	18	1.80	10.00	2.50	13.89	4.00	2.86	15.87	9.00	4.82	26.79	1.00	5.56	93.18
	6000	100	18	2.70	15.00	3.00	16.67	3.40	2.43	13.49	8.00	4.29	23.81	0.50	2.78	92.21
	6000 - Biochar	100	18	0.90	5.00	2.00	11.11	6.70	4.79	26.59	10.00	5.36	29.76	2.00	11.11	96.14
R3	1000	100	18	0.71	3.97	2.00	11.11	6.10	4.36	24.21	10.00	5.36	29.76	2.00	11.11	95.71
	2000	100	18	1.07	5.94	2.00	11.11	7.70	5.50	30.56	10.00	5.36	29.76	2.00	11.11	96.86
	3000	100	18	0.93	5.17	2.00	11.11	8.40	6.00	33.33	10.00	5.36	29.76	2.00	11.11	97.36
	4000	100	18	0.70	3.89	2.00	11.11	6.50	4.64	25.79	10.00	5.36	29.76	2.00	11.11	96.00
	5000	100	18	1.90	10.56	2.50	13.89	4.50	3.21	17.86	9.00	4.82	26.79	0.50	2.78	93.04
	6000	100	18	2.30	12.78	3.00	16.67	4.40	3.14	17.46	8.00	4.29	23.81	1.00	5.56	93.43
	6000 - Biochar	100	18	1.00	5.56	2.00	11.11	7.70	5.50	30.56	10.00	5.36	29.76	2.00	11.11	96.86

Table B.1 Parameter of interest in sulfur balance

Reactor	Influent sulfate mg SO_4/L	Effluent sulfate mg SO_4/L	Dissolved sulfide mg S/L	Unionized (H_2S_{aq}) mg S/L	Biogas sulfide (H_2S_{gas}) NmL/d
R1	1000	6.14	2.70	0.41	93.44
	2000	2.25	24.46	3.67	172.52
	3000	9.10	59.71	8.96	164.00
	4000	5.03	79.10	11.86	249.10
	5000	4.72	124.10	18.61	358.03
	6000	40.00	163.95	24.59	450.61

	6000 Biochar	6.00	33.88	5.08	92.20
R2	1000	11.71	1.12	0.17	56.33
	2000	3.07	30.46	4.57	182.36
	3000	4.40	62.43	9.36	159.07
	4000	6.75	79.23	11.88	272.27
	5000	14.20	113.79	17.07	339.33
	6000	53.00	143.70	21.56	436.16
	6000 Biochar	10.00	73.69	11.05	51.09
R3	1000	13.14	2.40	0.36	63.65
	2000	2.92	30.64	4.60	170.90
	3000	6.40	61.10	9.17	187.73
	4000	6.00	81.60	12.24	269.93
	5000	12.00	118.17	17.73	331.33
	6000	22.00	157.60	23.64	391.48
	6000 Biochar	18.00	72.11	10.82	165.95

Table B.2 Conversion of all sulfur species into equivalent sulfur

Reactor	Influent sulfate mg SO4/L	Influent - S g SO4-S/d	Effluent -S, g S/d			Biogas sulfide H_2S-S/d	Sulfur recovery g S/d
			SO_4-S	Ionized -S	Un-ionized -S		
	1000	166.32	10.24	8.12	2.03	116.79	29.13

R1	2000	332.64	3.75	36.76	18.35	215.65	58.13
	3000	498.97	15.18	59.83	44.78	205.00	174.17
	4000	665.29	8.39	59.44	59.32	311.30	226.76
	5000	831.61	7.87	74.61	93.07	447.53	208.53
	6000	997.94	66.72	82.14	122.96	563.26	162.85
	6000 Biochar	997.94	10.00	16.97	25.41	115.25	830.30
R2	1000	166.32	19.53	3.36	0.84	70.41	72.18
	2000	332.64	5.12	45.78	22.85	227.95	30.95
	3000	498.97	7.34	62.55	46.82	198.84	183.41
	4000	665.29	11.26	59.54	59.42	340.34	194.73
	5000	831.61	23.68	68.41	85.34	424.16	230.01
	6000	997.94	88.41	71.99	107.78	545.20	184.55
	6000 Biochar	997.94	16.68	36.92	55.27	63.86	825.21
R3	1000	166.32	21.92	7.21	1.80	79.56	55.83
	2000	332.64	4.87	46.05	22.98	213.63	45.12
	3000	498.97	10.67	61.22	45.83	234.66	146.58
	4000	665.29	10.00	61.32	61.20	337.41	195.35
	5000	831.61	20.01	71.04	88.63	414.16	237.76
	6000	997.94	36.70	78.96	118.20	489.35	274.73
	6000 Biochar	997.94	30.02	36.12	54.08	207.43	670.27

Table B.3 Fate of sulfur as percent of influent sulfate sulfur

Reactor	Influent sulfate mg SO_4/L	Influent SO_4-S %	Effluent -S, %			Biogas sulfide %	Sulfur recovery g %
			SO_4-S	Ionized -S	Un ionized-S		
R1	1000		6.15	4.88	1.21	70.22	82.48
	2000		1.12	11.05	5.51	64.82	82.53
	3000		3.04	11.99	8.97	41.08	65.09
	4000		1.26	8.93	8.91	46.80	65.92
	5000		0.94	8.97	11.19	53.81	74.92
	6000		6.68	8.23	12.32	56.44	83.68
	6000 - Biochar		1.00	1.70	2.54	11.54	16.80
R2	1000		11.74	2.02	0.50	42.33	56.61
	2000		1.53	13.76	6.86	68.52	90.70
	3000		1.47	12.53	9.38	39.85	63.24
	4000		1.69	8.95	8.93	51.15	70.73
	5000		2.84	8.22	10.26	51.00	72.34
	6000		8.85	7.21	10.79	54.63	81.51
	6000 - Biochar		1.67	3.69	5.53	6.39	17.31
	1000		13.17	4.33	1.08	47.83	66.43

R3	2000	100	1.46	13.84	6.908	64.21	86.44
	3000		2.13	12.27	9.18	47.02	70.62
	4000		1.50	9.21	9.19	50.71	70.64
	5000		2.40	8.54	10.65	49.80	71.41
	6000		3.67	7.91	11.84	49.03	72.47
	6000 - Biochar		3.00	3.62	5.41	20.78	32.83

APPENDIX C

MICROBIOLOGY SAMPLE PREPARATION

Table C.1 Multivariate statistics. Sample preparation.

Sample ID	Reactor	Sulfate (mg/L)	Raw Reads (PE)	Clean Reads (PE)	Raw Tags	Clean Tags	MaxLen (nt)	MinLen (nt)	AvgLen (nt)	GC (%)	No. of seqs	Effective (%)
1A	1	4000	28006	26885	26777	26147	393	358	371.56	54.19	20644	78.95
1B	1	4000	21079	20307	20240	19751	388	352	371.12	53.57	15795	79.97
1C	1	4000	22208	21345	21276	20797	390	354	371.07	53.52	16493	79.3
1D	1	5000	23086	22205	22135	21675	380	360	371.12	55.11	18393	84.86
1E	1	5000	21580	20724	20653	20221	382	363	371.26	54.32	16872	83.44
1F	1	5000	25706	24614	24545	24098	397	358	371.39	54.73	20489	85.02
1G	1	6000	24177	23122	23034	22597	394	357	370.91	55.23	19284	85.34
1H	1	6000	26311	25169	25096	24646	380	347	370.84	55.62	21169	85.89
1I	1	6000 after biochar	28779	27804	27725	27122	379	357	371.4	54.2	22429	82.7
2A	2	4000	23177	22126	22050	21503	393	358	371.41	55.26	17028	79.19
2B	2	4000	25590	24635	24560	24040	393	345	370.78	53.86	19546	81.31
2C	2	4000	24256	23052	22988	22566	381	365	371.04	55.1	18905	83.78
2D	2	5000	25043	24083	24022	23627	381	351	370.81	55.21	20495	86.74

2E	2	5000	22854	21901	21835	21442	389	361	370.88	55.2	18000	83.95
2F	2	5000	23664	22684	22627	22247	381	355	370.75	55.2	18741	84.24
2G	2	6000	25460	24560	24495	24023	382	358	370.94	55.58	20547	85.53
2H	2	6000	26269	25274	25205	24803	382	358	370.97	55.33	20825	83.96
2I	2	6000 after biochar	23343	22623	22574	22192	381	353	370.85	53.92	18789	84.67
3A	3	4000	23360	22250	22189	21790	382	361	370.33	54.12	17906	82.18
3B	3	4000	24574	23381	23289	22899	386	365	370.47	54.4	18839	82.27
3C	3	4000	21877	20750	20698	20328	391	350	370.49	54.81	16984	83.55
3D	3	5000	16981	16227	16180	15932	398	360	370.44	54.8	13630	85.55
3E	3	5000	22129	21158	21091	20751	399	357	370.42	54.57	17476	84.22
3F	3	5000	21770	20797	20746	20422	393	355	370.49	54.3	17524	85.81
3G	3	6000	21903	21068	20997	20625	384	359	370.75	54.67	16992	82.39
3H	3	6000	21186	20255	20195	19819	382	356	370.69	54.72	16299	82.24
3I	3	6000 after biochar	22189	21296	21230	20815	386	357	370.87	53.64	17194	82.6

APPENDIX D

LIST OF PUBLICATIONS

Peer-Reviewed Articles

Submitted:

Oliveira, F. R., Jaisi, D. P., Lu, H & Khanal, S. K. (2019). Alleviating sulfide toxicity using biochar during anaerobic treatment of sulfate-laden wastewater with simultaneous recovery of sulfur-rich biochar as soil macro-nutrient. Bioresource Technology

Published:

Oliveira, F. R., Patel, A. K., Jaisi, D. P., Adhikari, S., Lu, H., & Khanal, S. K. (2017). Environmental application of biochar: Current status and perspectives. Bioresource Technology. [Most downloaded article].

Kanjanarong, J., Giri, B. S., Jaisi, D. P., **Oliveira, F. R.,** Boonsawang, P., Chaiprapat, S., ... & Khanal, S. K. (2017). Removal of hydrogen sulfide generated during anaerobic treatment of sulfate-laden wastewater using biochar: Evaluation of efficiency and mechanisms. *Bioresource Technology*, *234*, 115-121.

Oral and Poster Presentation

Oliveira, F. R., Surendra, K. C., Jaisi, D. P., Lu, H. and Khanal, S. K. Alleviating sulfide toxicity using biochar during anaerobic treatment of high-sulfate wastewater with sulfur recovery. 16th IWA World Congress on Anaerobic Digestion (AD-16), June 23-27, 2019, Delft- Netherlands.

Oliveira, F.R. and Khanal, S. K. High rate anaerobic treatment of sulfate-laden industrial wastewater with simultaneous removal of hydrogen sulfide using biochar. 30th Annual CTAHR Student Research Symposium (2018). University of Hawaii at Manoa, HI, USA.

Oliveira, F.R. and Khanal, S. K. Hydrogen sulfide removal from biogas using biochar. 28th Annual CTAHR Student Research Symposium (2016). University of Hawaii at Manoa, HI, USA.